Performance Evaluation of a Solar Chimney Power Plant.

by

Richard Anthony Hedderwick

Thesis presented in partial fulfilment of the requirements for the degree of Master of Engineering at the University of Stellenbosch

Thesis Supervisor: Prof. D.G. Kröger

Department of Mechanical Engineering
University of Stellenbosch

December 2000

DECLARATION

I the undersigned, hereby declare that the work contained in this thesis is my own original work and that I have not previously, in its entirety or in part, submitted it at any university for a degree.

Signature: ..... Date: 13.02.21

Richard Hedderwick

ABSTACT

A solar chimney power plant consists of a central chimney that is surrounded by a transparent canopy located a few meters above ground level. The ground beneath this canopy or collector as it is known is heated by the solar radiation that is effectively trapped by the collector. This in turn heats the air in the collector, which flows radially inwards towards the chimney. This movement is driven by the difference between the hydrostatic pressure of the air inside- and outside the solar chimney system. The energy is extracted from the air by a turbine driven generator situated at the base of the chimney.

The performance of such a solar chimney power plant is evaluated in this study making use of a detailed mathematical model. In this model the relevant discretised energy and draught equations are deduced and solved to determine the performance of a specific plant referred to as the "reference plant". This plant is to be located at a site near Sishen in the Northern Cape in South Africa where meteorological data is available.

The performance characteristics of this plant are presented using values from the 21st of December as an example. These characteristics include the instantaneous and integrated power output, as well as the absorption of the solar radiation of each of the parts of the collector. The air temperatures throughout the plant and the convective heat transfer coefficients in the collector in the region of developing and fully developed flow are presented. The pressure of the air throughout the system is presented as well as the pressure drop over the turbine. Temperature distributions in the ground below the collector are also presented and discussed.

OPSOMMING

'n Sonkrag toring aanleg bestaan uit 'n sentrale toring omring deur 'n deurskynende bedekking wat 'n paar meter bo die grondvlak verhef is. Die grond wat onder die bedekking is staan bekend as die versamelaar. Die son bestraling word effektief deur die versamelaar vasgevang en dit verhit die grond wat die versamelaar bedek. Hierdie grond verhit die lug teenwoordig in die versamelaar en die lug vloei in 'n radiale rigting inwaarts na die toring toe. Die dryfkrag agter hierdie beweging is die verskil in hidrostatiese druk van onderskeildelik die lug binne en buite die sonkrag toring sisteem. Energie word uit die lug onttrek deur 'n turbien aangedrewe opwekker geleë by die basis van die toring.

Die werksverrigting van die toring word geëvalueer in hierdie studie deur van 'n gedetaileerde wiskundige model gebruik te maak. In hierdie model word die relevante gediskritiseerde energie en vloei vergelykings afgelei en opgelos om sodoende die werksverrigting van 'n spesifieke aanleg te bereken. Die aanleg word na verwys as die "verwysings aanleg". Die ligging van hierdie verwysings aanleg is naby Sishen in die Noord-Kaap in Suid Afrika waar meteorologiese data beskikbaar is.

Die werksverrigtings-karakterisiteke van die verwysings aanleg word voorgelê deur gebruik te maak van waardes vanaf die 21ste Desember. Hierdie karakterisiteke sluit die onmiddelike en geintegreerde krag wat opgewek word, sowel as die absorpsie van die son bestraling in elke deel van die toring in. Die lug temperatuuur deurgaans in die stelsel asook die konveksie warmte oordrag koeëfisiente in die versamelaar, in die gebied van ontwikkelde én ten volle ontwikkelde vloei word voorgelê. Die druk van die lug in die stelsel word voorgelê sowel as die drukval oor die turbine. Temperatuur verspreidings in die grond onder die versamelaar word ook voorgelê en bespreek.

ACKNOWLEDGEMENTS

I am very grateful for the absolutely accurate and unhurried help that I received from my promoter Prof. D.G. Kröger. I hope to carry traces of his character in my work always.

I would like to acknowledge the advice that I received from Francois Lombaard especially with regards to the calculations involving solar radiation. His unselfish support and friendship were also invaluable.

I am especially grateful to the Lord who teaches me continuously. May this work serve His kingdom.

DEDICATION

To my father, an engineer at heart.

TABLE OF CONTENTS

NOMENCLATURE

A	Area (m^2)
b	Exponent in collector roof height
C	Drag coefficient
c_p	Specific heat at constant pressure (J/kgK)
d	Diameter (m)
F	Force (N)
f	Friction factor
g	Gravitational acceleration (m/s^2)
H	Height (m)
h	Heat transfer coefficient (W/m^2K)
I	Solar radiation (W)
K	Static pressure change factor
k	Thermal conductivity (W/mK)
M	Momentum (kgm/s)
m	Mass flow rate (kg/s)
n	Number
P	Power (W) or pitch (m)
p	Pressure (Pa)
q	Heat flux (W/m^2)
R	Universal gas constant (J/kgK)
r	Radius (m)
T	Temperature (°C or K)
t	Time (s) or thickness (m)
v	Velocity (m/s)
z	Depth (m)

Symbols

α	Absorbtance
∞	Infinity
∂	Partial derivative
Δ	Differential
δ	Boundary layer thickness (m)
ε	Surface roughness
ϕ	Angle (radians)

μ	Viscosity (kg/ms)
π	Pi
θ	Angle (radians or degrees)
ρ	Density (kg/m^3)
σ	Boltzmann's constant (W/m^2K^4)
τ	Transmittance or frictional force (N)
υ	Kinematic viscosity (m^2/s)
ω	Hour angle (radians)

Dimensionless Numbers

Fr	Froude number
Pr	Prandtl number
Re	Reynolds number

Subscripts

α	Radiation absorbed by roof or due to absorption only
10	Base 10
a	Ambient
aHco	Ambient at elevation of chimney outlet
b	Beam
ci	Chimney inlet
co	Collector outlet
d	Diffuse or declination
$\Delta\theta$	Relevant to differential portion of angle
D	Darcy or drag or densimetric
f	Friction
g	Ground
h	Total
i	Radiation entering ground or collector inlet or radial index
j	Axial index
lat	Latitude
nlayg	Number of layers modelled in ground
o	Collector outlet
old	From previous time step
r	Roof or radial or due to reflectance only
ra	Convective from roof to ambient air

rgr	Radiative from ground to roof
rrs	Radiative between roof an sky
s	Collector support
sky	Sky
t	Tangential
ti	Turbine inlet
to	Turbine outlet
w	Wind

Current electricity production from fossil fuels like natural gas, oil or coal is damaging to the environment and bares the limitation that it relies upon non-renewable energy sources. Many developing countries cannot afford these conventional energy sources, and in some of these locations nuclear power is considered an unacceptable risk. It has been shown that a lack of energy may be connected to poverty and poverty to population explosions. The need for an environmentally friendly and cost effective electricity generating scheme is thus obvious and will become more pronounced in the future.

A possible solution to the ever-increasing problem is solar energy. It is an abundant, renewable source of energy that only needs to be harnessed to be of use to man. Solar power plants in use in the world are equipped to transform solar radiation into electrical energy via any one of a number of cycles or natural phenomena. Few however have the ability to store sufficient energy during the day so that a supply can be maintained during the night as well, when the solar radiation is negligible. The necessary capacity of this storage is usually too high to be practically viable.

The solar chimney power plant concept proposed by Schlaich [94SC1] in the late 1970's is possibly a good solution to the problems involved with conventional power generators. A solar chimney power plant consists of a central chimney that is surrounded by a transparent canopy located a few metres above ground level as

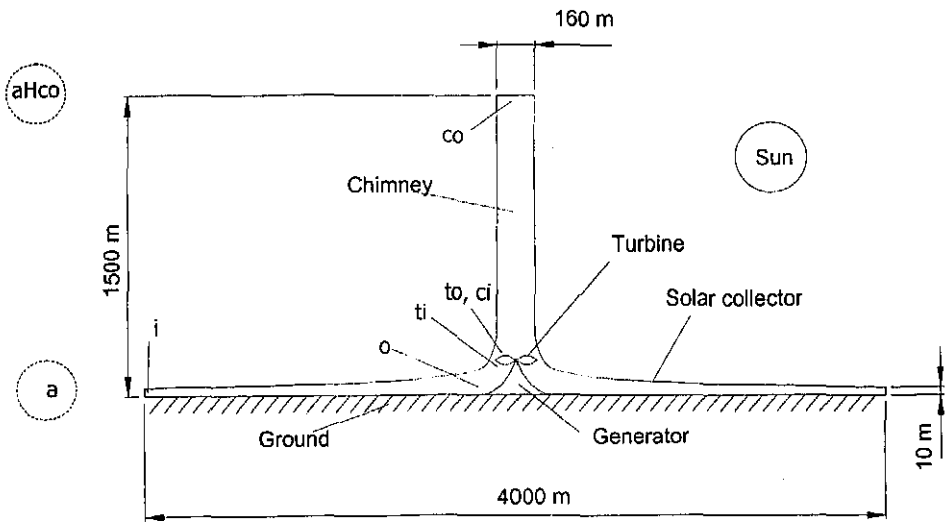

Figure 1.1: The Solar chimney showing the labelling convention used.

shown schematically in figure 1.1. The ground beneath the collector is heated by the solar radiation that is effectively trapped by the collector. This in turn heats the air in the collector which flows radially inwards towards the chimney. This movement is driven by the difference of the hydrostatic pressure of the air inside- and outside the solar chimney system. Energy is extracted from the air by a turbine driven generator situated at the base of the chimney.

Schlaich conducted detailed theoretical research and extensive wind tunnel experiments which were followed by the design, construction and commissioning of a 50 kW experimental plant. This plant was erected in Manzanares, and had a 240 m diameter collector and a 195 m high chimney. Various properties and effects were studied namely:

- Different roof coverings were tested for durability, structural suitability, and effects on plant performance.
- Effects of ground temperature, humidity, and absorbtance on plant performance.
- Various mass flow control algorithms were tested.
- Running costs and maintenance requirements were assessed.

These experiments took place between 1982 and 1986, after which the plant was left to run under its own automated control until 1989. Various plant sizes were studied using a thermodynamic model and the dimensions, costs and performance of these plants were presented in numerous tables.

Schlaich also did research into the economic viability of the system and found that it approached that of conventional power generating systems. Later supplements to his book discuss the results of his studies into the effects of water bags used to improve the ground storage capability. These studies reveal that a water layer 0.2 m thick will even out the daily fluctuation in power generation, at a value approximately half that of the midday peak of a similar plant with no water storage.

Haaf et al. [83HA1] presented the results of their investigations into the proposed Manzanares plant and then in a later study Haaf [84HA1] presented preliminary test results from the experiments done on the same plant.

Mullet [87MU1] presented a simple analysis of the solar chimney, neglecting the variation of temperature, and pressure of air with variation in height, and losses in the chimney. Expressions for the overall efficiency were suggested.

Relevant governing differential equations that describe chimney performance were derived by Padki et al. [88PA1] and later they presented the results of their study of the viability of medium-to-large scale power generation [89PA1] and power generation in rural areas [89PA1]. More recently they discussed various effects of geometrical and operating parameters on the overall performance of the solar chimney.

Blaine and Kröger [99BL1] studied the validity of various driving potential models for prevailing ambient conditions (especially conditions that are elevation dependant) around the solar chimney. They show that power output increases with humidity and that condensation may occur in the chimney.

Gannon and von Backström. [00GA1] applied an ideal air standard cycle analysis to the solar chimney to find its limiting efficiency and performance. This cycle was then refined to include a simple collector model and system losses.

2.1. INTRODUCTION

The energy equations are used to determine the temperature distribution throughout the collector of the solar chimney power plant. The derivation of these equations is discussed in the following section.

2.2. ENERGY EQUATION FOR AIR

Consider the elementary control volume of collector air as shown in figure 2.1.

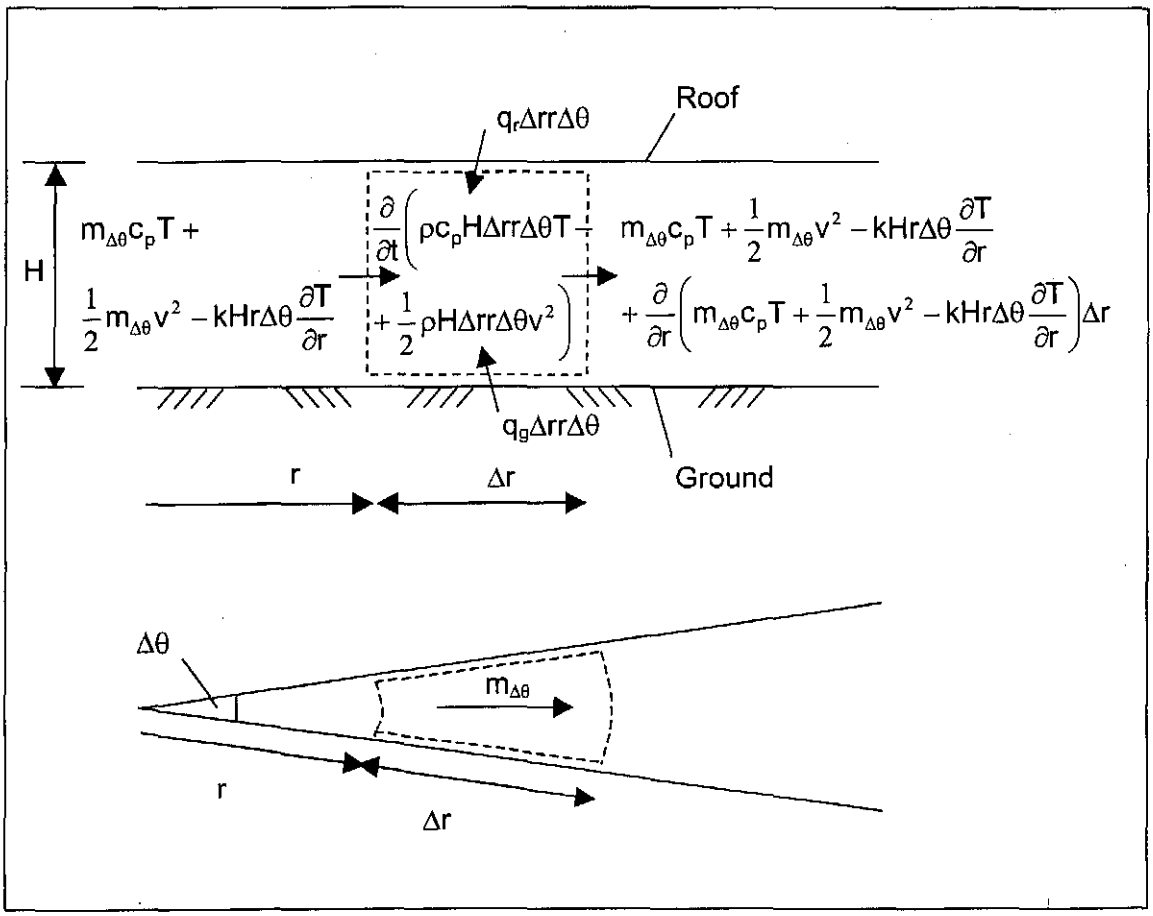

Figure 2.1: Energy equation applied to an elementary control volume of air.

Assuming a constant temperature distribution in the vertical plane the energy equation applicable to this control volume can be written as follows:

$$m_{\Delta\theta}c_pT+\frac{1}{2}m_{\Delta\theta}v^2-kHr\Delta\theta\frac{\partial T}{\partial r}+q_r\Delta\theta r\Delta r+q_g\Delta\theta r\Delta r$$
$$=m_{\Delta\theta}c_pT+\frac{1}{2}m_{\Delta\theta}v^2-kHr\Delta\theta\frac{\partial T}{\partial r}+\frac{\partial}{\partial r}\left(m_{\Delta\theta}c_pT+\frac{1}{2}m_{\Delta\theta}v^2-kHr\Delta\theta\frac{\partial T}{\partial r}\right)\Delta r \qquad (2.1)$$
$$+\frac{\partial}{\partial t}\left(\rho c_p\Delta\theta r\Delta rHT+\frac{1}{2}\rho\Delta\theta r\Delta rHv^2\right)$$

where $m_{\Delta\theta}$ is the mass flow that passes through the control volume. Changes in the kinetic energy and conduction terms are negligible and it can be assumed that the specific heat c_p remains essentially constant. (For details about these approximations see Appendix 5.) With these approximations equation (2.1) is simplified to read

$$q_r+q_g=\frac{m_{\Delta\theta}c_p}{\Delta\theta r}\frac{\partial T}{\partial r}+\frac{c_pT}{\Delta\theta r}\frac{\partial m_{\Delta\theta}}{\partial r}+Hc_p\frac{\partial}{\partial t}(\rho T) \qquad (2.2)$$

According to the perfect gas law $\rho=p/(RT)$. Since changes in absolute pressure are essentially negligible in the collector, substitution of the expression for ρ into the last term of equation (2.2) results in its elimination leading to the following relation

$$q_r+q_g=\frac{m_{\Delta\theta}c_p}{\Delta\theta r}\frac{\partial T}{\partial r}+\frac{c_pT}{\Delta\theta r}\frac{\partial m_{\Delta\theta}}{\partial r} \qquad (2.3)$$

Applying the conservation of mass to the control volume of air as shown in figure 2.1 yields the following equation:

$$m_{\Delta\theta}=m_{\Delta\theta}+\frac{\partial m_{\Delta\theta}}{\partial r}\Delta r+\frac{\partial(\rho\Delta\theta rH\Delta r)}{\partial t} \qquad (2.4)$$

Substitute $\rho=p/(RT)$ into equation (2.4) and find

$$\frac{\partial m_{\Delta\theta}}{\partial r}=-\Delta\theta rH\frac{p}{RT^2}\frac{\partial T}{\partial t} \qquad (2.5)$$

For fully developed flow the convective heat entering the control volume from the underside of the roof q_r can be written as

$$q_r = h_r(T_r - T) \tag{2.6}$$

where h_r is given by the relation [75GN1]

$$h_r = \frac{k\left(f_D/16\right)(Re-1000)Pr}{H\left[1.07+12.7(f_D/8)^{0.5}\left(Pr^{0.67}-1\right)\right]} \tag{2.7}$$

where

$$Re = 2\rho vH/\mu \tag{2.8}$$

If the surface of the roof is assumed to be smooth the Darcy friction factor f_D is given by

$$f_D = \left(1.82\log_{10}Re - 1.64\right)^{-2} \tag{2.9}$$

Similarly, the convective heat q_g entering the control volume from the ground with roughness ε_g can be written as

$$q_g = h_g(T_g - T) \tag{2.10}$$

where h_g is given by equation (2.7) with f_D being given by [83HA2]

$$f_D = 0.3086\left[\log_{10}\left\{\frac{6.9}{Re}+\left(\frac{\varepsilon_g/H}{7.4}\right)^{1.11}\right\}\right]^{-2} \tag{2.11}$$

Substituting equations (2.5), (2.6) and (2.10) into equation (2.3) yields for fully developed flow

$$\frac{m_{\Delta\theta}c_p}{\Delta\theta r}\frac{\partial T}{\partial r} + c_pH\frac{p}{RT}\frac{\partial T}{\partial t} = h_g(T_g - T) + h_r(T_r - T) \tag{2.12}$$

Applying this to the entire annulus (i.e. the control volume formed by increasing the inner angle to 2π) we find

$$\frac{mc_p}{2\pi r}\frac{\partial T}{\partial r}+c_pH\frac{p}{RT}\frac{\partial T}{\partial t}=h_g\left(T_g-T\right)+h_r\left(T_r-T\right) \tag{2.13}$$

Repeating the process for the region of developing flow near the inlet of the collector where the heat transfer coefficients are defined with respect to the free stream temperature yields

$$\frac{mc_p}{2\pi r}\frac{\partial T}{\partial r}+c_pH\frac{p}{RT}\frac{\partial T}{\partial t}=h_g\left(T_g-T_a\right)+h_r\left(T_r-T_a\right) \tag{2.14}$$

where h_r and h_g are now given by the developing flow equations as given by Kröger and Buys [99KR1] namely:

$$h_r=\frac{k}{r_i-r}0.0032Pr^{0.333}\left(1-\frac{r}{r_i}\right)\left(\frac{m}{\mu H_i}\right)^{0.833}\left(\frac{r_i}{r}\right)^{0.8(1-b)}\left\{\frac{6.218-15.08b}{\left(\frac{r}{r_i}\right)^{1.2-0.2b}-\left(\frac{r}{r_i}\right)^{2.743-3.943b}}\right\}^{1/6} \tag{2.15}$$

for a smooth surface and

$$h_g=\frac{k}{r_i-r}0.001325Pr^{0.333}\left(1-\frac{r}{r_i}\right)\left(\frac{m}{\mu H_i}\right)\left(\frac{\varepsilon_g}{r_i}\right)^{0.2026}\left(\frac{r_i}{r}\right)^{1-b}$$
$$\times\frac{4.953q\left(\frac{r}{r_i}\right)^{0.51(1-b)}+1}{\left\{q\frac{\left(\frac{r}{r_i}\right)^{1.51-0.51b}-\left(\frac{r}{r_i}\right)^{2.866-4.120b}}{2.550-6.787b}+\frac{\left(\frac{r}{r_i}\right)-\left(\frac{r}{r_i}\right)^{2.886-4.120b}}{17.38-38.37b}\right\}^{0.2026}} \tag{2.16}$$

with

$$q=\left(\frac{\mu H_i r_i}{\varepsilon_g m}\right)^{0.51} \tag{2.17}$$

for a rough surface.

2.3. ENERGY EQUATION FOR GROUND

Consider an elementary control volume as shown in figure 2.2 in the ground of the collector.

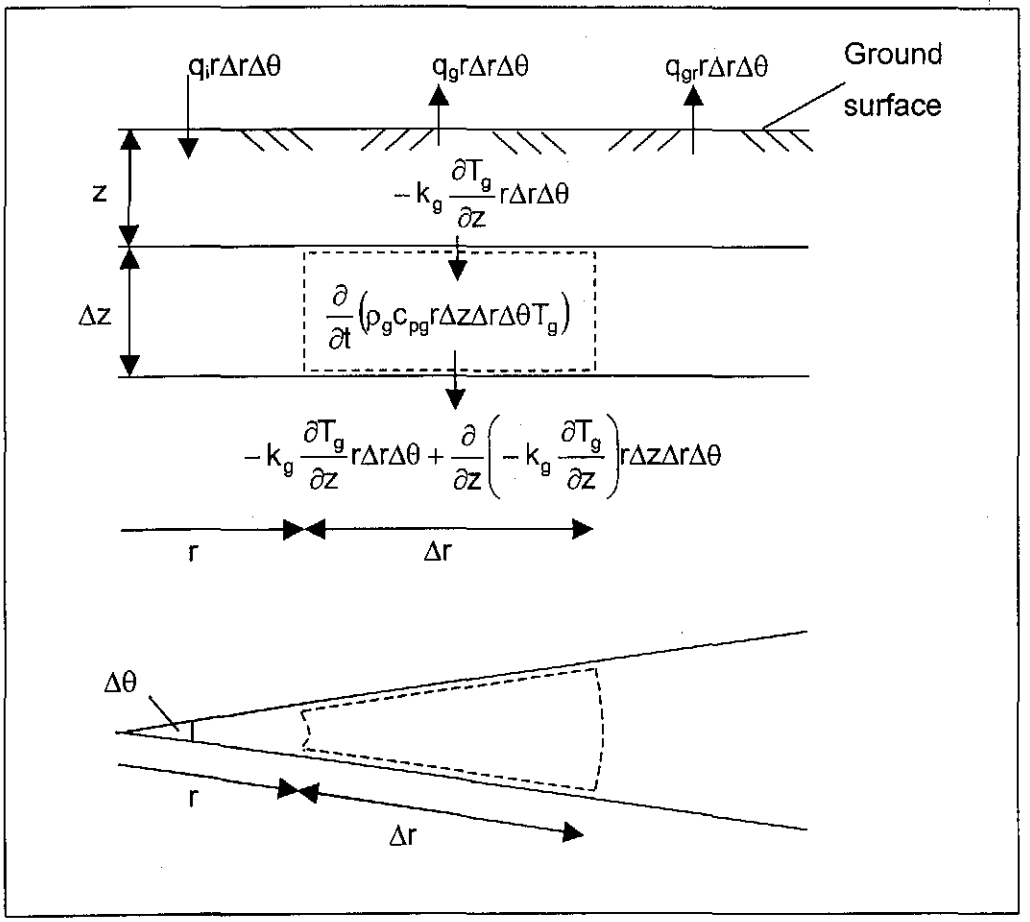

Figure 2.2: Energy equation applied to an elementary control volume of ground.

Since the temperature gradient with respect to varying depth is orders of magnitude higher than in the radial direction a one-dimensional analysis will be appropriate. The energy equation applicable to the elementary control volume shown in figure 2.2 is written as follows:

$$\frac{\partial}{\partial t}\left(\rho_g c_{pg} r\Delta r\Delta\theta\Delta z T_g\right) = \frac{\partial}{\partial z}\left(k_g \frac{\partial T_g}{\partial z}\right) r\Delta r\Delta\theta\Delta z \qquad (2.18)$$

For constant ρ_g, c_{pg} and k_g this becomes

$$\rho_g c_{pg} \frac{\partial T_g}{\partial t} = k_g \frac{\partial^2 T_g}{\partial z^2} \tag{2.19}$$

To solve this equation two boundary conditions and an initial condition are necessary. The boundary conditions are given as:

$$k_g \frac{\partial T_g}{\partial z} = q_g + q_{gr} - q_i \tag{2.20}$$

at $z = 0$, and at $z = \infty$

$$\frac{\partial T_g}{\partial z} = 0 \tag{2.21}$$

(This boundary condition is given more attention in Appendix 9.) Because of the transient nature of the model, the initial condition will be given as some initial temperature. The most accurate way to define initial conditions is to allow the model to run using approximate initial values for as long as it takes to reach a sustained convergence, and to use the output of this preliminary run as the initial conditions of the actual run.

The fraction of solar radiation entering the surface of the ground is given by

$$q_i = (\tau_b \alpha)_g I_b + (\tau_d \alpha)_g I_d \tag{2.22}$$

The beam and diffuse transmittance-absorptance products are given in Appendix 6. I_b and I_d are the beam and diffuse radiation components of the total radiation I_h such that

$$I_b + I_d = I_h \tag{2.23}$$

The radiative heat flux between the ground and the roof is given by

$$q_{gr} = \frac{1}{1/\varepsilon_g + 1/\varepsilon_r - 1} \sigma \left(T_g^4 - T_r^4 \right) \tag{2.24}$$

To facilitate the discretisation of equation (2.20), equation (2.24) can be written as

$$q_{gr} = h_{rgr}\left(T_g - T_r\right) \tag{2.25}$$

where the radiative heat transfer coefficient is given by

$$h_{rgr} = \frac{1}{1/\varepsilon_g + 1/\varepsilon_r - 1}\sigma\left(T_g^2 + T_r^2\right)\left(T_g + T_r\right) \tag{2.26}$$

Substituting equations (2.10), (2.22) and (2.25) into equation (2.20) we find a new expression for the surface boundary condition in the region of fully developed flow at z = 0, namely

$$k_g \frac{\partial T_g}{\partial z} = h_g\left(T_g - T\right) + h_{rgr}\left(T_g - T_r\right) - \left(\tau_b\alpha\right)_g I_b - \left(\tau_d\alpha\right)_g I_d \tag{2.27}$$

For the region of developing flow the boundary condition can be written as

$$k_g \frac{\partial T_g}{\partial z} = h_g\left(T_g - T_a\right) + h_{rgr}\left(T_g - T_r\right) - \left(\tau_b\alpha\right)_g I_b - \left(\tau_d\alpha\right)_g I_d \tag{2.28}$$

2.4. ENERGY EQUATION FOR ROOF

Consider an elementary control volume in the roof of the collector as shown in figure 2.3. In this control volume the axial heat fluxes are orders of magnitude higher than the radial conduction fluxes and so the terms for the latter are negligible. It can also be shown that in order to determine the surface fluxes, the mean temperature of the roof can be used as an approximation of the surface temperature and so only one control volume will be used in the axial direction in the roof. (For details about these approximations see Appendix 5.)

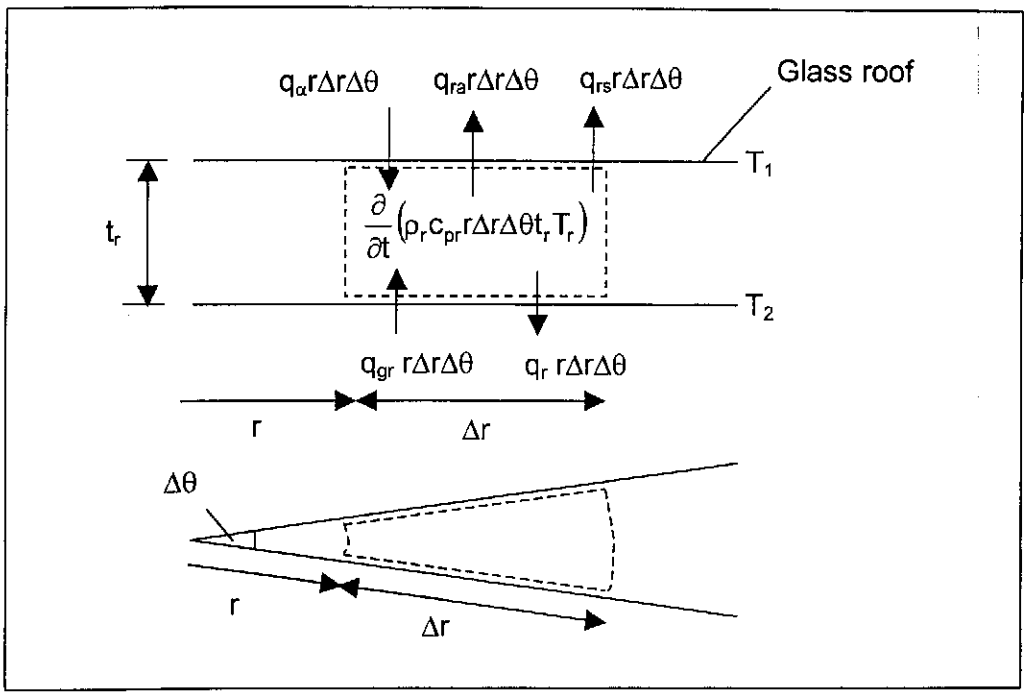

Figure 2.3: Energy equation applied to an elementary roof control volume.

The energy equation applicable to the roof control volume can thus be written as follows:

$$(q_\alpha + q_{gr} - q_r - q_{rs} - q_{ra}) r\Delta r\Delta\theta = \frac{\partial}{\partial t}(\rho_r c_{pr} t_r T_r r\Delta r\Delta\theta) \tag{2.29}$$

For constant ρ_r, and c_{pr} this can be written as

$$q_\alpha + q_{gr} - q_r - q_{rs} - q_{ra} = \rho_r c_{pr} t_r \frac{\partial T_r}{\partial t} \tag{2.30}$$

where q_α is the fraction of solar radiation that is absorbed by the roof and is given by

$$q_\alpha = (1-\rho_b)(1-\tau_{b\alpha}) I_b + (1-\rho_d)(1-\tau_{d\alpha}) I_d \tag{2.31}$$

The reflectances and transmittances are given in Appendix 6.

The convective heat flux between the roof and the ambient air is given by

$$q_{ra} = h_{ra}(T_r - T_a) \tag{2.32}$$

where h_{ra} is the convective heat transfer coefficient between the roof and the ambient air. This can be found using the relation suggested by Duffie and Beckman [74DU1] namely

$$h_{ra} = 5.7 + 3.8v_w \tag{2.33}$$

The radiative heat flux between the roof and the ambient air q_{rs} can be found using the equation

$$q_{rs} = \varepsilon_r \sigma \left(T_r^4 - T_{sky}^4 \right) \tag{2.34}$$

Once again to facilitate the discretisation of equation (2.30) this can be written as

$$q_{rs} = h_{rrs} \left(T_r - T_{sky} \right) \tag{2.35}$$

where h_{rrs} is the effective radiative heat transfer coefficient between the roof and the sky and is given by

$$h_{rrs} = \varepsilon_r \sigma \left(T_r^2 + T_{sky}^2 \right) \left(T_r + T_{sky} \right) \tag{2.36}$$

where T_{sky} is an approximation for the product of the apparent temperature of the sky and the emissivity thereof. The value of T_{sky} can be found using the relation suggested by Swinbank [63SW1]

$$T_{sky} = 0.0552 T_a^{1.5} \tag{2.37}$$

Substituting equations (2.6), (2.25), (2.31), (2.32) and (2.35) into equation (2.30) for the region of fully developed flow we find

$$\left(1-\rho_b\right)\left(1-\tau_{b\alpha}\right) I_b + \left(1-\rho_d\right)\left(1-\tau_{d\alpha}\right) I_d + h_{rgr}\left(T_g - T_r\right) - h_{rrs}\left(T_r - T_{sky}\right) - h_r\left(T_r - T\right) - h_{ra}\left(T_r - T_a\right) = \rho_r c_{pr} t_r \frac{\partial T_r}{\partial t} \tag{2.38}$$

Repeating this process for the region of developing flow we find

$$(1-\rho_b)(1-\tau_{b\alpha})I_b + (1-\rho_d)(1-\tau_{d\alpha})I_d + h_{rgr}(T_g - T_r) - h_{rrs}(T_r - T_{sky}) - h_r(T_r - T_a) - h_{ra}(T_r - T_a) = \rho_r c_{pr} t_r \frac{\partial T_r}{\partial t}$$

(2.39)

3.1. INTRODUCTION

The draught equation which is coupled to the energy equation applicable to the air is used to determine the pressure distribution through the solar chimney power plant and to determine the power available from the turbine. The derivation of the draught equation and of the equations for the various pressure changes will be discussed in this section.

3.2. SYSTEM PRESSURE CHANGES

3.2.1. Collector inlet pressure drop

The total pressure outside the collector far from the collector inlet is p_a. As the air is drawn towards the collector it undergoes a decrease in pressure due to its acceleration and a loss at the collector inlet. This collector inlet pressure drop is given by

$$\Delta p_i = \frac{1}{2}\rho_i v_i^2 K_i + \frac{1}{2}\rho_i v_i^2 \tag{3.1}$$

where the subscript i refers to the conditions in the collector inlet as shown in figure 1.1. For a well-rounded inlet the value of the loss coefficient is approximately zero while a value of unity is more appropriate for the case of the sharp edged inlet. Any possible error in this approximation will be negligible since the inlet pressure drop is orders of magnitude smaller than the total pressure drop in the system.

3.2.2. Collector drag pressure drop

The collector roof is supported above the surface of the ground by the collector supports. These are positioned on radii with a radial pitch P_r and spaced tangentially on these radii P_t apart as shown in figure 3.1.

To find the radial pressure gradient due to the drag effects of the collector supports on the air in the collector consider the force exerted by each support on the air given by

$$F_{sD} = C_{sD} d_s H \rho v^2 / 2 \tag{3.2}$$

where v is the local free stream velocity and is given by

$$v = m/(2\rho\pi r H) \tag{3.3}$$

where H is the height of the collector at radius r and m is the mass flow rate. Substitute equation (3.3) into equation (3.2) and find

$$F_{sD} = \frac{C_{sD}}{8\pi^2}\left(\frac{d_s}{H}\right)\frac{m^2}{\rho r^2} \tag{3.4}$$

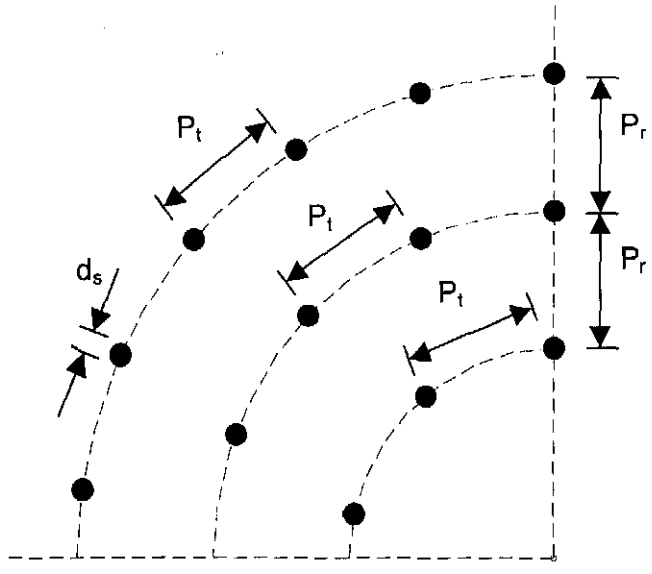

Figure 3.1: Schematic plan view of a portion of the collector showing the position of the collector supports.

With a tangential pitch P_t, the number of supports along the circumference at radius r is

$$n_{st} = (2\pi r)/P_t \tag{3.5}$$

The drag on all the supports at radius r is obtained by multiplying equation (3.4) by equation (3.5) thus

$$F_{srD} = F_{sD} n_{st} = C_{sD} m^2 d_s / (4\pi r P_t H \rho) \tag{3.6}$$

This is the force required by the air to move radially inwards through one row of supports. The resultant corresponding pressure difference required is thus given by

$$\Delta p_s = \frac{F_{srD}}{2\pi rH} = \frac{C_{sD} m^2 d_s}{8\pi^2 \rho P_t H^2 r^2} \tag{3.7}$$

Since H is given by

$$H = H_i (r_i / r)^b \tag{3.8}$$

equation (3.7) can be written as follows

$$\Delta p_s = \frac{C_{sD} m^2 d_s r^{2(b-1)}}{8\pi^2 \rho P_t H_i^2 r_i^{2b}} \tag{3.9}$$

3.2.3. Accelerational pressure drop

The radial pressure gradient due to the momentum changes in the collector (acceleration) can be found as discussed in the this section. Consider the control volume shown in figure 3.2. The force exerted on the control volume at a radius of r is given by

$$F_r = pHr\Delta\theta \tag{3.10}$$

Similarly the force at a radius of $r + \Delta r$ is

$$F_{r+\Delta r} = -pHr\Delta\theta - \frac{\partial}{\partial r}(pHr\Delta\theta)\Delta r \tag{3.11}$$

Applying the partial derivative operator on the right hand side yields

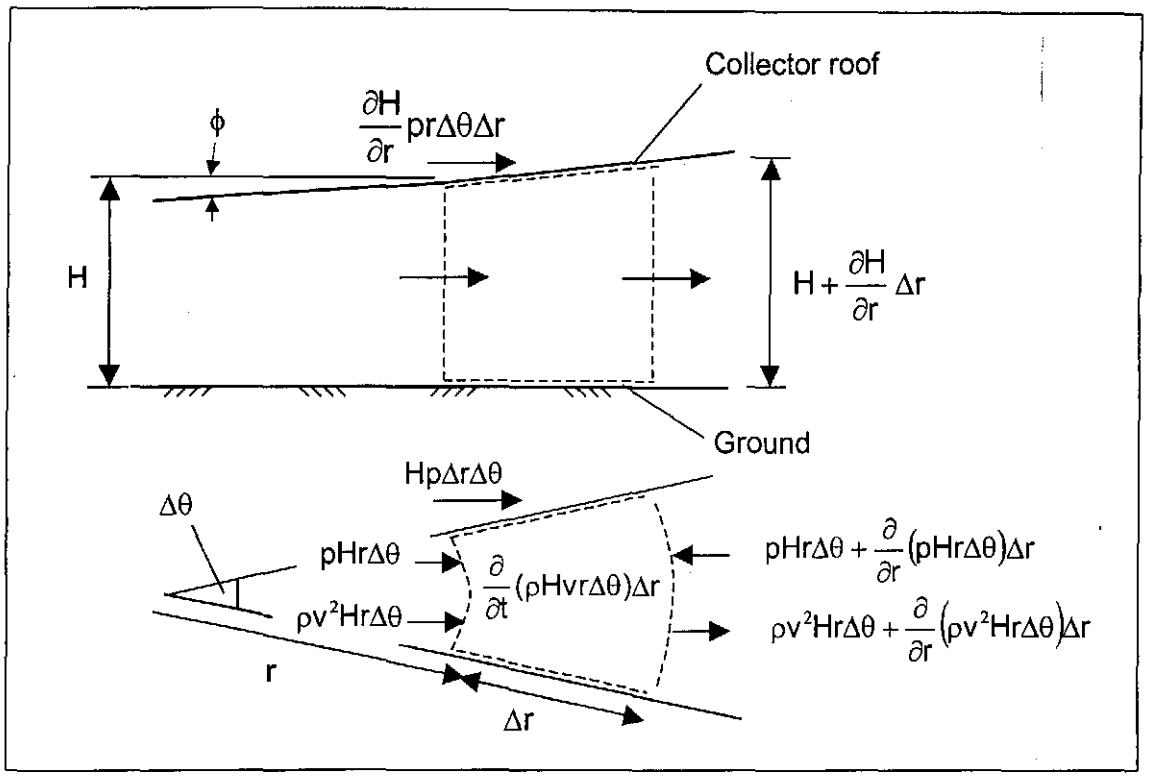

Figure 3.2: Conservation of momentum applied to an elementary contro volume of air.

$$F_{r+\Delta r} = -(pHr + pH\Delta r + \frac{\partial p}{\partial r} Hr\Delta r + \frac{\partial H}{\partial r} pr\Delta r)\Delta\theta \tag{3.12}$$

The forces on the sides of the control volumes are calculated using the average height and pressure along each side wall. Thus the height and pressure are given by the following relations respectively

$$H_{side} = 0.5(H + \frac{\partial H}{\partial r}\Delta r + H) \tag{3.13}$$

$$p_{side} = 0.5(p + \frac{\partial p}{\partial r}\Delta r + p) \tag{3.14}$$

The sum of the tangential forces acting on the sides is thus

$$F_{side,\,tan} = 0.5(H + \frac{\partial H}{\partial r}\Delta r + H)(p + \frac{\partial p}{\partial r}\Delta r + p)\Delta r \tag{3.15}$$

To find the radial component of the force exerted on the sides this can be multiplied by sin(θ/2). For small angles of θ this can be approximated by (θ/2) hence

$$\begin{aligned} F_{side} &= 0.5(H+\frac{\partial H}{\partial r}\Delta r+H)(p+\frac{\partial p}{\partial r}\Delta r+p)\Delta r\Delta\theta/2 \\ &= 0.25(4Hp\Delta r+2\frac{\partial p}{\partial r}H\Delta r^2+2\frac{\partial H}{\partial r}p\Delta r^2+\frac{\partial p}{\partial r}\frac{\partial H}{\partial r}\Delta r^3)\Delta\theta \end{aligned} \tag{3.16}$$

Once again neglecting the second and third order terms this can be simplified to

$$F_{side} = Hp\Delta r\Delta\theta \tag{3.17}$$

There also exists a force on the roof of the control volume that has a radial component.

$$F_{roof\ axial} = pr\Delta\theta\left(\left(\frac{\partial H}{\partial r}\Delta r\right)^2+\Delta r^2\right)^{0.5} = pr\Delta\theta\Delta r\left(\left(\frac{\partial H}{\partial r}\right)^2+1\right)^{0.5} \tag{3.18}$$

Since the height gradient is small, the square of the gradient is negligible when compared to unity. The relation for the roof force can thus be approximated as

$$F_{roof\ axial} = pr\Delta\theta\Delta r(1)^{0.5} = pr\Delta\theta\Delta r \tag{3.19}$$

Multiplying this by $\sin(\phi)\approx\frac{\partial H}{\partial r}$ the force in the radial direction is found to be

$$F_{roof} = \frac{\partial H}{\partial r}pr\Delta\theta\Delta r \tag{3.20}$$

Summing all the forces in the radial direction we find

$$\begin{aligned} \sum F &= prH\Delta\theta+Hp\Delta r\Delta\theta+\frac{\partial H}{\partial r}pr\Delta\theta\Delta r-(pHr+pH\Delta r+\frac{\partial p}{\partial r}Hr\Delta r+\frac{\partial H}{\partial r}pr\Delta r)\Delta\theta \\ &= -\frac{\partial p}{\partial r}Hr\Delta\theta\Delta r \end{aligned} \tag{3.21}$$

The momentum change across the control volume is given by

$$\Delta M = \left(\rho v^2 Hr\Delta\theta + \frac{\partial}{\partial r}(\rho v^2 Hr\Delta\theta)\Delta r\right) + \frac{\partial}{\partial t}(\rho Hvr\Delta\theta)\Delta r - \rho v^2 Hr\Delta\theta \qquad (3.22)$$

The transient term in equation (3.22) is negligible as is shown in Appendix 5. Equating equations (3.21) and (3.22) and using the relation $m_{\Delta\theta} = \rho vHr\Delta\theta$ we find

$$\frac{\partial p}{\partial r} Hr\Delta\theta\Delta r = -\frac{\partial}{\partial r}(\rho v^2 Hr\Delta\theta)\Delta r \qquad (3.23)$$

or

$$\frac{\partial p}{\partial r} = -\frac{m_{\Delta\theta}}{Hr\Delta\theta}\frac{\partial v}{\partial r} \qquad (3.24)$$

Since $v = m_{\Delta\theta}/\rho Hr\Delta\theta$ and $\rho = p/RT$ equation (3.24) can be written as

$$\frac{\partial p}{\partial r} = -\frac{m_{\Delta\theta}}{Hr\Delta\theta}\frac{\partial}{\partial r}\left(\frac{m_{\Delta\theta}RT}{pHr\Delta\theta}\right) \qquad (3.25)$$

Since R is constant and p and $m_{\Delta\theta}$ remain essentially constant with varying r, this can be simplified to

$$\frac{\partial p}{\partial r} = -\frac{Rm_{\Delta\theta}^{\ 2}}{pHr\Delta\theta^2}\frac{\partial}{\partial r}\left(\frac{T}{Hr}\right) \qquad (3.26)$$

Substituting equation (3.8) into equation (3.26) we find

$$\frac{\partial p}{\partial r} = -\frac{Rm_{\Delta\theta}^{\ 2} r^{b-1}}{pH_i r_i^b \Delta\theta^2}\frac{\partial}{\partial r}\left(\frac{Tr^{b-1}}{H_i r_i^b}\right) \qquad (3.27)$$

Simplify equation (3.27) to read

$$\frac{\partial p}{\partial r} = -\frac{Rm_{\Delta\theta}^{\ 2} r^{b-1}}{pH_i^2 r_i^{2b}\Delta\theta^2}\left(\frac{\partial T}{\partial r}r^{b-1} + (b-1)r^{b-2}T\right) \qquad (3.28)$$

Equation (3.28) can be written in terms of the total mass flow using the relation

$$m_{\Delta\theta} = \frac{\Delta\theta}{2\pi} m \tag{3.29}$$

then

$$\frac{\partial p}{\partial r} = -\frac{Rm^2 r^{b-1}}{pH_i^2 r_i^{2b} 4\pi^2}\left(\frac{\partial T}{\partial r} r^{b-1} + (b-1) r^{b-2} T\right) \tag{3.30}$$

where m is negative in the solar chimney power plant. Equation (3.30) can be used to approximate the pressure differential over one control volume hence

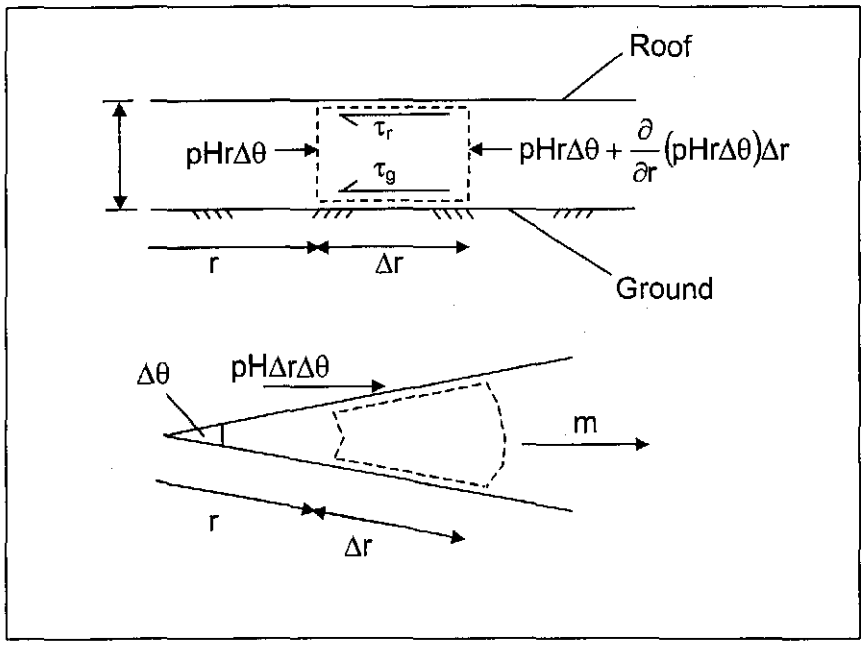

Figure 3.3: Momentum equation applied to the air, taking only the frictional pressure drop into account.

$$\Delta p_{acc} = -\frac{Rm^2 r^{b-1}}{pH_i^2 r_i^{2b} 4\pi^2}\left(\frac{\partial T}{\partial r} r^{b-1} + (b-1) r^{b-2} T\right)\Delta r \tag{3.31}$$

3.2.4. Collector frictional pressure drop

The radial pressure gradient due to the frictional drag on the ground and the under side of the roof can be found as follows [99KR1]:

Applying the conservation of momentum to the control volume as shown in figure 3.3 considering only the pressure drop due to the shear stresses on the ground and roof and ignoring the change in collector height yields

$$pHr\Delta\theta - pHr\Delta\theta - \frac{\partial}{\partial r}(pHr\Delta\theta)\Delta r + pH\Delta r\Delta\theta = r\Delta r\Delta\theta(\tau_g + \tau_r) \tag{3.32}$$

Dividing throughout by $\Delta\theta$ and neglecting the higher order terms since they are orders of magnitude smaller than the others we find

$$\frac{\partial p}{\partial r} = -\frac{(\tau_g + \tau_r)}{H} \tag{3.33}$$

Substitute the height as given by equation (3.8) into equation (3.33) to give

$$\frac{\partial p}{\partial r} = -\frac{1}{H_i}\left(\frac{r}{r_i}\right)^b(\tau_g + \tau_r) \tag{3.34}$$

According to Kröger and Buys [99KR1], the shear stress exerted by the roof (assuming that it is smooth) on the air in the region of developing flow can be given approximately by

$$\tau_r = -0.01392\rho v^{1.8}\left(\frac{\upsilon}{\delta}\right)^{0.2} \tag{3.35}$$

where the core velocity is given approximately by

$$v = \frac{m}{2\pi r\rho H} \tag{3.36}$$

and the boundary layer thickness for flow moving radially inwards across a smooth plate is given by

$$\delta(r) = H_i\left\{\frac{1}{6.218 - 15.08b}\left(\frac{r_i}{H_i}\right)\left(\frac{\mu r_i}{m}\right)^{0.2}\left[\left(\frac{r}{r_i}\right)^{1.2-.02b} - \left(\frac{r}{r_i}\right)^{2.743-3.943b}\right]\right\}^{5/6} \tag{3.37}$$

Similarly the following relation may be used to find the shear stress for developing radial flow over a rough disc

$$\tau_g = -0.008326\rho v^2 \left(\frac{\varepsilon}{\delta}\right)^{0.254} \left[1.94\left(\frac{\mu}{\rho v \varepsilon}\right)^{0.51} + 1\right] \tag{3.38}$$

with the boundary layer thickness being given by

$$\delta(r) = H_i \left(\frac{\varepsilon_g}{H_i}\right)^{0.2026} \left(\frac{r_i}{H_i}\right)^{0.7974} \left\{ q \frac{\left(\frac{r}{r_i}\right)^{1.51-0.51b} - \left(\frac{r}{r_i}\right)^{2.866-4.120b}}{2.550 - 6.787b} + \frac{\left(\frac{r}{r_i}\right) - \left(\frac{r}{r_i}\right)^{2.866-4.120b}}{17.38 - 38.37b} \right\}^{0.7974} \tag{3.39}$$

with $b \neq 0.3757$, $b \neq 0.453$ and

$$q = \left(\frac{\mu H_i r_i}{\varepsilon_g m}\right)^{0.51} \tag{3.40}$$

Substituting equations (3.35) and (3.38) into equation (3.34) we find the pressure gradient due only to the frictional forces on the roof and the ground for the region of developing flow

$$\Delta p_f = \frac{1}{H_i}\left(\frac{r}{r_i}\right)^b \left[0.01392 \frac{\rho v^{1.8} \upsilon^{0.2}}{H_i^{0.2}} \left(\frac{H_i}{r_i}\right)^{1/6} \left(\frac{m}{\mu r_i}\right)^{1/30} \left\{ \frac{6.218 - 15.08b}{\left(\frac{r}{r_i}\right)^{1.2-0.2b} - \left(\frac{r}{r_i}\right)^{2.743-3.943b}} \right\}^{1/6} \right.$$

$$+ 0.008326 \rho v^2 \varepsilon_g^{0.254} \left\{ 1.94 \left(\frac{\mu}{\rho v \varepsilon_g}\right)^{0.51} + 1 \right\} \frac{1}{H_i^{0.254}} \left(\frac{H_i}{\varepsilon_g}\right)^{0.0515} \left(\frac{H_i}{r_i}\right)^{0.2025} \qquad (3.41)$$

$$\left. \times \left\{ q \frac{\left(\frac{r}{r_i}\right)^{1.51-0.51b} - \left(\frac{r}{r_i}\right)^{2.866-4.120b}}{2.550 - 6.787b} + \frac{\left(\frac{r}{r_i}\right) - \left(\frac{r}{r_i}\right)^{2.866-4.120b}}{17.38 - 38.37b} \right\}^{-0.2025} \right] \Delta r$$

Kröger and Buys [99KR1] suggest that for the region of fully developed flow the shear stress on the roof and ground are given by

$$\tau_r = -\frac{0.02 \rho^{0.8} v^{1.8} \mu^{0.2}}{H^{0.2}} \qquad (3.42)$$

and

$$\tau_g = -0.02975 \left(\frac{\varepsilon_g}{2H}\right)^{0.254} \left[1.75 \left(\frac{\mu}{\rho v \varepsilon}\right)^{0.51} + 1 \right] \frac{\rho v^2}{2} \qquad (3.43)$$

respectively. Substituting equations (3.42) and (3.43) into equation (3.34) we find for the region of fully developed flow

$$\Delta p_f = \frac{1}{H_i}\left(\frac{r}{r_i}\right)^b \left\{ 0.02975 \left(\frac{\varepsilon_g r^b}{2 H_i r_i^b}\right)^{0.254} \left[1.75 \left(\frac{\mu}{\rho v \varepsilon_g}\right)^{0.51} + 1 \right] \frac{\rho v^2}{2} + \frac{0.02 \rho^{0.8} v^{1.8} \mu^{0.2} r^{0.2b}}{H_i^{0.2} r_i^{0.2b}} \right\} \Delta r \qquad (3.44)$$

3.2.5. Chimney inlet pressure drop

The pressure drop caused by friction and momentum changes between the collector outlet and the turbine inlet is given by

$$\Delta p_{ti} = \frac{1}{2}\rho_{ti} v_{ti}^{2} K_{ti} \tag{3.45}$$

where K_{ti} is the turbine inlet loss coefficient. The loss coefficient is dependant on the geometry of the region of the plant at the inlet to the turbine and is thus specified in the reference plant specifications.

3.2.6. Turbine pressure drop

The pressure drop over the turbine can be found using the relation $P = V\Delta p_t$ where P and V are the turbine power and the volume flow rate respectively. Thus the turbine pressure drop is given by

$$\Delta p_t = P / V \tag{3.46}$$

3.2.7. Chimney appurtenances drag pressure drop

The approximate pressure drop caused by the appurtenances in the chimney is given by

$$\Delta p_{cs} = \frac{1}{2}\rho_{ti} v_{ti}^{2} K_{cs} \tag{3.47}$$

where K_{cs} is defined relative to the conditions at the turbine inlet. This coefficient is also dependant on the geometry of the system and is specified in the reference plant specifications.

3.2.8. Chimney frictional pressure drop

The approximate pressure drop caused by the frictional drag in the chimney is given by

$$\Delta p_{cf} = f_D\left(H_c / d_c\right)\left(\rho_c v_c^{2} / 2\right) \tag{3.48}$$

Haaland's [83HA1] equation for the Darcy friction factor is best suited to the fully developed turbulent flow with ε/d_c small i.e.

$$f_D = 2.7778\left[\log_{10}\left\{\left(\frac{7.7}{Re_{dc}}\right)^3 + \left(\frac{\varepsilon_g/d_c}{3.75}\right)^{3.33}\right\}\right]^{-2} \tag{3.49}$$

3.2.9. Chimney accelerational pressure drop

The approximate pressure differential due to the momentum changes in the chimney is given by

$$\Delta p_{cacc} = \frac{1}{A_c}\left[m(v_{co} - v_{ci}) + \frac{\partial}{\partial t}(\rho_c A_c H_c v_c)\right] \approx \left(\frac{4m}{\pi d_c^{\,2}}\right)^2\left(\frac{1}{\rho_{co}} - \frac{1}{\rho_{ci}}\right) \tag{3.50}$$

where the transient term is shown in Appendix 5 to be negligible.

3.2.10. Chimney exit pressure change (recovery)

The pressure of the air leaving the chimney differs from the ambient pressure at the chimney exit height by

$$\Delta p_{co} = \frac{1}{2}\rho_{co} v_{co}^{\,2} K_{co} \tag{3.51}$$

where the chimney outlet pressure loss coefficient is given by

$$K_{co} = -0.28 Fr_D^{\,-1} + 0.04 Fr_D^{\,-1.5} \tag{3.52}$$

with the densimetric Froude number being given by

$$Fr_D = \left(\frac{m_{co}}{A_c}\right)^2 \Big/ \left[\rho_{co}(\rho_{aHco} - \rho_{co}) g d_{co}\right] \tag{3.53}$$

where the subscript aHco refers to ambient conditions at the elevation of the chimney outlet. The densities at this elevation outside and inside respectively of the chimney are found using the relations

$$\rho_{aHco} = \frac{p_a T_a}{R}\left(1 - 0.00975 H_c / T_a\right)^{2.5} \tag{3.54}$$

$$\rho_{co} = \frac{p_o T_o}{R}\left(1 - 0.00975 H_c / T_o\right)^{2.5} \tag{3.55}$$

The kinetic energy lost at the exit of the chimney is expressed as

$$\text{Dynamic loss} = 0.5\alpha_e \rho_{co} v_{co}^{\ 2} \tag{3.56}$$

where α_e is the kinetic energy correction factor. Du Preez and Kröger [94DU1] find that for $1/Fr_D \leq 3$ at the exits of dry cooling towers α_e is equal to unity. Since the exit of the chimney may be approximated as dry cooling tower exit and Fr_D is approximately two, the kinetic energy correction factor is taken as unity.

3.3. PRESSURE DRIVING POTENTIAL

Having discussed the system losses it is now appropriate to discuss the driving potential of the solar chimney. The driving potential is essentially the difference between pressure potentials caused by the column of cold (ambient) air outside the chimney and the equivalent column of warm air inside the chimney. This can be written as

$$\left(p_a - p_{aHco}\right) - \left(p_o - p_{co}\right) \tag{3.57}$$

Since the pressure at the exit plane of the chimney (p_{co}) and the pressure outside the chimney but at the same elevation as the chimney exit (p_{aHco}) are approximately equal, the driving potential given in expression (3.55) can be reduced to

$$\left(p_a - p_{aHco}\right) - \left(p_o - p_{co}\right) \approx p_a - p_o \tag{3.58}$$

The values for p_{co} and p_{aHco} are given by the following equations respectively (if it is assumed that an adiabatic lapse rate and isentropic expansion are applicable and if the air is assumed dry).

$$p_{co} = p_o\left(1 - 0.00975 H_c / T_o\right)^{3.5} \tag{3.59}$$

$$p_{aHco} = p_a\left(1 - 0.00975 H_c / T_a\right)^{3.5} \tag{3.60}$$

Once again making use of the fact that the exit pressure of the chimney is very close to the ambient pressure at the same height the following is applicable.

$$p_o(1-0.00975H_c/T_o)^{3.5} = p_a(1-0.00975H_c/T_a)^{3.5} \quad (3.61)$$

or

$$p_o = p_a\{(1-0.00975H_c/T_a)/(1-0.00975H_c/T_o)\}^{3.5} \quad (3.62)$$

This can be rewritten to give an expression for the driving potential as follows,

$$p_a - p_o = p_a\left[1-\{(1-0.00975H_c/T_a)/(1-0.00975H_c/T_o)\}^{3.5}\right] \quad (3.63)$$

This is the net driving potential in the solar chimney power plant.

The draught available to the turbine is thus the driving potential less the sum of the pressure drops throughout the system and is given by the draught equation namely

$$\Delta p_t = p_a - p_o - \Delta p_i - \Delta p_s - \Delta p_{acc} - \Delta p_f - \Delta p_{ti} - \Delta p_{cs} - \Delta p_{cacc} - \Delta p_{cf} - \Delta p_{co} - 0.5\rho_{co}v_{co}^2$$

4.1. INTRODUCTION

The energy equations derived in Chapter 2 will be solved throughout the collector. Because of the nature of the equations a numerical solution will be required. For this reason each one of the energy equations will be discretised to be transformed from differential equations to explicit algebraic equations. This process is discussed in this section.

4.2. CONTROL VOLUME CONVENTION

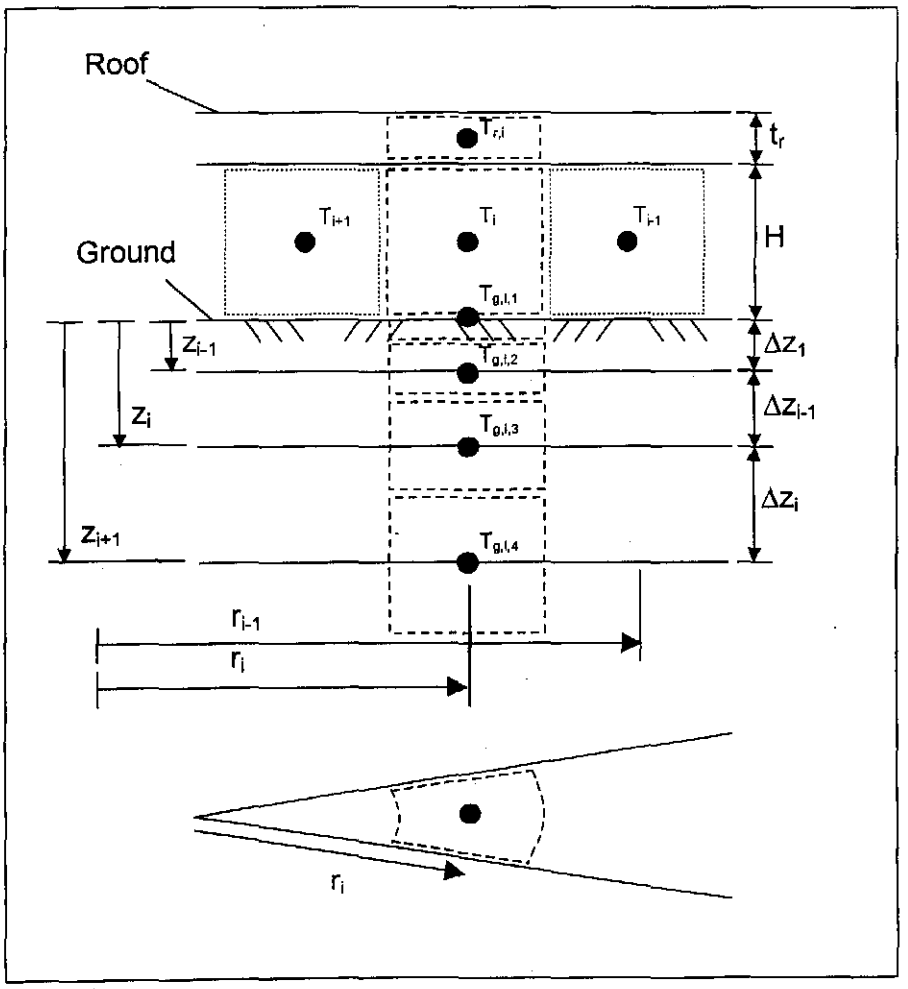

Figure 4.1: A set of control volumes and two neighbouring air control volumes.

A set of control volumes (hereafter a *control volume set* will refer to the roof, air and ground control volumes whose nodes occur on a particular radius) is shown in figure

4.1 (two neighbouring air control volumes are shown in dotted lines as well because they are used in the air calculations). These control volumes are annular in shape and are arranged in horizontal layers. Each control volume is represented by a node occurring on a circular line at the average radius of the control volume. The nodes in the roof and air control volumes are also situated at the average height of the control volumes while the ground control volumes are divided by planes midway between the nodes.

4.3. THE DISCRETISATION SCHEMES

A finite difference scheme is employed to discretise the energy equations Although a central difference scheme is more accurate than an upwind finite difference scheme the latter is more suitable for the radial temperature gradients in the collector air because it does not cause decoupling. (The difference between the two approximations is discussed in Appendix 4.1.) It approximates the gradient at a node with the finite difference between a control volume and its upwind neighbour. The time gradients will be modelled with the finite difference between the present and past property value. Thus the well known scheme namely the backward time – backward space scheme (or BTBS) is employed.

The heat transfer in the ground is of such a nature that a simple backward time – central space (BTCS) scheme can be used. This models the temperature gradients with the average difference between the two neighbouring control volumes and the one in question.

4.4. THE DISCRETISED AIR EQUATION

The energy equation applicable to the air is according to equation (2.13) for the region of fully developed flow given by

$$\frac{mc_p}{2\pi r}\frac{\partial T}{\partial r} + c_p \rho H \frac{\partial T}{\partial t} = h_g\left(T_g - T\right) + h_r\left(T_r - T\right) \tag{4.1}$$

or applying the BTBS scheme

$$\left(\frac{mc_{p,i}}{2\pi r_i}\right)\left(\frac{T_i - T_{i-1}}{r_i - r_{i-1}}\right) + \rho_i c_{p,i} H_i \frac{T_i - T_{old,i}}{dt} = h_{g,i}\left(T_{g,i} - T_i\right) + h_{r,i}\left(T_{r,i} - T_i\right) \tag{4.2}$$

where the subscripted index refers to the radial position of the point at which the value is taken. (See figure 4.1) Manipulating this equation yields

$$T_i = \frac{\frac{mc_{p,i}}{2\pi r_i(r_i - r_{i-1})}T_{i-1} + \frac{\rho_i c_{p,i} H_i}{dt}T_{old,i} + h_{r,i}T_{r,i} + h_{g,i}T_{g,i}}{\frac{mc_{p,i}}{2\pi r_i(r_i - r_{i-1})} + \frac{\rho_i c_{p,i} H_i}{dt} + h_{r,i} + h_{g,i}} \tag{4.3}$$

Applying these steps to the region of developing flow results in a similar equation namely

$$T_i = \frac{\frac{mc_{p,i}}{2\pi r_i(r_i - r_{i-1})}T_{i-1} + \frac{\rho_i c_{p,i} H_i}{dt}T_{old,i} + h_{r,i}(T_{r,i} - T_a) + h_{g,i}(T_{g,i} - T_a)}{\frac{mc_{p,i}}{2\pi r_i(r_i - r_{i-1})} + \frac{\rho_i c_{p,i} H_i}{dt}} \tag{4.4}$$

The inlet boundary condition can be implemented by replacing T_{i-1} in equation (4.4) with the collector inlet temperature T_a.

4.5. THE DISCRETISED GROUND EQUATION

The energy equation applicable to the ground is a simple time-dependant one-dimensional conduction equation and is according to equation (2.19)

$$\rho_g c_{pg} \frac{\partial T_g}{\partial t} = k_g \frac{\partial^2 T_g}{\partial z^2} \tag{4.5}$$

The time derivative can be approximated using a backward difference hence

$$\frac{\partial T_{g,j}}{\partial t} \approx \frac{T_{g,j} - T_{g,old,j}}{dt} \tag{4.6}$$

where the subscripted indexes once again refer to the position (depth) at which the temperature is taken. (See figure 4.1)

The second derivative applied to the ground temperature with respect to depth (z) is approximated with the central difference scheme. This is done while making provision for the variation of consecutive control volume thicknesses as follows (with the distance Δz_j being the distance between the node at z_j and the node below it z_{j+1}).

$$\frac{\partial^2 T_{g,j}}{\partial z^2} \approx \frac{\frac{\partial T_{g,j+1/2}}{\partial z} - \frac{\partial T_{g,j-1/2}}{\partial z}}{\frac{1}{2}\left(\Delta z_j + \Delta z_{j-1}\right)} \tag{4.7}$$

Applying the second derivatives we find

$$\frac{\partial^2 T_{g,j}}{\partial z^2} \approx \frac{T_{gi+j} - T_{g,j}}{\frac{1}{2}\left(\Delta z_j + \Delta z_{j-1}\right)\cdot \Delta z_j} - \frac{T_{g,j} - T_{g,j-1}}{\frac{1}{2}\left(\Delta z_j + \Delta z_{j-1}\right)\cdot \Delta z j_{j-1}} \tag{4.8}$$

Substituting equations (4.6) and (4.8) into equation (4.5) yields

$$\rho_g c_{pg} \frac{T_{g,j} - T_{g,old,j}}{dt} = k_g \left[\frac{T_{g,j+1} - T_{g,j}}{\frac{1}{2}\left(\Delta z_j + \Delta z_{j-1}\right)\cdot \Delta z_j} - \frac{T_{g,j} - T_{g,j-1}}{\frac{1}{2}\left(\Delta z_j + \Delta z_{j-1}\right)\cdot \Delta z_{j-1}} \right] \tag{4.9}$$

Solving this equation for $T_{g,i}$ yields

$$T_{g,j} = \left[\frac{T_{g,j+1}}{\frac{1}{2}\left(\Delta z_j + \Delta z_{j-1}\right)\cdot \Delta z_j} + \frac{T_{g,j-1}}{\frac{1}{2}\left(\Delta z_j + \Delta z_{j-1}\right)\cdot \Delta z_{j-1}} + \frac{T_{g,old,j}}{dt}\frac{\rho_g c_{pg}}{k_g} \right] / \left[\frac{\rho_g c_{pg}}{k_g}\frac{1}{dt} + \frac{1}{\frac{1}{2}\left(\Delta z_j + \Delta z_{j-1}\right)\cdot \Delta z_j} + \frac{1}{\frac{1}{2}\left(\Delta z_j + \Delta z_{j-1}\right)\cdot \Delta z_{j-1}} \right] \tag{4.10}$$

This equation can be applied to the control volumes in the ground from the second one to the penultimate one. For the first control volume (the one just below the surface) the following analysis is applicable. Applying an energy balance over the control volume as shown in figure 4.2 yields for the region of fully developed flow

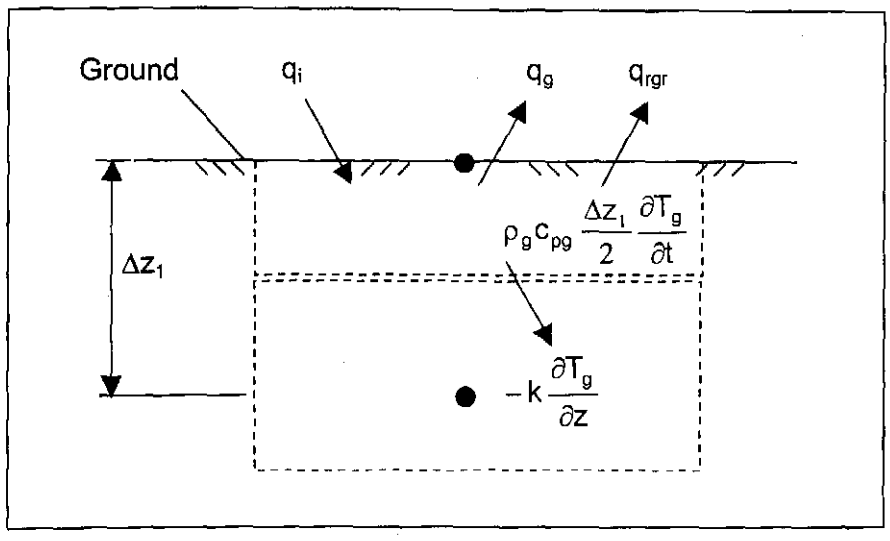

Figure 4.2: An energy balance applied to the ground control volume just below the surface.

$$q_i = q_g + q_{gr} - k_g \frac{\partial T_{g,1}}{\partial z} + \frac{1}{2} \rho_g c_{pg} \frac{\Delta z_1}{2} \frac{\partial T_{g,1}}{\partial t} \tag{4.11}$$

This can be approximated using the BTBS scheme as

$$q_i = h_g \left(T_{g,1} - T\right) + h_{rgr} \left(T_{g,1} - T_r\right) + k_g \frac{T_{g,1} - T_{g,2}}{\Delta z_1} + \rho_g c_{pg} \frac{\Delta z_1}{2} \frac{\left(T_{g,1} - T_{g,old,1}\right)}{\partial t} \tag{4.12}$$

Manipulating this gives

$$T_{g,1} = \frac{q_i + h_g T + h_{rgr} T_r + k_g T_{g,2} / \Delta z_1 + \rho_g c_{pg} \frac{\Delta z_1}{2} T_{g,old,1} / \partial t}{h_g + h_{rgr} + k_g / \Delta z_1 + \rho_g c_{pg} \frac{\Delta z_1}{2} / \partial t} \tag{4.13}$$

The derivation of an equation for $T_{g,i}$ for the region of developing flow is done in a similar manner to that used to find equation (4.13). The resulting equation follows

$$T_{g,i} = \frac{q_i + h_g T_a + h_{rgr} T_r + k_g T_{g,2} / \Delta z_1 + \rho_g c_{pg} \frac{\Delta z_1}{2} T_{g,old,1} / \partial t}{h_g + h_{rgr} + k_g / \Delta z_1 + \rho_g c_{pg} \frac{\Delta z_1}{2} / \partial t} \tag{4.14}$$

The temperature at the last node $T_{g,nlayg}$ (where nlayg is the number of layers used to model the ground) can be found by using the boundary condition given by equation (2.21) namely at $z = \infty$

$$\frac{\partial T_g}{\partial z} = 0 \tag{4.15}$$

This can be approximated as follows

$$\frac{T_{nlayg-1} - T_{nlayg}}{z_{nlayg-1} - z_{nlayg}} = 0 \tag{4.16}$$

or

$$T_{nlayg} = T_{nlayg-1} \tag{4.17}$$

This boundary condition is given more attention in Appendix 5.1.

4.6. THE DISCRETISED ROOF EQUATION

The equation describing the heat transfer in the roof in the region of fully developed flow is given by equation (2.38) as

$$(1-\rho_b)(1-\tau_{b\alpha})I_b + (1-\rho_d)(1-\tau_{d\alpha})I_d + h_{rgr}(T_g - T_r) - h_{rrs}(T_r - T_{sky}) - h_r(T_r - T) - h_{ra}(T_r - T_a) = \rho_r c_{pr} t_r \frac{\partial T_r}{\partial t} \tag{4.18}$$

Approximating the time gradient with a backward difference, equation (4.18) can be written as

$$(1-\rho_b)(1-\tau_{b\alpha})I_b + (1-\rho_d)(1-\tau_{d\alpha})I_d - h_{rgr}(T_r - T_g) - h_{rrs}(T_r - T_{sky}) - h_r(T_r - T) - h_{ra}(T_r - T_a) = \rho_r c_{pr} t_r (T_r - T_{r,old})/dt \tag{4.19}$$

This can be solved for T_r to yield the following

$$T_r = \frac{(1-\rho_b)(1-\tau_{b\alpha})I_b + (1-\rho_d)(1-\tau_{d\alpha})I_d + h_{rgr}T_g + h_r T + h_{rrs}T_{sky} + h_{ra}T_a + \rho_r c_{pr} t_r T_{r,old}/dt}{h_{rgr} + h_r + h_{rrs} + h_{ra} + \rho_r c_{pr} t_r/dt} \quad (4.20)$$

The equivalent equation for the region of developing flow is written as follows

$$T_r = \frac{(1-\rho_b)(1-\tau_{b\alpha})I_b + (1-\rho_d)(1-\tau_{d\alpha})I_d + h_{rgr}T_g + h_r T_a + h_{rrs}T_{sky} + h_{ra}T_a + \rho_r c_{pr} t_r T_{r,old}/dt}{h_{rgr} + h_r + h_{rrs} + h_{ra} + \rho_r c_{pr} t_r/dt} \quad (4.21)$$

5. SOLUTION OF ENERGY AND DRAUGHT EQUATIONS FOR REFERENCE PLANT (SPECIFIED IN APPENDIX 1)

5.1. INTRODUCTION

In order to model the solar chimney power plant (in this case the reference solar chimney power plant with dimensions specified in Appendix 1 and meteorological conditions specified in Appendix 2) the energy and draught equations will be solved within the time varying environment as would be present at the proposed plant location. This solution would be focused on determining the time-varying power generated by the solar chimney power plant. This section describes the solution method used. First an overview is presented to introduce the main features of the solution code and then a more detailed description is provided. The latter will be presented in a step-by-step format following the course taken by the code.

5.2. OVERVIEW OF SOLUTION PROCEDURE

The draught and energy equations are solved subject to boundary conditions as modelled using the radiation data and ambient temperature present at the proposed location of the plant. In this way the daily and yearly variations are introduced into the solution.

The solution of the energy equations is achieved using a simple upwind time marching scheme. Thus the roof, air and ground energy equations are solved at the collector inlet radius first and then at each smaller radius until the collector outlet is reached. This solution at each radius is done using the well known Gauss-Seidel method. When the energy equations are solved, the draught equation is used to determine the pressure throughout the plant and the instantaneous power output delivered by the plant. These temperatures, pressures, and instantaneous power output values are recorded with other information in output files.

This code not only solves the equations but also optimises the plant performance by determining the turbine pressure drop which yields the highest instantaneous power output, and using this pressure drop at each time step.

5.3. THE ALGORITHM

This section describes in detail the operation of the 'solchim' code. Each subroutine is described in the order in which it is accessed in the code. The code may be divided into three phases namely the initiation phase, solution phase and conclusion phase. The following discussion is presented in similar divisions.

A flow chart showing the main algorithm is shown in figure 5.1. It shows how the various time loops are nested and how the time marching is controlled. Also evident are the levels in which each property is updated. It is clear that all the properties that change continuously with time are only recalculated every minute. The changes are so small that it not necessary to update these values at every time step.

5.3.1. Initiation Phase

This procedure is performed once at the beginning of the solution process.

The reference to the 'var&aray.inc' file at the start of the main program and each subroutine contains the 'dimension' and 'common' commands for all the variables that are used in the code. This ensures that all variables are global (available to all routines). This simplifies the programming process and facilitates a shorter, more readable code.

All variables are defined as double precision numbers and are thus precise up to 16 digits. This is necessary to capture the values of very small differences between certain terms in the energy and draught equations.

5.3.1.1 Subroutine ***constants*** defines the following constants as shown in table 5.1.

Table 5.1: Constants as defined in subroutine *constants*.

Constant name	**Value**
Stefan-Boltzmann's constant, σ	5.6710e-8 W/m^2K^4
Gravitational acceleration, g	9.81 m/s^2
Pi, π	3.1415926536
Gas constant, R	287.08 Nm/kgK

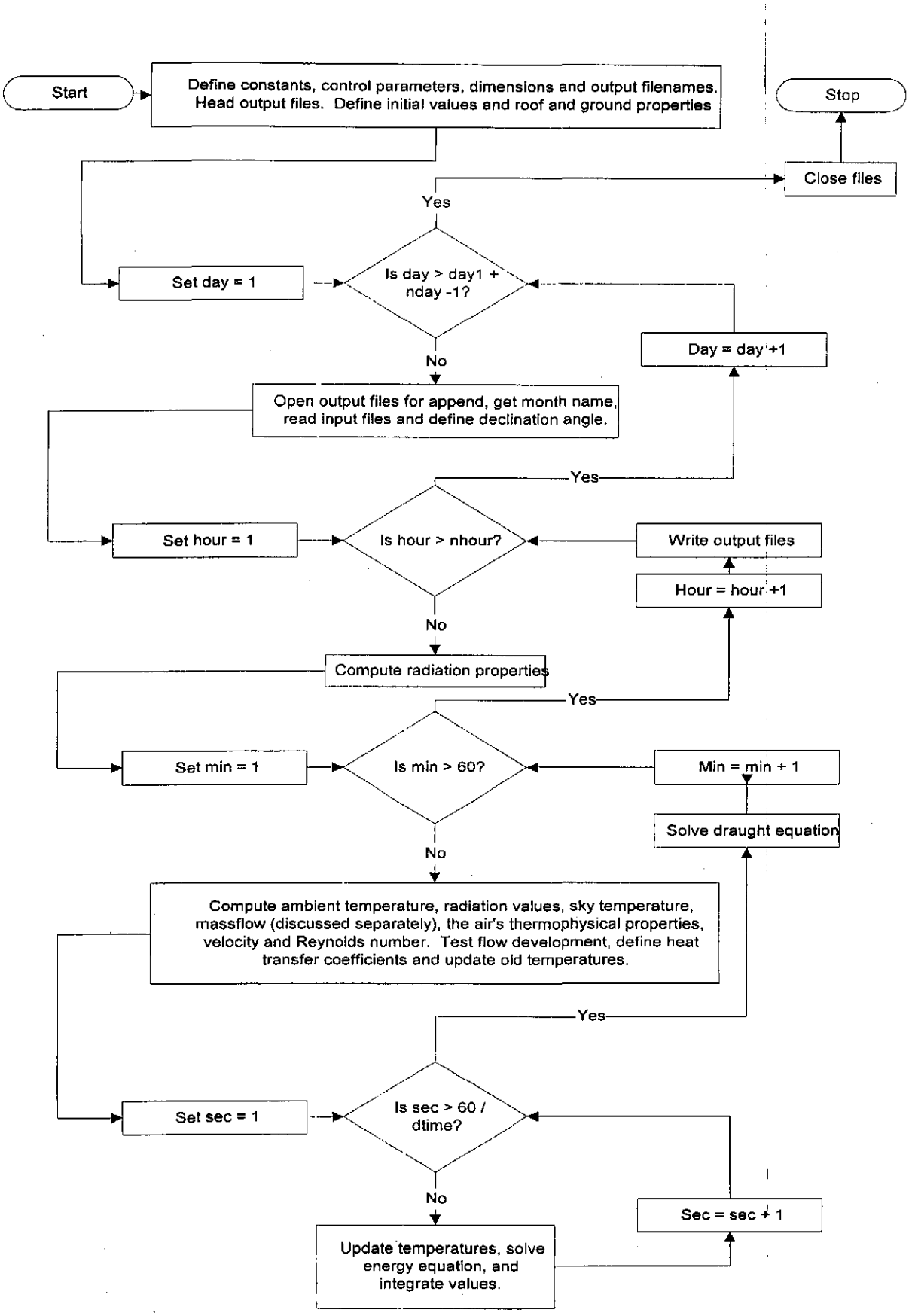

Figure 5.1: A flow chart showing the algorithm used by the 'solchim' code.

5.3.1.2. Subroutine ***runcontrol*** reads the control parameters listed in table 5.2 from a list of values stored in the input file 'runcon.inp'. These values have been set according to the conditions stated below.

The number of control volumes (ncv) is the number of control volume sets on a radian of the collector. It can be set to any integer greater than two, but to ensure accurate results a larger value should be used. Since there is no generally valid method of determining the smallest number of control volumes (maximum control length size) for the upwinding scheme, Bejan [84BE1] suggests that successively smaller grid spacing be used until change in grid size has no marked effect on the results. A value of 100 was used in the calculations, since the use of a larger number had an insignificant effect on the results.

The time step (dtime) determines the step in time from one calculation to the next during the time marching. Since the energy equations for the ground were discretised using an implicit scheme the time step is not limited by stability considerations there. The upwinding scheme used in the discretisation of the energy equation for the air does however present limits.

Table 5.2: Parameters defined in subroutine *runcon.*

Parameter symbol	**Explanation**
Ncv	Number of control volumes in radial direction
Dtime	Time step used in transient terms
Nday	Number of days to model
Day1	Day to start modelling (1-365)
Hour_sam	Hour to record radial distribution
cv_sam	Control volume to use for time distribution
mtest	Period used to test different mass flow rates
mhold	Period over which present mass flow rate is used
EBaccuracy	Maximum tolerable error made in solving energy equations
iniupd	1 = update initial.inp file, 0 = leave initial.inp values

When finite differencing is used in situations involving fluid flow, the time step must be smaller than the shortest time taken for the fluid to pass through a control volume [99HA1].

The number of layers in the ground (nlayg) that are used in each control volume set is defined in this routine. This was set equal to 14 (although somewhat arbitrary) since this yielded a fine enough grid in the modelled region near the ground surface to capture the gradients there, while not causing redundant calculation of the ground temperatures.

5.3.1.3. Subroutine ***dimensions*** defines the following dimensions from a list of values stored in the input file 'dimension.inp'. The file contains the dimensions as specified in Appendix 1 but can be altered to model a plant with different dimensions.

Following these definitions the radial increment is calculated using the following formula

$$\Delta r = (r_i - r_o)/ncv \tag{5.1}$$

and the average height and radius of each control volume are calculated using the following equations respectively (where the index i is used to define the number of the control volume starting from 1 at the collector inlet with control volume number ncv at the collector outlet).

$$r = r_i - (i-1)\Delta r - \Delta r/2 \tag{5.2}$$

$$H = H_i\left(\frac{r_i}{r}\right)^b \tag{5.3}$$

The average depth of each ground control volume is found using the following relations (where the index j is used to define the number of the control volume starting from 1 at the surface of the ground with control volume number nlayg at the deepest control volume). For j = 1 and j = 2 respectively

$$z_1 = 0.0 \tag{5.4}$$

and

$$z_2 = 0.002 \tag{5.5}$$

while for j = 3 until j = nlayg

$$z_j = \text{multiplier}(z_{j-1} - z_{j-2}) + z_{j-1} \tag{5.6}$$

The resulting depths are as shown in table 5.3 with a multiplier value of 2.15 (rounded off to millimetres)

Table 5.3: Depths of centres of control volumes with multiplier equal to 2.15.

CV	z_1	z_2	z_3	z_4	z_5	z_6	z_7	z_8	z_9	z_{10}	z_{11}	z_{12}	z_{13}	z_{14}
Depth [m]	0	0.002	0.006	0.015	0.035	0.078	0.17	0.367	0.792	1.705	3.668	7.889	16.96	36.47

Since the energy equation for the ground is solved using the fully implicit method the solution is stable for all depths and time steps [99BU1]. The average depth of the deepest control volume should be such that the maximum annual temperature variation of this control volume is negligible when compared to the maximum temperature variation experienced by the uppermost control volume. This is true for the application of the zero gradient boundary at this lower surface.

The distances between each control volume's average height and the average height of the control volume below it are determined and defined as Δz as follows

$$\Delta z_j = z_{j+1} - z_j \tag{5.7}$$

Finally this subroutine determines the chimney cross sectional area and the collector outlet area respectively as follows

$$A_c = 0.25\pi d_c^{\,2} \tag{5.8}$$

$$A_o = 2\pi r_o H_o \tag{5.9}$$

5.3.1.4. Subroutine ***headoutfiles*** opens the 'time.out', 'radi.out' and 'ground.out' files, making use of the ***openoutfiles*** routine. It then heads these files with details of the origin of each file. The details as discussed are shown in figures 5.2, 5.3 and 5.4.

```
day1  :   1
radius:   2.0000000000000000E+02
day hour   Tsky      Tr       T       Ta      Tg1  Power     Dpt          m
           [°C]    [°C]    [°C]    [°C]    [°C]    [MW]    [Pa]     [kg/s]
```

Figure 5.2: The 'time.out' file after it has been opened.

```
day1  :   1
Hour_sam:   14
radius   T_am       Tr        T        Tg        P     hg     hr
   [m]    [°C]     [°C]     [°C]     [°C]     [Pa]      [W/mK]
```

Figure 5.3: The 'radi.out' file after it has been opened.

```
day1  :  365
cv_sam:  100
.000 .002 .006 .015 .034 .072 .154 .326 .686 1.442 3.031
[°C] [°C] [°C] [°C] [°C] [°C] [°C] [°C] [°C]  [°C] [°C]
```

Figure 5.4: The 'ground.out' file after it has been opened.

5.3.1.5. Subroutine ***initialval*** assigns initial values to the temperature and pressure arrays throughout the system. These values are read from the 'initial.inp' file. The ambient pressure, initial chimney density, and initial mass flow rate are also defined as listed in table5.4.

Table 5.4: Values defined internally in the *initialval* routine.

Variable	Symbol	Value
p_a	Pa	90 000 Pa
ρ_c	Rhoc	1 kg/m^3
M	M	180 000 kg/s

5.3.1.6. Subroutine ***properties*** accesses the material files namely 'granite.mat' and 'glass.mat' and reads the ground and roof properties as are listed in Appendix 1.

5.3.2. Solution Phase

The solution is found for each point in time spaced dtime seconds apart in the solution time domain (nday – day1 + 1). To initiate the solution time domain the largest of the time loops namely the day loop is entered. This loop runs until all the days in the time domain have been modelled. Nested in the day loop are the hour, minute and time step loops respectively. These will be discussed in later paragraphs.

5.3.2.1. Subroutine ***getmonth*** is responsible to determine the month in which the day being modelled is found. This is important so that the corresponding data is accessed from the data files. It assigns to the variable month the value of 'jan' , 'feb', 'mar', etc. This is used later to build a filename in which that month's data can be found.

5.3.2.2. Subroutine ***openinpfiles*** opens the input files which contain radiative data as well as ambient temperature data. These files are stored in the directories according to the meteorological property that they contain and are named according to the month for which they are valid. For example the radiation data for January will be accessed by the path and filename 'radiat\jan.inp' while the ambient temperature in December will be accessed by the path and filename 'tambient\dec.inp'. The data stored in these files can be found in Appendix 2.

The beam and diffuse radiation values as well as the ambient temperature values for the particular month are read from the respective files and stored in the computer's memory. These values are the average hourly values taken from the average of all the days in each month. This means for example, that for each day in August the radiation and ambient temperatures during the twenty fourth hour remain the same. This is not actually the case since each day in August is warmer than the previous one. This averaging of the values over entire months would cause a discontinuity in the radiation and ambient temperature when the model moves from one month to the next. This introduces the need to smooth the ambient temperature variation between subsequent months. For this reason the respective month's data is read, as well as

the previous and following month's data. These values for each hour of the day are used to find the ambient temperature for any given day and hour in that month. This is discussed in more detail later in this section. The files are closed immediately after being read.

5.3.2.3. Subroutine ***getdeclination*** determines the declination using equation A6.2.

The hourly loop is entered and it is run repeatedly until 24 hours have been modelled after which a new daily loop is entered if necessary. This loop contains the following subroutines.

5.3.2.4. Subroutine ***getradproperty*** determines the values of the beam and diffuse radiation properties. The hour angle is determined using the following relation

$$\omega = 15(\text{hour} - 12) \tag{5.10}$$

The zenith angle is determined using equation (A6.1). The subroutine then determines the beam reflectance, transmittance due to reflection, the transmittance due to absorption and the transmittance-absorbtance product using the zenith angle and equation (A6.3), (A6.4), (A6.7) and (A6.9) respectively. The diffuse reflectance, transmittance due to reflection, the transmittance due to absorption and the transmittance-absorbtance product are then found approximating the diffuse case with a zenith angle of 60°.

The minutely loop is entered and it is run repeatedly until 60 minutes have been modelled after which a new hourly loop is entered if necessary. The loop contains the following subroutines:

5.3.2.5. Subroutine ***runhalt*** provides the user with an opportunity to stop the code at the beginning of each minute. If any key is pressed (if the buffer contains an entry) at any time during the solution process the program is referred to the end of the code where the files are closed and the program is stopped. (This option is deactivated in the Microsoft compiled version.)

5.3.2.6. Subroutine ***gettambient*** uses the data stored in the pretta (previous month's ambient temperature data), tta (present month's ambient temperature data) and the

nxttta (next month's ambient temperature data) arrays to interpolate between the monthly average ambient temperatures to find a smoother representation of the ambient temperature. The following equations are used for this interpolation. The hourly data for each month is interpolated to find the particular minutes ambient temperature. These would represent the temperatures at the particular minute on the fifteenth of each of the three months.

$$preT_a = pretta(hour) + 273.15 + min(pretta(hour+1) - pretta(hour))/60 \quad (5.11)$$

$$T_a = tta(hour) + 273.15 + min(tta(hour+1) - tta(hour))/60 \quad (5.12)$$

$$nxtT_a = nxttta(hour) + 273.15 + min(nxttta(hour+1) - nxttta(hour))/60 \quad (5.13)$$

where min, pretta, tta and nxttta represent the number of current minute and the arrays used to store the hourly ambient temperatures.

These three temperatures on the averages of each month are then used with the following equation to find the ambient temperature on the specific day (interpolation between months)

$$T_a = (currday + 15) * (T_a - preT_a)/30 + preT_a \quad \text{if currday < 15} \quad (5.14)$$

$$T_a = (currday - 15) * (nxtT_a - T_a)/30 + T_a \quad \text{if currday > 15} \quad (5.15)$$

where currday is the number of the day starting with 1 on the first of the particular month. These equations make use of the assumption that an average day of each month is the 15th of that month.

5.3.2.7. Subroutine ***getradiation*** uses equations similar to equation (5.12) to find interpolated values of the beam and diffuse radiation. The equations are stated here for clarity.

$$I_d = iid(hour) + min(iid(hour+1) - iid(hour))/60 \quad (5.16)$$

where iid is the array used to store the hourly diffuse radiation values.

To find I_b equation (2.23) is used in conjunction with the interpolation equation to yield

$$I_b = \text{iih(hour)} + \min(\text{iih(hour}+1) - \text{iih(hour)})/60 - I_d \quad (5.17)$$

where once again iih is the array used to store the hourly total radiation values.

5.3.2.8. Subroutine ***getsky*** determines the apparent sky temperature using equation (2.37)

5.3.2.9. Since it is not necessary to update the mass flow rate at every time step subroutine ***getmassflow*** is called at intervals of a number of minutes. This number of minutes is defined by the mhold value specified in the 'runcon.inp' file. This subroutine is responsible for finding the mass flow rate that results in the maximum power output for the particular conditions prevalent in the plant.

The algorithm used to find the mass flow rate that yields the maximum power output of the plant is outlined in figure 5.5. The pressures and temperatures throughout the plant are recorded by the ***sendstore*** subroutine so that after the power optimisation has been completed these properties can be returned to their original state. The code solves the energy and draught equations over a number of minutes given by mtest (read form the 'runcon.inp' file) using the previous mhold period's mass flow rate. The power generated with this mass flow rate is recorded and the properties are returned to there original state by the ***fetchstore*** subroutine.

The power is then calculated in the same manner but using mass flow rates 100kg/s (given by the Daccuracy parameter) higher and lower than the original mass flow rate respectively and these powers are also recorded.

These three sample mass flow rates and their respective powers are used to generate a parabolic function which is subsequently optimised (position of zero gradient determined) to find the mass flow rate that would have yielded the highest power. This optimisation process is contained in the following equation [96RA1]

$$m_{opt} = \frac{P_{+100}\left(m^2 + (m-100)^2\right) + P\left((m-100)^2 - (m+100)^2\right) + P_{-100}\left((m+100)^2 - m^2\right)}{2\left[P_{+100}\left(m + (m-100)\right) + P\left((m-100) - (m+100)\right) + P_{-100}\left((m+100) - m\right)\right]} \quad (5.18)$$

where P_{+100} and P_{-100} are the powers calculated using a mass flow rate 100 kg/s

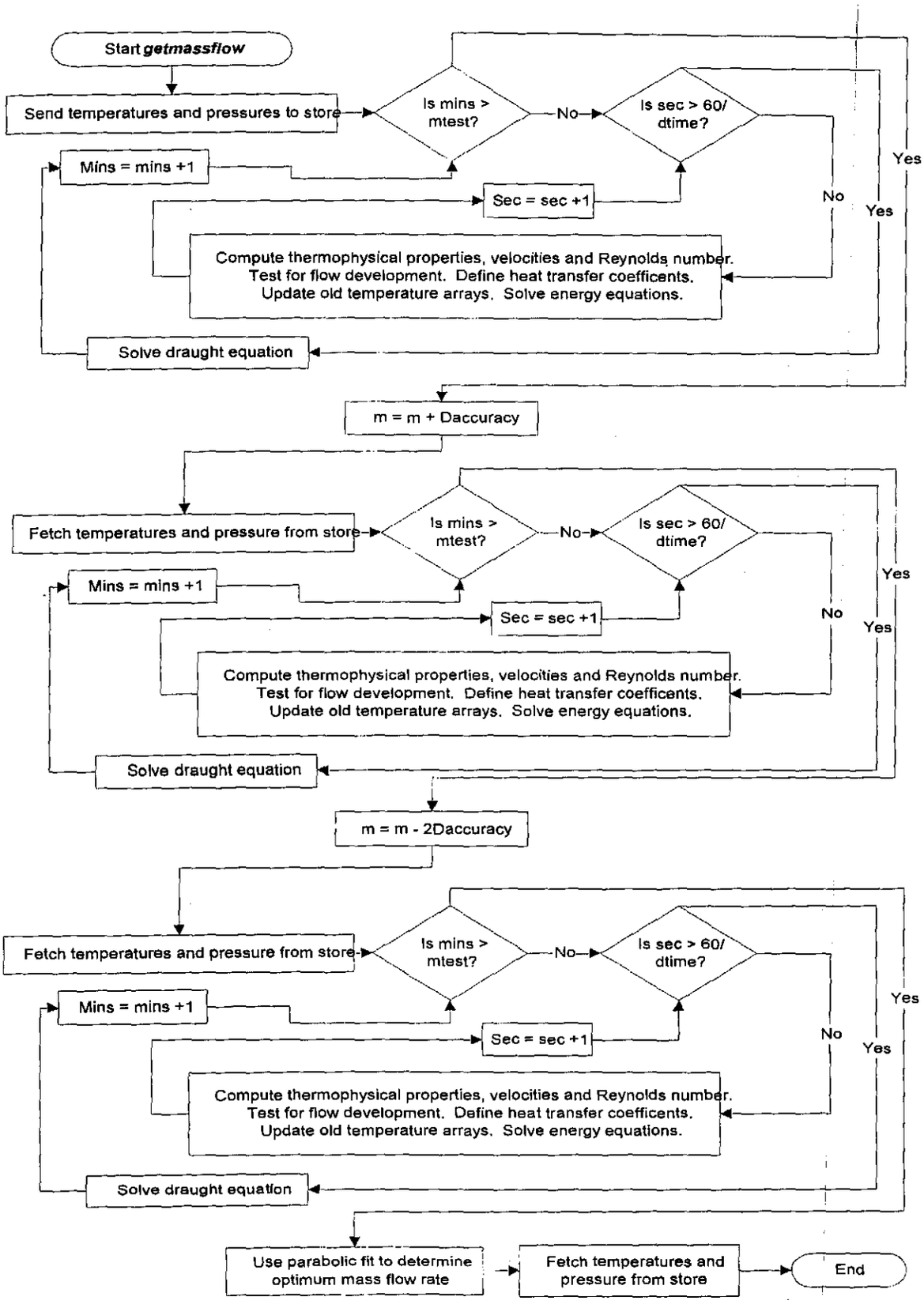

Figure 5.5: The algorithm used to determine the optimum mass flow rate.

higher than m and 100 kg/s lower than m respectively. The value of m is replaced with the value of this optimum mass flow rate m_{opt}.

5.3.2.10. Subroutine ***getthermop*** determines the thermophysical properties of the air at each control volume using the equations and correlations [98KR1] listed in Appendix 8.

5.3.2.11. Subroutine ***getvelocity*** determines the average air velocity in each control volume using the equation

$$v = m/(2\rho H r\pi) \tag{5.19}$$

5.3.2.12. Subroutine ***getreynolds*** determines the Reynolds number based on the collector height (in fact the hydraulic diameter of the collector) at each control volume using the equation

$$Re_h = 2\rho v H/\mu \tag{5.20}$$

5.3.2.13. Subroutine ***testdevelopment*** determines the value of the array devel for each air control volume in the collector. This array is used by subsequent subroutines to ascertain whether or not the air flow in each control volume has reached the state of being hydrodynamically fully developed or if it is still developing. This is determined by testing whether or not the sum of the boundary layer thicknesses is less than the collector height. The subroutine will not define flow in a control volume as developing if at any larger radius it is defined as fully developed. The equation used to find the boundary layer thickness for the roof (assumed smooth) follows [99KR1]

$$\delta = H_i\left\{\frac{1}{6.218-15.08b}\left(\frac{r_i}{H_i}\right)\left(\frac{\mu r_i}{m}\right)^{0.2}\left[\left(\frac{r}{r_i}\right)^{1.2-0.2b}-\left(\frac{r}{r_i}\right)^{2.743-3.943b}\right]\right\}^{\frac{5}{6}} \tag{5.21}$$

while for the ground (rough surface) the equation can be written as

$$\delta = H_i\left(\frac{\varepsilon}{H_i}\right)^{0.2026}\left(\frac{r_i}{H_i}\right)^{0.7974}\left\{q\frac{\left(\frac{r}{r_i}\right)^{1.51-0.51b}-\left(\frac{r}{r_i}\right)^{2.866-4.120b}}{2.550-6.787b}+\frac{\frac{r}{r_i}-\left(\frac{r}{r_i}\right)^{2.866-4.120b}}{17.38-38.37b}\right\}^{0.7974} \quad (5.22)$$

5.3.2.14. Subroutine ***getheatcoeffs*** determines the average convection heat transfer coefficients between the ground and the air, and the underside of the roof and the air (h_g and h_r respectively) for every control volume using equations (2.15) an (2.16) respectively for the region of developing flow and equation (2.7) for the fully developed region. This subroutine also determines the average effective radiation heat transfer coefficients between the ground and the roof and between the roof and the sky for each radius using equations (2.26) and (2.36) respectively. These effective radiation heat transfer coefficients are only updated every minute to help linearise the solution of the energy equations. (If they were solved at every new energy equation iteration, the solution of these equations would have required many more iterations or become unstable in nature. This is an acceptable approximation since the coefficients don't change dramatically over a period of a minute.) Finally this routine determines the convection heat transfer coefficient between the upperside of the roof and the air above the collector using equation (2.33).

5.3.2.15. Subroutine ***tempupdate*** replaces the values of the old temperature arrays (T_{old}, $T_{g,old}$ and $T_{r,old}$) with the latest temperatures. These so-called old temperatures are used in the dicretised transient terms in the energy equations.

5.3.2.16. Subroutine ***energyeqn*** iteratively solves the energy equations for the roof, collector air and the various layers of ground. This solution makes use of two discretisation methods namely the fully implicit Forward Time – Central Space (BTCS) and the upwind finite difference schemes for the ground and air respectively. (Details on the discretisation can be found in Chapter 4.) The equations generated by this discretisation are solved using the successive substitution or Gauss-Seidel method until convergence is attained. The solutions are defined to have reached convergence when the errors measured (in Watts per square metre) while applying energy balances to the roof, air and ground are less than the value of the parameter EBaccuracy defined in the 'runcon.inp' file. This routine makes use of four routines namely ***rooftemperature***, ***airtemperature***, ***groundtemperature*** and ***energy_balance*** and these will be discussed in the following sections.

It is evident in figure 5.6 that the energy equations are solved completely (until convergence) starting at the outer most radius and subsequently at smaller radii until the collector outlet is reached. This is another advantage of the upwinding scheme, namely that the solutions of the equations at a particular radius are independent of the solutions in radii at smaller radii.

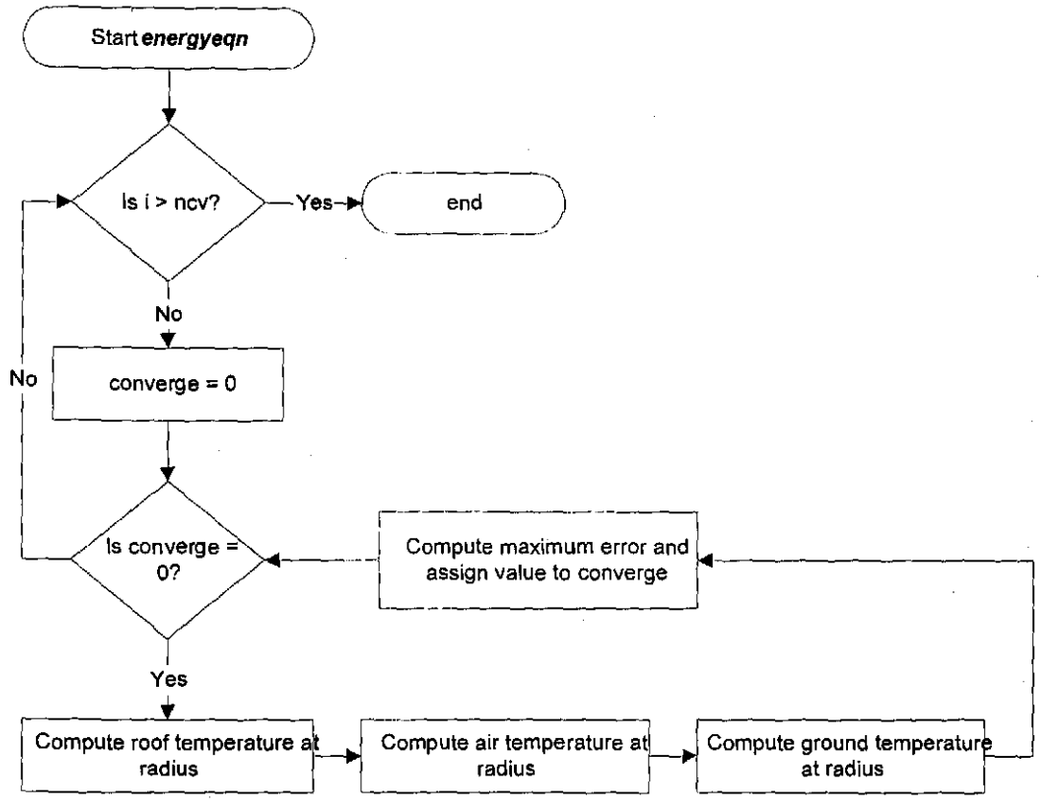

Figure 5.6: The algorithm used to solve the energy equations.

Subroutine ***rooftemperature*** solves the roof energy equation for the particular control volume using equation (4.20) for the regions of fully developed flow and equation (4.21) for regions of developing flow.

Subroutine ***airtemperature*** solves the air energy equation for the particular control volume using equation (4.3) for the regions of fully developed flow and equation (4.4) for regions of developing flow.

Subroutine ***groundtemperature*** solves the ground energy equation for the particular control volume using for the surface equation (4.13) for the regions of fully developed

flow and equation (4.14) for regions of developing flow. The temperatures of each layer below the surface are also determined using equation (4.10)

Once each new temperature in the particular control volume set has been determined an energy balance is done in order to establish whether or not the solution is sufficiently converged. This process is explained in the next section.

Subroutine ***energy_balance*** determines the maximum error made in solving the energy equations in Watts per square metre and compares this to the parameter EBaccuracy. It determines these errors (for each radii) for the roof, air and ground using the following equations: For the roof the equations can be written as follows (based on equations (4.19))

$$EBr = (1-\rho_b)(1-\tau_{b\alpha})I_b + (1-\rho_d)(1-\tau_{d\alpha})I_d - h_{rgr}(T_r - T_g) - h_r(T_r - T) - h_{rrs}(T_r - T_{sky}) - h_{ra}(T_r - T_a) - \rho_r c_{pr} t_r (T_r - T_{r,old})/dt \quad (5.23)$$

for the region of fully developed flow and

$$EBr = (1-\rho_b)(1-\tau_{b\alpha})I_b + (1-\rho_d)(1-\tau_{d\alpha})I_d - h_{rgr}(T_r - T_g) - h_r(T_r - T_a) - h_{rrs}(T_r - T_{sky}) - h_{ra}(T_r - T_a) - \rho_r c_{pr} t_r (T_r - T_{r,old})/dt \quad (5.24)$$

for the region of developing flow. For the air the equations are written as (based on equation (4.2))

$$EBa = \left(\frac{mc_{p,i}}{2\pi r_i}\right)\left(\frac{T_i - T_{i-1}}{r_i - r_{i-1}}\right) + \rho_i c_{p,i} H_i \frac{T_i - T_{old,i}}{dt} - h_{r,i}(T_{r,i} - T_i) + h_{g,i}(T_{g,i} - T_i) \quad (5.25)$$

for the region of fully developed flow and

$$EBa = \left(\frac{mc_{p,i}}{2\pi r_i}\right)\left(\frac{T_i - T_{i-1}}{r_i - r_{i-1}}\right) + \rho_i c_{p,i} H_i \frac{T_i - T_{old,i}}{dt} - h_{r,i}(T_{r,i} - T_a) + h_{g,i}(T_{g,i} - T_a) \quad (5.26)$$

for the region of developed flow. For the surface of the ground the equations can be written as (based on equations (4.9) and (4.12) respectively)

$$Ebg = q_{gi} - h_g\left(T_{g,1} - T\right) + h_{rgr}\left(T_{g,1} - T_r\right) + k_g \frac{T_{g,1} - T_{g,2}}{\Delta z_1} + \rho_g c_{pg} \Delta z_1 \frac{\left(T_{g,1} - T_{g,old,1}\right)}{\partial t} \qquad (5.27)$$

for the region of fully developed flow and

$$Ebg = q_{gi} - h_g\left(T_{g,1} - T_a\right) + h_{rgr}\left(T_{g,1} - T_r\right) + k_g \frac{T_{g,1} - T_{g,2}}{\Delta z_1} + \rho_g c_{pg} \Delta z_1 \frac{\left(T_{g,1} - T_{g,old,1}\right)}{\partial t} \qquad (5.28)$$

for the region of developing flow. The equation used to determine the error made solving the energy equations for the layers of ground below the surface is written as follows

$$EBg = \rho_g c_{pg} \frac{T_{g,j} - T_{g,old,j}}{dt} - k_g \left[\frac{T_{g,j+1} - T_{g,j}}{\frac{1}{2}\left(\Delta z_j + \Delta z_{j-1}\right) \cdot \Delta z_j} - \frac{T_{g,j} - T_{g,j-1}}{\frac{1}{2}\left(\Delta z_j + \Delta z_{j-1}\right) \cdot \Delta z_{j-1}} \right] \qquad (5.29)$$

The subroutine then determines the maximum entry in each of the EB arrays, and in so doing finds the maximum error made in the roof, air and ground energy equations. If all of these errors are smaller than the parameter accuracy then the convergence parameter (converge) is assigned a value of 1 which allows the code to move to the next control volume. At this point the time step loop is complete.

5.3.2.17 Subroutine ***drafteqn*** is used to determine the power available to the turbine. This is achieved by determining the pressure potential available and subtracting from it the system pressure losses. The difference is the pressure drop over the turbine and this is used to find the power available. The calculations are done as follows:

The inlet pressure drop is determined using equation (3.1).

Subroutine ***colldp*** uses equations (3.9), (3.31), (3.41) and (3.44) to find the various pressure drops over each control volume. These are added to find the total pressure drop over the collector (dpcoll).

The turbine inlet pressure drop is found using equation (3.45).

Subroutine ***getpahco*** determines the ambient pressure at the height of the chimney exit using the equation using equation (3.59) which makes use of the assumption that the air is dry, and that adiabatic expansion is applicable.

Subroutine ***averagechim*** determines the average properties in the chimney so that the chimney pressure drop can be found based on average values. The following equations are used to find the average values

$$p_c = 0.5(p_{aHco} + p_o) \tag{5.30}$$

$$T_c = T_o - 0.5 \cdot 0.00975 H_c \tag{5.31}$$

$$\rho_c = p_c / (T_c R) \tag{5.32}$$

The average chimney viscosity is determined using the average chimney temperature in equation (A8.3). The Reynolds number based on the chimney diameter number is then found using

$$v_c = m / \left(0.25 \rho_c \pi d_c^{\,2}\right) \tag{5.33}$$

$$Re_c = \rho_c v_c d_c / \mu_c \tag{5.34}$$

Subroutine ***chimdp*** uses the average chimney properties and equations (3.48), (3.50) and (3.51) to determine the total pressure drop in the chimney.

The driving potential is determined using the equation (3.62) and then the power available to the turbine is found using the following equations

$$\Delta p_t = p_a - p_o - (\Delta p_i + \Delta p_{coll} + \Delta p_{ti} + \Delta p_{chim} + 0.5 \rho_{co} v_{co}^{\,2}) \tag{5.35}$$

$$\text{Power} = \Delta p_t m / \rho_{ti} \tag{5.36}$$

In order to determine the integrated power output, this value of the instantaneous power is multiplied by 60 (the number of seconds in a minute) to find the energy generated in the last minute and this is added to a running total of the energy

generated up to that time beginning with zero at the start of each new year. At his point the minutely loop is complete.

5.3.2.18. Subroutine ***write_output*** writes a line of output information to the 'time.out' file using the data from the control volume specified by the cv_sam (control volume to sample) paramter where applicable.

If the current hour is equal to the parameter hour_sam (hour to sample) then the current days data is added to the 'radi.out' file.

The current hours ground temperatures are added as a new line in the 'ground.out' file.

At his point the hourly loop and the daily loops are complete.

5.3.3. Conclusion phase

Subroutine ***closefiles*** closes all the files that have been accessed but not closed.

6. VERIFICATION OF SOLUTION OF ENERGY AND DRAUGHT EQUATIONS

6.1. INTRODUCTION

In order to check the validity of the solution attained with the 'solchim' code discussed in Chapter 5 it is necessary to substitute the results obtained into the governing equations. If these results satisfy the governing equations then the solution is valid. This process is discussed in this section.

The results of the simulation are discrete in nature and for this reason the discretised energy equations are used instead of the differential form of the energy equations.

The values used throughout this Chapter are found in Appendix 4

6.2. THE AIR ENERGY EQUATION

The discretised form of the air energy equation for the region of fully developed flow equation (4.1) is repeated here for clarity.

$$\left(\frac{mc_{p,i}}{2\pi r_i}\right)\left(\frac{T_i - T_{i-1}}{r_i - r_{i-1}}\right) + \rho_i c_{p,i} H_i \frac{T_i - T_{old,i}}{dt} = h_{r,i}\left(T_{r,i} - T_i\right) + h_{g,i}\left(T_{g,i} - T_i\right) \qquad (6.1)$$

Substituting the values from Appendix 4 into the left hand side yields

$$\begin{aligned} \text{LHS.} &= \left(\frac{mc_{p,i}}{2\pi r_i}\right)\left(\frac{T_i - T_{i-1}}{r_i - r_{i-1}}\right) + \rho_i c_{p,i} H_i \frac{T_i - T_{old,i}}{dt} \\ &= \left(\frac{-216442.204096 \cdot 1007.211369}{2\pi \cdot 254}\right)\left(\frac{306.709481 - 306.665054}{254 - 290}\right) \\ &\quad + 1.021676 \cdot 1007.211369 \cdot 28.060677\left(\frac{306.709481 - 306.705549}{4}\right) \\ &= 196.9599 \text{ W/m}^2 \end{aligned}$$

Substituting the values into the right hand side yields

$$\begin{aligned}\text{RHS.} &= h_{r,i}(T_{r,i} - T) + h_{g,i}(T_{g,i} - T) \\ &= 4.706022(307.507588 - 306.709481) + 12.295963(322.422016 - 306.709481) \\ &= 196.9567 \text{ W/m}^2\end{aligned}$$

Note that the L.H.S and the R.H.S are essentially the same i.e. a satisfactory energy balance is achieved.

The discretised form of the air energy equation for the region of developing flow is written as

$$\left(\frac{mc_{p,i}}{2\pi r_i}\right)\left(\frac{T_i - T_{i-1}}{r_i - r_{i-1}}\right) + \rho_i c_{p,i} H_i \frac{T_i - T_{old,i}}{dt} = h_{r,i}(T_{r,i} - T_a) + h_{g,i}(T_{g,i} - T_a) \qquad (6.2)$$

Substituting the values from Appendix 4 into the left hand side yields

$$\begin{aligned}\text{LHS.} &= \left(\frac{mc_{p,i}}{2\pi r_i}\right)\left(\frac{T_i - T_{i-1}}{r_i - r_{i-1}}\right) + \rho_i c_{p,i} H_i \frac{T_i - T_{old,i}}{dt} \\ &= \left(\frac{-216442.204096 \cdot 1006.891419}{2\pi \cdot 1910}\right)\left(\frac{298.281361 - 297.891695}{1910 - 1946}\right) \\ &\quad + 1.0511 \cdot 1006.891419 \cdot 10.23289\left(\frac{298.281361 - 298.279541}{4}\right) \\ &= 201.4904 \text{ W/m}^2\end{aligned}$$

Substituting the values into the right hand side yields

$$\begin{aligned}\text{RHS.} &= h_{r,i}(T_{r,i} - T_a) + h_{g,i}(T_{g,i} - T_a) \\ &= 2.88198(306.540335 - 297.233327) + 6.657858(323.468219 - 297.233327) \\ &= 201.4908 \text{ w/m}^2\end{aligned}$$

Once again, an energy balance is achieved.

6.3. THE GROUND ENERGY EQUATION

The discretised form of the ground energy equation applicable to the surface for the region of fully developed flow equation (4.12) is repeated here for clarity.

$$q_i = h_g\left(T_{g,j} - T\right) + h_{rgr}\left(T_{g,j} - T_r\right) + k_g \frac{T_{g,j} - T_{g,j+1}}{\Delta z_j} + \rho_g c_{pg} \frac{\Delta z_j}{2} \frac{\left(T_{g,j} - T_{g,old,j}\right)}{\partial t} \qquad (6.3)$$

Substituting the values from Appendix 4 into the left hand side yields

$$\text{LHS.} = q_i = 530.269208 \text{ W/m}^2$$

Substituting the values into the right hand side yields

$$\begin{aligned}\text{RHS.} &= h_g\left(T_{g,1} - T\right) + h_{rgr}\left(T_{g,1} - T_r\right) + k_g \frac{T_{g,1} - T_{g,2}}{\Delta z_1} + \rho_g c_{pg} \frac{\Delta z_1}{2} \frac{\left(T_{g,1} - T_{g,old,1}\right)}{\partial t} \\ &= 12.295963(322.422016 - 306.709481) + 5.620415(322.422016 - 307.507588) \\ &\quad + 1.73 \frac{322.422016 - 322.13334}{0.002} + 2640 \cdot 820 \cdot \frac{0.002}{2} \frac{(322.422016 - 322.41558)}{4} \\ &= 530.2139 \text{ W/m}^2\end{aligned}$$

The discretised form of the ground energy equation applicable to the surface for the region of developing flow is written as

$$q_i = h_g\left(T_{g,j} - T_a\right) + h_{rgr}\left(T_{g,j} - T_r\right) + k_g \frac{T_{g,j} - T_{g,j+1}}{\Delta z_j} + \rho_g c_{pg} \frac{\Delta z_j}{2} \frac{\left(T_{g,j} - T_{g,old,j}\right)}{\partial t} \qquad (6.4)$$

Substituting the values from table 4 into the left hand side yields

$$\begin{aligned}\text{LHS.} &= q_i \\ &= 530.269208 \text{ W/m}^2\end{aligned}$$

Substituting the values into the right hand side yields

$$\begin{aligned}\text{RHS.} &= h_g\left(T_{g,1} - T_a\right) + h_{rgr}\left(T_{g,1} - T_r\right) + k_g \frac{T_{g,1} - T_{g,2}}{\Delta z_1} + \rho_g c_{pg} \frac{\Delta z_1}{2} \frac{\left(T_{g,1} - T_{g,old,1}\right)}{\partial t} \\ &= 6.657858(323.468219 - 297.233327) + 5.623413(323.468219 - 306.540335) \\ &\quad + 1.73 \frac{323.468219 - 323.171357}{0.002} + 2640 \cdot 820 \cdot \frac{0.002}{2} \frac{(323.468219 - 323.461629)}{4} \\ &= 530.2128 \text{ W/m}^2\end{aligned}$$

In both cases since the L.H.S is essentially the same as the R.H.S, a satisfactory energy balance is achieved.

6.4. THE ROOF ENERGY EQUATION

The discretised form of the roof energy equation for the region of fully developed flow equation (4.19) is repeated here for clarity.

$$(1-\rho_b)(1-\tau_{b\alpha})I_b + (1-\rho_d)(1-\tau_{d\alpha})I_d - h_{rgr}(T_r - T_g) - h_r(T_r - T) - h_{rrs}(T_r - T_{sky}) - h_{ra}(T_r - T_a) = \rho_r c_{pr} t_r (T_r - T_{r,old})/dt \quad (6.5)$$

Substituting the values from Appendix 4 into the left hand side yields

$$\begin{aligned}\text{LHS.} &= (1-\rho_b)(1-\tau_{b\alpha})I_b + (1-\rho_d)(1-\tau_{d\alpha})I_d - h_{rgr}(T_r - T_g) - h_r(T_r - T) - h_{rrs}(T_r - T_{sky}) \\ &\quad - h_{ra}(T_r - T_a) \\ &= (1-0.044426)(1-0.845492)638.28333 + (1-0.093463)(1-0.823391)126.16667 \\ &\quad - 5.620415(307.507588 - 322.422016) - 4.706022(307.507588 - 306.709481) \\ &\quad - 5.08258(307.50758 - 282.868982) - 5.7(307.507588 - 297.233327) \\ &= 10.7166\ \text{W/m}^2\end{aligned}$$

Substituting the values into the right hand side yields

$$\begin{aligned}\text{RHS.} &= \rho_r c_{pr} t_r (T_r - T_{r,old})/dt \\ &= 2700 \cdot 840 \cdot 0.005(307.507588 - 307.503808)/4 \\ &= 10.7163\ \text{W/m}^2\end{aligned}$$

The discretised form of the roof energy equation for the region of developing flow is written as

$$(1-\rho_b)(1-\tau_{b\alpha})I_b + (1-\rho_d)(1-\tau_{d\alpha})I_d - h_{rgr}(T_r - T_g) - h_r(T_r - T_a) - h_{rrs}(T_r - T_{sky}) - h_{ra}(T_r - T_a) = \rho_r c_{pr} t_r (T_r - T_{r,old})/dt \quad (6.6)$$

Substituting the values from Appendix 4 into the left hand side yields

$$\begin{aligned}\text{LHS.} &= (1-\rho_b)(1-\tau_{b\alpha})I_b + (1-\rho_d)(1-\tau_{d\alpha})I_d - h_{rgr}(T_r - T_g) - h_r(T_r - T) - h_{rrs}(T_r - T_{sky}) \\ &\quad - h_{ra}(T_r - T_a) \\ &= (1-0.044426)(1-0.845492)638.28333 + (1-0.093463)(1-0.823391)126.16667 \\ &\quad - 5.623413(306.540335 - 323.468219) - 2.88198(306.540335 - 297.233327) \\ &\quad - 5.057084(306.540335 - 282.868982) - 5.7(306.540335 - 297.23327) \\ &= 10.0501\ \text{W/m}^2\end{aligned}$$

Substituting the values into the right hand side yields

$$\begin{aligned}\text{RHS.} &= \rho_r c_{pr} t_r (T_r - T_{r,old})/dt \\ &= 2700 \cdot 840 \cdot 0.005(306.540335 - 306.536791)/4 \\ &= 10.0472\ \text{W/m}^2\end{aligned}$$

Once again a satisfactory energy balance is achieved.

6.5. THE DRAUGHT EQUATION

To test the validity of the draught equation it is necessary to determine all the pressure drops in the system and ultimately the power output for a point in time and compare this to the code's predicted pressure drops and power output. This is done in an order starting from the collector inlet and moving through the system until the chimney outlet is reached

The inlet pressure drop is given by equation (3.1). Substituting the values given in Appendix 4 into this equation yields

$$\begin{aligned}\Delta p_i &= \frac{1}{2}\rho_i v_i^2 K_i + \frac{1}{2}\rho_i v_i^2 \\ &= \frac{1}{2}1.053962 \cdot 1.641611^2 \cdot 1 + \frac{1}{2}1.053962 \cdot 1.641611^2 \\ &= 2.8403\ \text{Pa}\end{aligned}$$

The code's predicted value is 2.8403 Pa. The pressure drop in the collector caused by the supports, the acceleration and the frictional effects in the developing region are calculated using equations (3.9), (3.31) and (3.41) respectively. Substituting the values from Appendix 4 find the pressure loss due to the collector supports

$$\Delta p_s = \frac{\Delta r}{P_r}\frac{C_{sD} m^2 d_s (0.5 * P_r + r)^{2(b-1)}}{8\pi^2 \rho P_t H_i^2 r_i^{2b}}$$

$$= \frac{(1946-1910)}{10}\cdot\frac{1\cdot 216442.204096^2\cdot 0.75\cdot(0.5*10+1910)^{2(0.5-1)}}{8\pi^2\cdot 1.0511\cdot 10\cdot 10^2\cdot 2000^{2\cdot 0.5}}$$

$$= 0.3979\ \text{Pa}$$

while the pressure differential due to acceleration is calculated as

$$\Delta p_{acc} = -\frac{Rm^2 r^{b-1}}{pH_i^2 r_i^{2b} 4\pi^2}\left(\frac{\partial T}{\partial r} r^{b-1} + (b-1) r^{b-2} T\right)\Delta r$$

$$= -\frac{287.079987\cdot(-216442.204096)^2\cdot 1910^{0.5-1}}{89996.082437\cdot 10^2\cdot 2000^{2\cdot 0.5}\cdot 4\cdot\pi^2}$$

$$\cdot\left(\frac{298.281361-297.891695}{1910-1946}1910^{0.5-1} + (0.5-1)1910^{0.5-2}\cdot 298.281361\right)(1946-1910)$$

$$= 0.0317\ \text{Pa}$$

The pressure differential due to the friction on the ground and roof in the collector

$$\Delta p_f = \frac{1}{H_i}\left(\frac{r}{r_i}\right)^b \left[0.01392\frac{\rho v^{1.8}\upsilon^{0.2}}{H_i^{0.2}}\left(\frac{H_i}{r_i}\right)^{1/6}\left(\frac{m}{\mu r_i}\right)^{1/30}\left\{\frac{6.218-15.08b}{\left(\frac{r}{r_i}\right)^{1.2-0.2b} - \left(\frac{r}{r_i}\right)^{2.743-3.943b}}\right\}^{1/6}\right.$$

$$+ 0.008326\rho v^2 \varepsilon_g^{0.254}\left\{1.94\left(\frac{\mu}{\rho v \varepsilon_g}\right)^{0.51}+1\right\}\frac{1}{H_i^{0.254}}\left(\frac{H_i}{\varepsilon_g}\right)^{0.0515}\left(\frac{H_i}{r_i}\right)^{0.2025}$$

$$\left.\times\left\{q\frac{\left(\frac{r}{r_i}\right)^{1.51-0.51b} - \left(\frac{r}{r_i}\right)^{2.866-4.120b}}{2.550-6.787b} + \frac{\left(\frac{r}{r_i}\right) - \left(\frac{r}{r_i}\right)^{2.866-4.120b}}{17.38-38.37b}\right\}^{-0.2025}\right]\Delta r$$

$$= \frac{1}{10}\left(\frac{1910}{2000}\right)^{0.5}\left[0.01392\frac{1.0511\cdot 1.838797\cdot 10^{-5}{}^{1.8}\left(\frac{1.838797\cdot 10^{-5}}{1.0511}\right)^{0.2}}{10^{0.2}}\left(\frac{10}{2000}\right)^{1/6}\right.$$

$$\left(\frac{216442.204096}{1.838797\cdot 10^{-5}\cdot 2000}\right)^{1/30}\cdot\left\{\frac{6.218-15.08\cdot 0.5}{\left(\frac{1910}{2000}\right)^{1.2-0.2\cdot 0.5}-\left(\frac{1910}{2000}\right)^{2.743-3.943\cdot 0.5}}\right\}^{1/6}$$

$$+0.008326\cdot 1.0511\cdot 1.676819^2\cdot 0.05^{0.254}\left\{1.94\left(\frac{1.838797\cdot 10^{-5}}{1.0511\cdot 1.676819\cdot 0.05}\right)^{0.51}+1\right\}$$

$$\frac{1}{10^{0.254}}\left(\frac{10}{0.05}\right)^{0.0515}\left(\frac{10}{2000}\right)^{0.2025}\times\left\{\left(\frac{1.838797\cdot 10^{-5}\cdot 10\cdot 2000}{0.05\cdot 216442.204096}\right)^{0.51}\right.$$

$$\left.\left.\frac{\left(\frac{1910}{2000}\right)^{1.51-0.51\cdot 0.5}-\left(\frac{1910}{2000}\right)^{2.866-4.120\cdot 0.5}}{2.550-6.787\cdot 0.5}+\frac{\left(\frac{1910}{2000}\right)-\left(\frac{1910}{2000}\right)^{2.866-4.120\cdot 0.5}}{17.38-38.37\cdot 0.5}\right\}^{-0.2025}\right](1946-1910)$$

$$= 0.0441\,\text{Pa}$$

The predicted values are 0.3979 Pa, 0.0317 Pa, and 0.0441 Pa respectively. These same pressure drops in the region of fully developed flow are given by equations (3.9), (3.31) and (3.44). Substituting in values from Appendix 4 yields the pressure drop in the chimney due to the collector supports

$$\Delta p_s = \frac{\Delta r}{P_r}\frac{C_{sD}m^2 d_s\left(0.5*P_r+r\right)^{2(b-1)}}{8\pi^2\rho P_t H_i{}^2 r_i{}^{2b}}$$

$$= \frac{(290-254)}{10}\frac{1\cdot 216442.204096^2\cdot 0.75\cdot\left(0.5*10+254\right)^{2(0.5-1)}}{8\pi^2\cdot 1.021676\cdot 10.\cdot 10^2\cdot 2000^{2\cdot 0.5}}$$

$$= 3.0270\,\text{Pa}$$

while the pressure differential due to acceleration of the collector air is found as

$$\Delta p_{acc} = -\frac{Rm^2 r^{b-1}}{pH_i^2 r_i^{2b} 2\pi^2}\left(\frac{\partial T}{\partial r} r^{b-1} + (b-1) r^{b-2} T\right)\Delta r$$

$$= -\frac{287.079987 \cdot (-216442.204096)^2 \cdot 254^{0.5-1}}{89938.521131 \cdot 10^2 \cdot 2000^{2 \cdot 0.5} \cdot 4\pi^2}$$

$$\left(\frac{306.709481 - 306.665054}{254 - 290} 254^{0.5-1} + (0.5-1) \cdot 254^{0.5-2} \cdot 306.709481\right)(254 - 290)$$

$$= 1.6239 \text{ Pa}$$

with the pressure differential due to friction on the ground and roof in the collector is given by

$$\Delta p_f = \frac{1}{H_i}\left(\frac{r}{r_i}\right)^b \left\{0.02975\left(\frac{\varepsilon_g r^b}{2H_i r_i^b}\right)^{0.254}\left[1.75\left(\frac{\mu}{\rho v \varepsilon_g}\right)^{0.51} + 1\right]\frac{\rho v^2}{2} + \frac{0.02\rho^{0.8} v^{1.8} \mu^{0.2} r^{0.2b}}{H_i^{0.2} r_i^{0.2b}}\right\}\Delta r$$

$$= \frac{1}{10}\left(\frac{254}{2000}\right)^{0.5}\left\{0.02975\left(\frac{0.05 \cdot 254^{0.5}}{2 \cdot 10 \cdot 2000^{0.5}}\right)^{0.254}\left[1.75\left(\frac{1.877356 \cdot 10^{-5}}{1.021676 \cdot 4.730609 \cdot 0.05}\right)^{0.51} + 1\right]\right.$$

$$\left.\times \frac{1.021676 \cdot 4.730609^2}{2} + \frac{0.02 \cdot 1.021676^{0.8} 4.730609^{1.8} 1.877356 \cdot 10^{-5^{0.2}} \cdot 254^{0.2 \cdot 0.5}}{10^{0.2} \cdot 2000^{0.2 \cdot 0.5}}\right\}$$

$$\times (290 - 254)$$

$$= 0.0992 \text{ Pa}$$

The predicted values are 3.0270 Pa, 1.6239 Pa and 0.0992 Pa. It is clear that the code is predicting accurate values for these pressure drops. The integrated pressure drop over the entire collector is found to be 89.136638 Pa.

The pressure drop at the inlet of the turbine is given by equation (3.45) with v_{ti} being given by the following equation

$$v_{ti} = m \Big/ \left(0.25 \cdot d_c^{\,2} \cdot \pi \cdot \rho_o\right)$$

Substituting values from Appendix 4 into this equation yields

$$v_{ti} = \frac{216442.204096}{0.25 \cdot 160^2 \cdot \pi \cdot 1.0214884} = 10.538497 \text{ m/s}$$

The pressure drop at the inlet to the turbine can thus be found as

$$\Delta p_{ti} = \frac{1}{2}\rho_{ti} v_{ti}^2 K_{ti}$$
$$= \frac{1}{2} 1.0214884 \cdot 10.538497^2 \cdot 0.25$$
$$= 14.1808 \text{ Pa}$$

The code predicts a value of 14.1808 Pa.

The pressure changes in the chimney caused by the supports, the frictional effects and the acceleration are given by equations (3.47), (3.48) and (3.50) respectively with f_D in equation (3.48) being given by equation (3.49). In order to find these pressure changes in the chimney, the average values of the properties were used. These are found as follows;

The average pressure in the chimney is found as

$$p_c = 0.5(p_{aHco} + p_o) = 0.5(75430.778141 + 89932.988978) = 82681.88356 \text{ Pa}$$

while the average temperature in the chimney is found as

$$T_c = T_o - 0.5 \cdot 0.00975 H_c = 306.74796 - 0.5 \cdot 0.00975 \cdot 1500 = 299.43546 \text{ K}$$

The average density in the chimney is

$$\rho_c = \frac{p_c}{RT_c} = \frac{82681.88356}{287.079987 \cdot 299.43546} = 0.961843 \text{ kg/m}^3$$

while the velocity is

$$v_c = \frac{m}{0.25\rho_c d_c^2 \pi} = \frac{216442.204096}{0.25 \cdot 0.961843 \cdot 160^2 \pi} = 11.19200 \text{ m/s}$$

The average viscosity is

$$\begin{aligned}\mu_c &= 2.287973\cdot10^{-6} + 6.259793\cdot10^{-8}T_c - 3.131956\cdot10^{-11}T_c^{\,2} + 8.15038\cdot10^{-15}T_c^{\,3}\\ &= 2.287973\cdot10^{-6} + 6.259793\cdot10^{-8}299.43546 - 3.131956\cdot10^{-11}299.43546^2\\ &\quad + 8.15038\cdot10^{-15}299.43546^3\\ &= 1.844267\ \text{kg/ms}\end{aligned}$$

These property values as well as the values from Appendix 4 will be used to determine the various pressure drops in the chimney.

The pressure drop due to the appurtenances is found using equation (3.47) as

$$\begin{aligned}\Delta p_{cs} &= \frac{1}{2}\rho_{ti}v_{ti}^{\,2}K_{cs}\\ &= \frac{1}{2}1.0214884\cdot10.538497^2\cdot0.1\\ &= 5.6723\ \text{Pa}\end{aligned}$$

The average Reynolds number in the chimney is

$$Re_{dc} = \frac{\rho_c d_c v_c}{\mu_c} = \frac{0.961843\cdot160\cdot11.19200}{1.844267\cdot10^{-5}} = 93.3917\cdot10^6$$

Thus the Darcy friction factor in the chimney is

$$\begin{aligned}f_D &= 2.7778\left[\log_{10}\left\{\left(\frac{7.7}{Re_{dc}}\right)^3 + \left(\frac{\varepsilon_c/d_c}{3.75}\right)^{3.33}\right\}\right]^{-2}\\ &= 2.7778\left[\log_{10}\left\{\left(\frac{7.7}{93.3917\cdot10^6}\right)^3 + \left(\frac{0.002/160}{3.75}\right)^{3.33}\right\}\right]^{-2}\\ &= 0.0083507\end{aligned}$$

Substituting this into the equation for friction in the chimney, equation (3.48) yields

$$\begin{aligned}\Delta p_{cf} &= f_D\left(H_c/d_c\right)\left(\rho_c v_c^{\,2}/2\right)\\ &= 0.0083507\left(1500/160\right)\left(0.961843\cdot11.19200^2/2\right)\\ &= 4.7161\ \text{Pa}\end{aligned}$$

The pressure differential in the chimney caused by the acceleration of the air is found using equation (3.50) as

$$\Delta p_{cacc} = \left(\frac{4m}{\pi d_c^{\,2}}\right)^2 \left(\frac{1}{\rho_{co}} - \frac{1}{\rho_{ci}}\right)$$
$$= \left(\frac{4 \cdot 216422.204096}{\pi \cdot 160^2}\right)^2 \left(\frac{1}{0.899456} - \frac{1}{1.0214884}\right)$$
$$= 15.3917 \text{ Pa}$$

The predicted values for these pressure changes respectively are 5.6723 Pa, 4.7161 Pa, and 15.3917 Pa. Thus it is clear that the code predicts these values accurately. The pressure change (recovery) at the exit of the chimney can be found using equations (3.51) through (3.55) as follows:

The density of the ambient air at the elevation of the exit of the chimney can be found as

$$\rho_{aHco} = \frac{p_a}{RT_a}\left(1 - 0.00975H_c / T_a\right)^{2.5}$$
$$= \frac{90000}{287.079987 \cdot 297.233327}\left(1 - 0.00975 \cdot 1500 / 297.233327\right)^{2.5} = 0.929738 \text{ kg/m}^3$$

(Since the exit pressure of the chimney is not known the density at this point is approximated using the ambient pressure at the same elevation as this is within one percent of the chimney exit pressure.) The density of the air at the chimney exit is given by

$$\rho_{co} = \frac{p_{aHco}}{\left(T_o - 0.00975H_c\right)R} = \frac{75430.778141}{\left(306.74796 - 0.00975 \cdot 1500\right)287.079987} = 0.899456 \text{ kg/m}^3$$

These densities are used to find the densimetric Frounde number as

$$Fr_D = \left(\frac{m_{co}}{A_c}\right)^2 \Big/ \left[\rho_{co}\left(\rho_{aHco} - \rho_{co}\right)g d_{co}\right]$$
$$= \left(\frac{216442.204096}{\pi \cdot 80^2}\right)^2 \Big/ \left[0.899456\left(0.929738 - 0.899456\right)9.81 \cdot 160\right]$$
$$= 2.7106$$

The pressure change coefficient is thus found as

$$K_{co} = -0.28Fr_D^{-1} + 0.04Fr_D^{-1.5} = -0.28 \cdot 2.7106^{-1} + 0.04 \cdot 2.7106^{-1.5} = -0.094334$$

The velocity at the chimney exit is

$$v_{co} = 4m/\rho_{co}\pi d_c^2 = 4 \cdot 216442.204096/0.899456 \cdot \pi \cdot 160^2 = 11.9683 \text{ m/s}$$

Substituting the density, velocity and pressure change coefficient into the equation for the pressure change at the chimney exit equation (3.51) yields

$$\Delta p_{co} = \frac{1}{2}\rho_{co} v_{co}^2 K_{co} = 0.5 \cdot 0899456 \cdot 11.9683^2 \cdot -0.094334 = -6.0769 \text{ Pa}$$

The pressure driving potential is given by equation (3.61). Substituting the values into this equation yield

$$\begin{aligned} p_a - p_o &= p_a\left[1 - \{(1 - 0.00975H_c / T_a)/(1 - 0.00975H_c / T_o)\}^{3.5}\right] \\ &= 90000\left[1 - \{(1 - 0.00975 \cdot 1500/297.23327)/(1 - 0.00975 \cdot 1500/306.74796)\}^{3.5}\right] \\ &= 503.80804 \text{ Pa} \end{aligned}$$

The net pressure driving potential (the pressure drop over the turbine) is given by the difference between the total potential and the sum of the pressure drops as follows:

$$\begin{aligned} \Delta p_t &= p_a - p_o - \Delta p_i - \Delta p_{coll} - \Delta p_{ti} - \Delta p_{chim} - \Delta p_{co} - 0.5\rho_{co} v_{co}^2 \\ &= 503.80804 - 2.840309 - 64.020637 - 14.180802 - 25.780142 + 6.076932 \\ &\quad - 0.5 \cdot 0.899456 \cdot 11.96829^2 \\ &= 338.6441 \text{ Pa} \end{aligned}$$

The predicted value is 338.6441 Pa. Thus it is shown that the draught equation is indeed satisfied by the solution obtained using the code.

7. SOLAR CHIMNEY POWER PLANT PERFORMANCE

7.1. INTRODUCTION

In this section some performance characteristics of a solar chimney power plant are presented. The reference plant's (dimensions given in Appendix 1 and meteorological conditions specified in Appendix 2) performance is discussed first and then the results of modifications to the reference plant's inlet height is presented.

7.2. REFERENCE PLANT PERFORMANCE

The performance of the reference plant was analysed by simulating it using the model and code discussed in chapters 2, 3 and 5 respectively. It is necessary to use correct initial values for the temperatures and pressures throughout the plant as the results of the simulation are dependant on these values. Since this dependence diminishes as the simulation time domain increases, initial values were obtained by running the simulation for a model time of four years and recording the temperatures and pressures at the end of this period in the 'initial.inp' file. In other words it took four years (modelling time) for the results to stabilise or to reach a state sometimes referred to as steady periodic- or sustained response. This stabilization time is proportional to the depth of ground to which the model is applied.

The energy that the reference plant delivers is 367 GWh/annum. This is generated at different rates throughout the year as can be seen in figure 7.1. Notice the significantly higher output in December compared to June. This is attributed to the higher radiation levels in December. It is also evident that the plant is considerably less effective in converting solar radiation into power in June than in December since the zenith angle is larger in June. This increases the relative amount of beam radiation that is reflected by the collector roof.

7.2.1. Conservation of solar radiation

The solar radiation that is available to the solar chimney power plant is shown in figure 7.2. It is clear that the data is given in solar time since the highest value of beam radiation occurs at a time of 12:00. The diffuse radiation has a less pronounced peak which seems to contribute only slightly to the shape and magnitude of the total solar radiation value. This solar radiation is utilised by the reference plant according to figure 7.3. The ground absorbs about 70% of the total solar radiation at

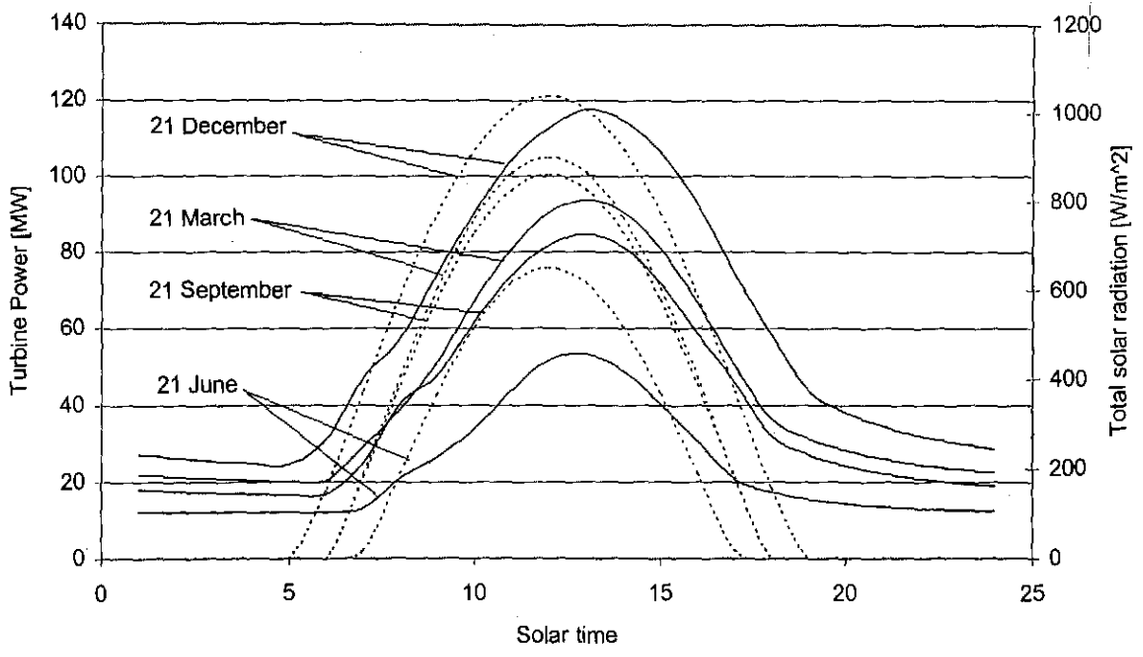

Figure 7.1: The turbine power output for the 21 of March, June, September and December, with the total radiation shown in broken lines.

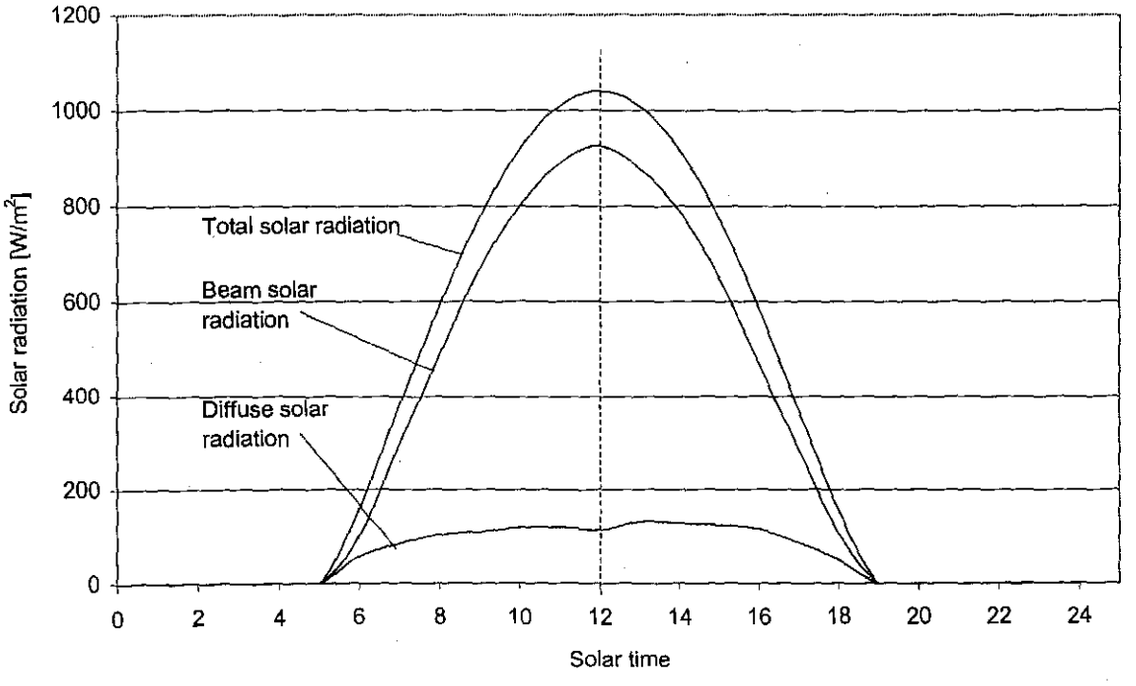

Figure 7.2: The beam, diffuse and total solar radiation incident on the collector roof on the 21 of December.

solar noon but less than fifty percent during the early morning and late afternoon. This is also attributed to the varying angle of incidence, which is lowest at noon. The glass absorbs 14% of the solar radiation at solar noon and is of the same order during the early morning and late afternoon. This relationship thus shows less dependence on the incidence angle and time of day. The beam radiation reflected by the roof shows (in figure 7.3) a high gradient during the early morning and late afternoon caused by the low position of the sun at these times. It is fairly constant throughout the rest of the day because the increase of the beam radiation before solar noon and the decrease during the afternoon are counteracted by the opposite trends in the reflectance during these parts of the day. The diffuse radiation reflected by the roof remains small throughout the day with a maximum value of 12 W/m^2. All of the above mentioned effects are approximately symmetrical about solar noon.

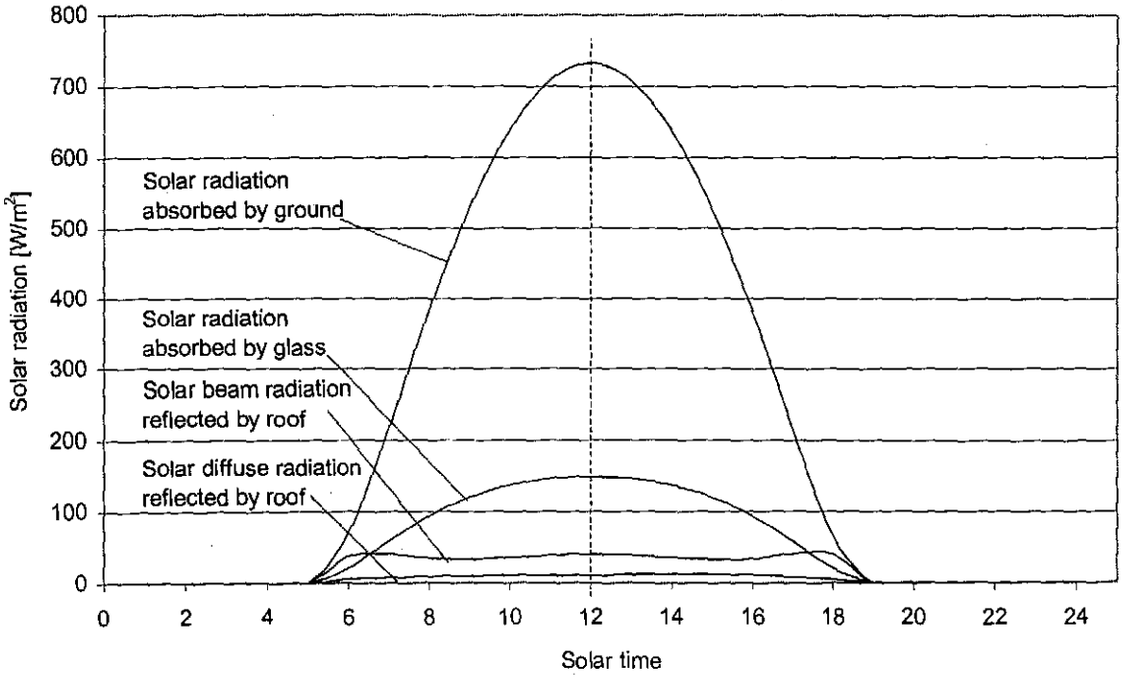

Figure 7.3: The solar radiation absorbed by the ground and glass and the solar radiation reflected by the roof on the 21 of December.

7.2.2. Conservation of thermal energy

An account of all the power throughout the day is given if figures 7.4 and 7.5. Figure 7.4 shows the heat that is lost to the environment via the top surface of the roof. The emission loss (radiation heat transfer between roof and sky) shows a maximum of approximately 160 W/m^2 at 13:00 and not solar noon since it is driven by the temperature of the roof relative to that of the sky and the former is affected by the thermal inertia of the roof material (transient term). The difference in time between

solar noon and the time at which a property has its maximum will be referred to from this point on as a time lag. The energy loss to the ambient air via convection has a maximum of approximately 95 W/m^2 at 13:00. This is less than the emission losses, but would increase if wind were present.

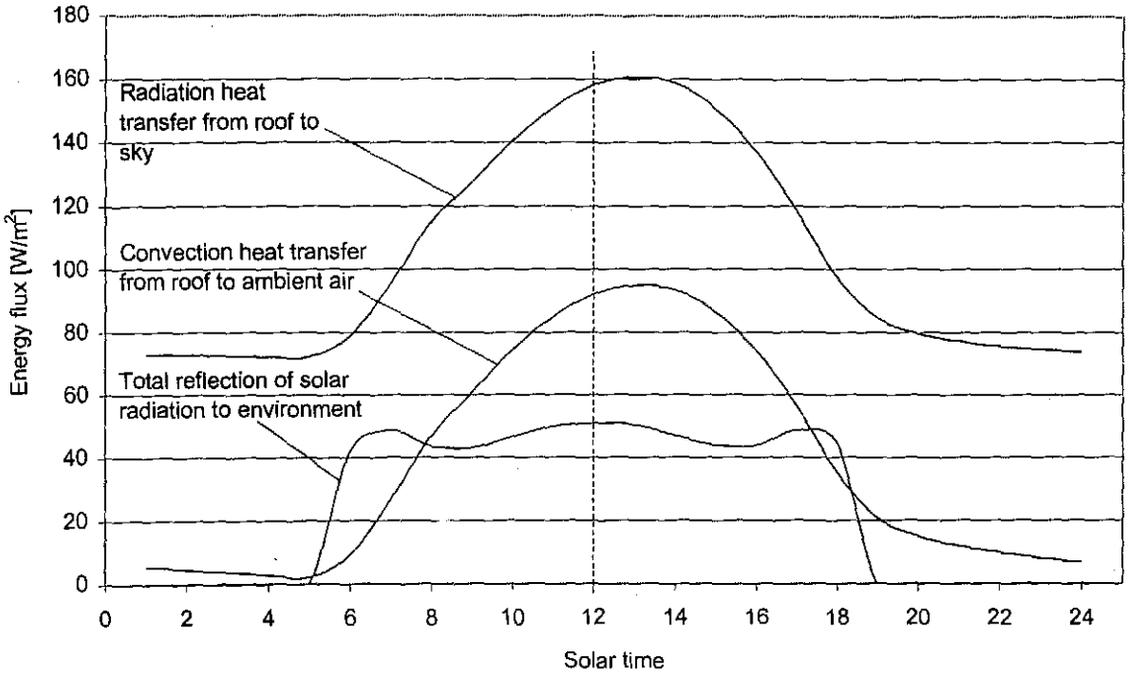

Figure 7.4: The heat lost to the environment via the collector roof on the 21 of December.

Figure 7.5 shows the heat transferred into the ground, air and glass. The net heat that is transferred into or out of the ground in a day is very small being positive in summer and negative in winter. This also is the case for the roof material. The air however shows a continuous absorption of energy since cool ambient air is drawn in continuously from the environment and the warm air is continuously returned from the chimney exit to the environment.

7.2.3. Collector performance

Figure 7.6 shows the collector air temperature at radii of 218 m, 1118 m, and 1982 m (The radii specified in the figures are the radii of the nodes closest to the inlet, midway and outlet radii). The increase in the air temperature as it passes through

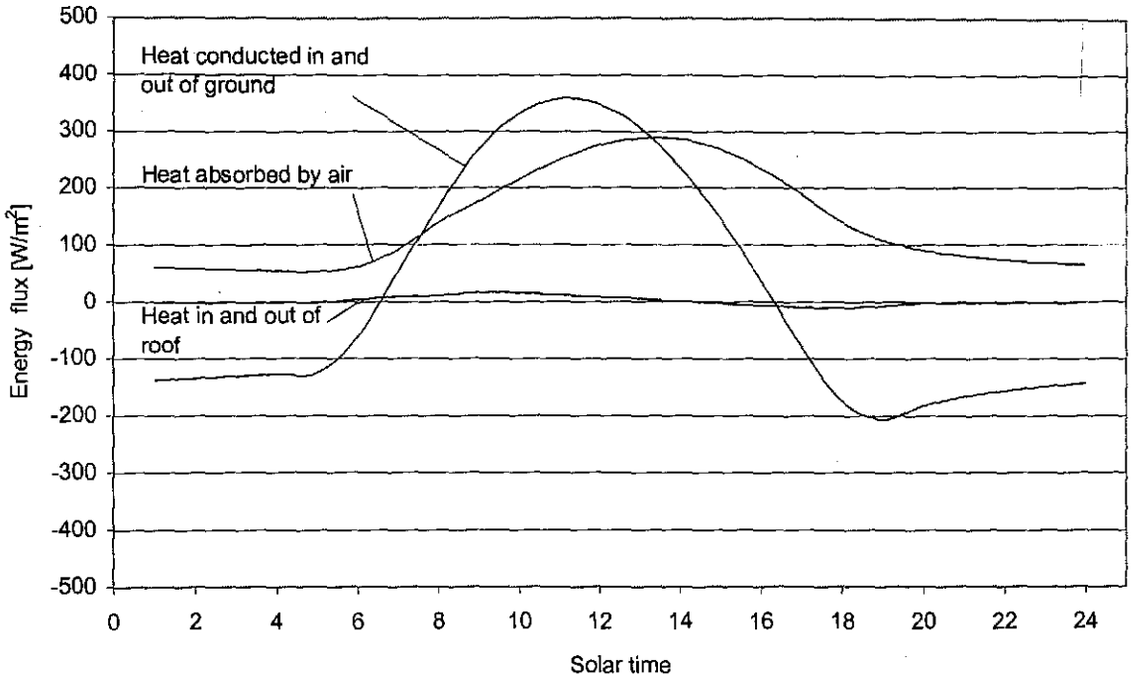

Figure 7.5: The power absorbed by the glass, ground and air on the 21 of December.

the collector (or ΔT over the collector) is a maximum at 14:00 of approximately 15 °C while at 5:00 it is only approximately 4.5°C. The time lag present in the air temperature is caused by the time lag present in the ground and roof temperatures as shown in figure 7.7. Figure 7.8 shows the radial temperature distribution of the ground, collector air and roof. It is clear from the figure that the collector air enters the collector at ambient temperature and is heated as it moves toward the chimney. The temperature gradient present in the air is steeper near the collector inlet since the boundary layer is thinner in this zone than closer to the chimney. The ground and roof temperatures also increase near to the collector inlet but show a decrease nearer to the collector outlet. This is attributed to the high heat transfer coefficients present near to the collector centre, which result from the higher collector air velocities there.

Transition from developing flow to fully developed flow occurs at a radius of approximately 1750 m. The discontinuity is due the difference between the results of the developing flow theory and the theory for the fully developed flow at that point.

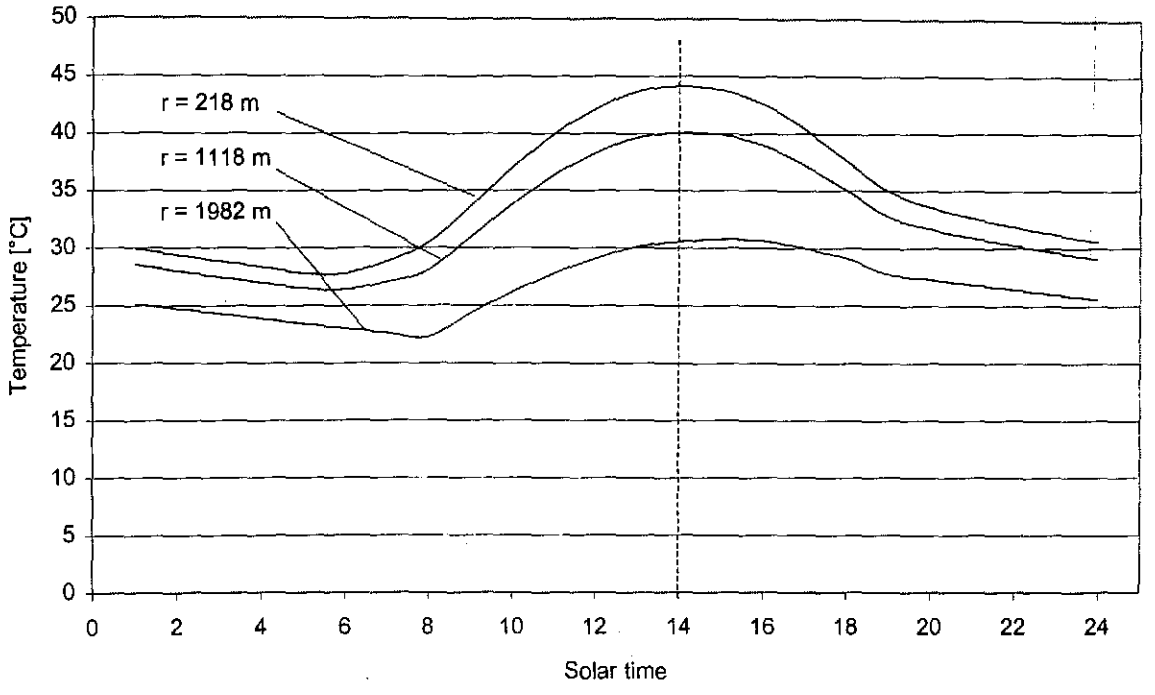

Figure 7.6: The collector air temperatures at radii of 218 m, 1118 m and 1982 m on the 21 of December.

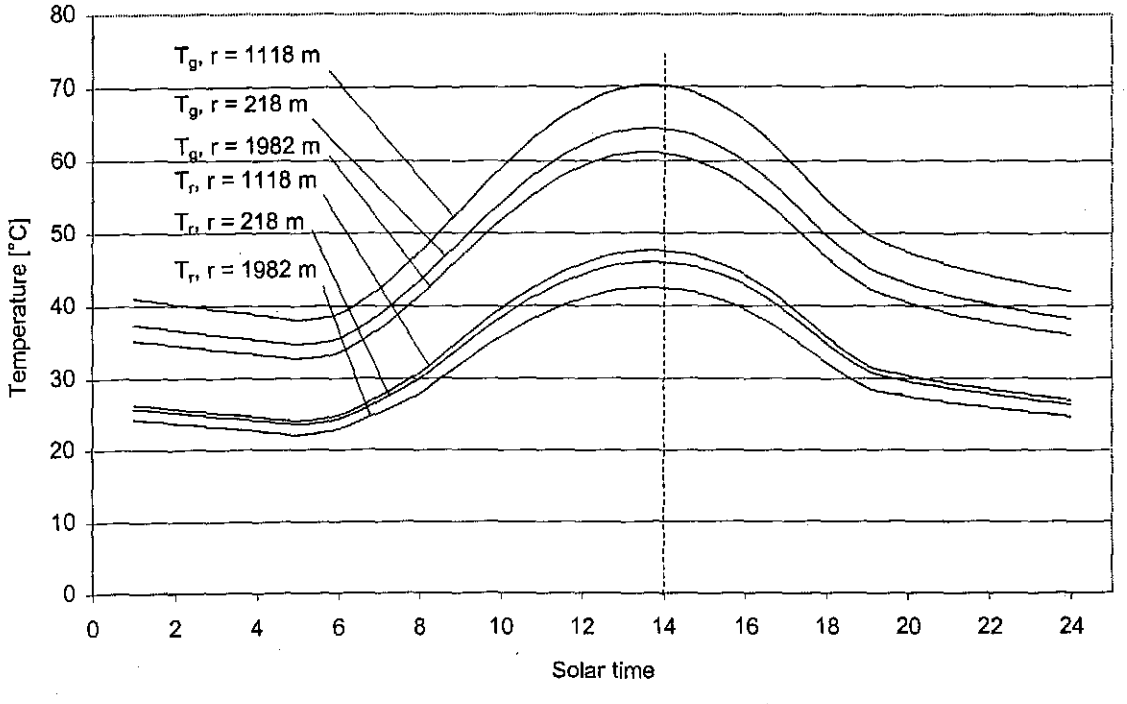

Figure 7.7: The ground and roof temperatures at radii of 218 m, 1118 m and 1982 m on the 21 of December.

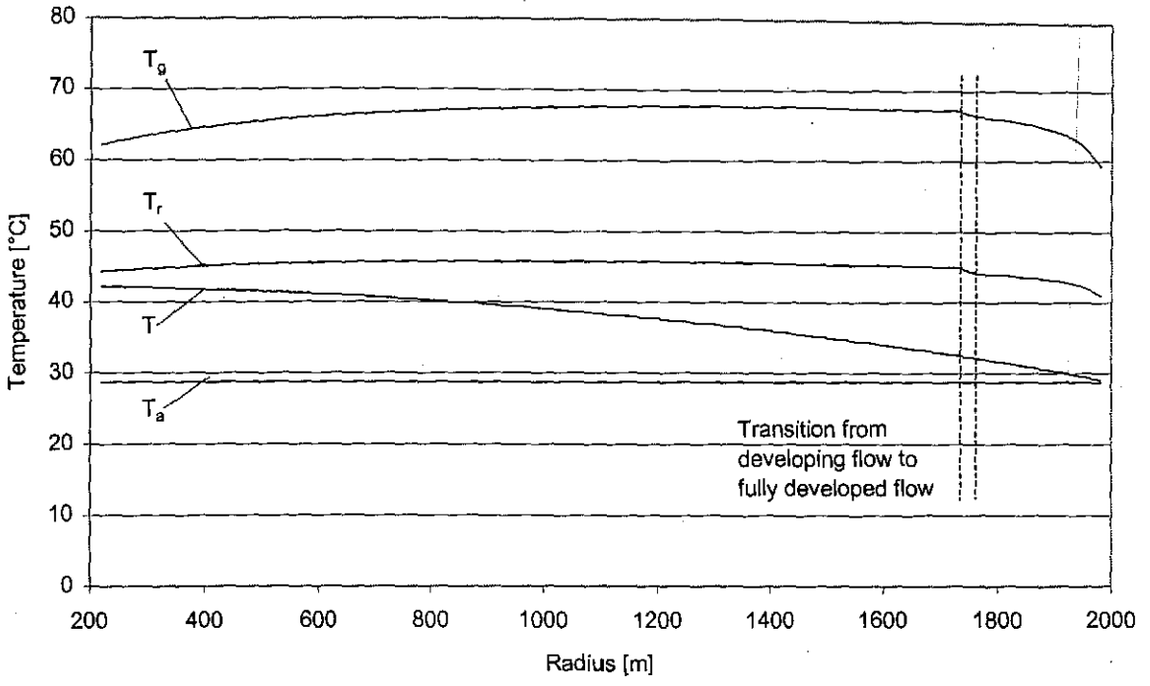

Figure 7.8: The radial distribution of the collector air, ambient air, roof and ground temperatures, at solar noon, on the 21 of December.

Figures 7.9 and 7.10 show the time and radial variation in the ground and roof heat transfer coefficients inside the collector. The ground heat transfer coefficient is considerably higher than the roof heat transfer coefficient since the former is modelled as a surface with roughness 0.05 m while the latter is modelled as smooth. Both figures show that the heat transfer coefficients are strongly dependant on the air velocity in the collector. The radial distributions however show high values near to the inlet, because of the thin boundary layer in the region of developing flow in spite of the low velocities present there.

Figures 7.11 and 7.12 respectively show how the collector air's velocity and density varies throughout the collector. As the air moves through the collector it is warmed and it's density decreases. This together with the reduced flow area caused by the radial flow geometry, causes the acceleration of the collector air. The roof height is increased to counteract this acceleration to reduce the frictional pressure losses in the collector. Note that the density only changes by 4% between the collector inlet and outlet at solar noon and less than that during the rest of the day.

Figure 7.13 shows the various pressure drops in the collector. The largest of these is the pressure drop caused the acceleration (momentum change) of the air as it moves

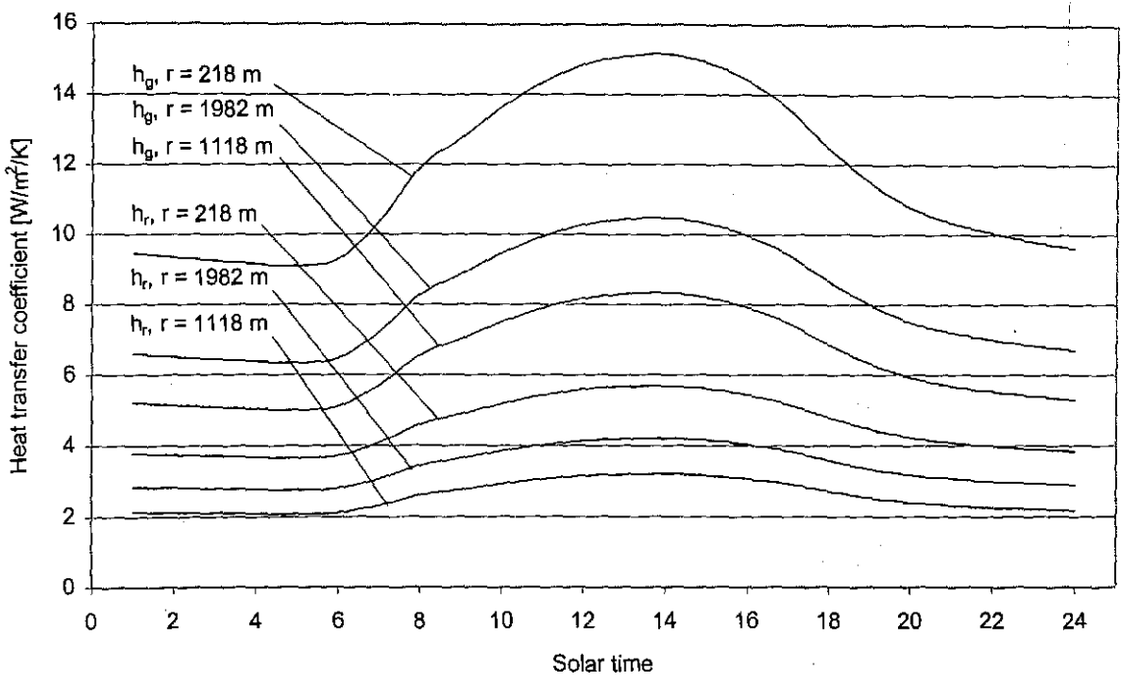

Figure 7.9: The heat transfer coefficients on the ground and roof in the collector at radii of 218 m, 1118 m and 1982 m on the 21 of December.

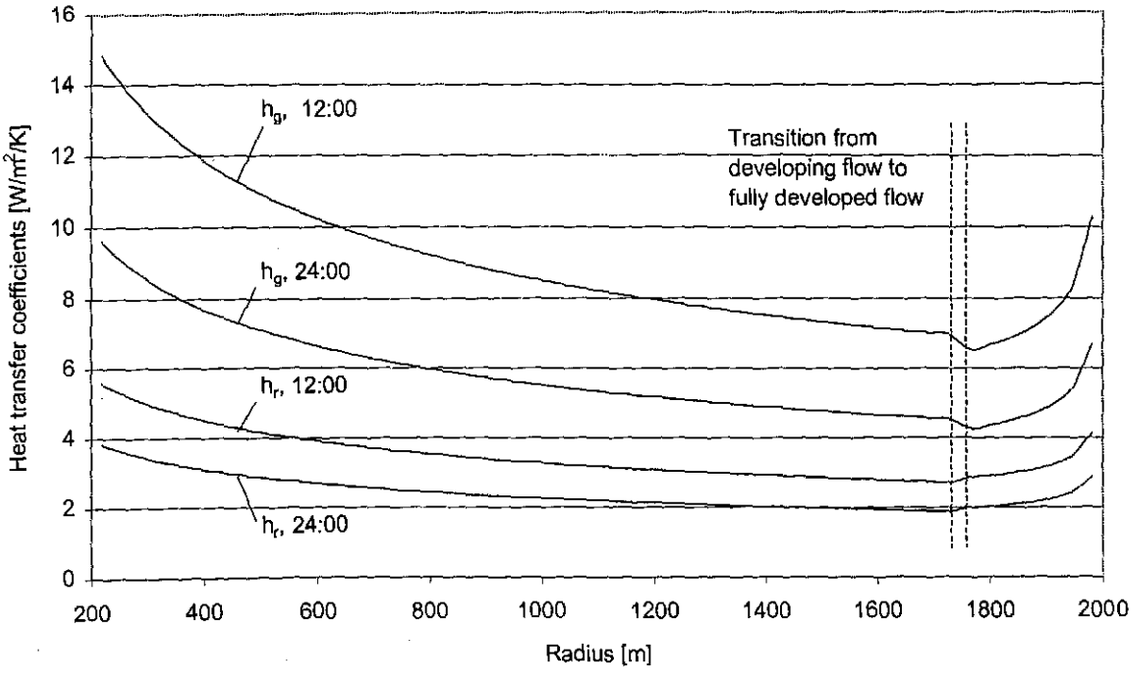

Figure 7.10: Radial variation of the ground and roof heat transfer coefficients on the 21 of December.

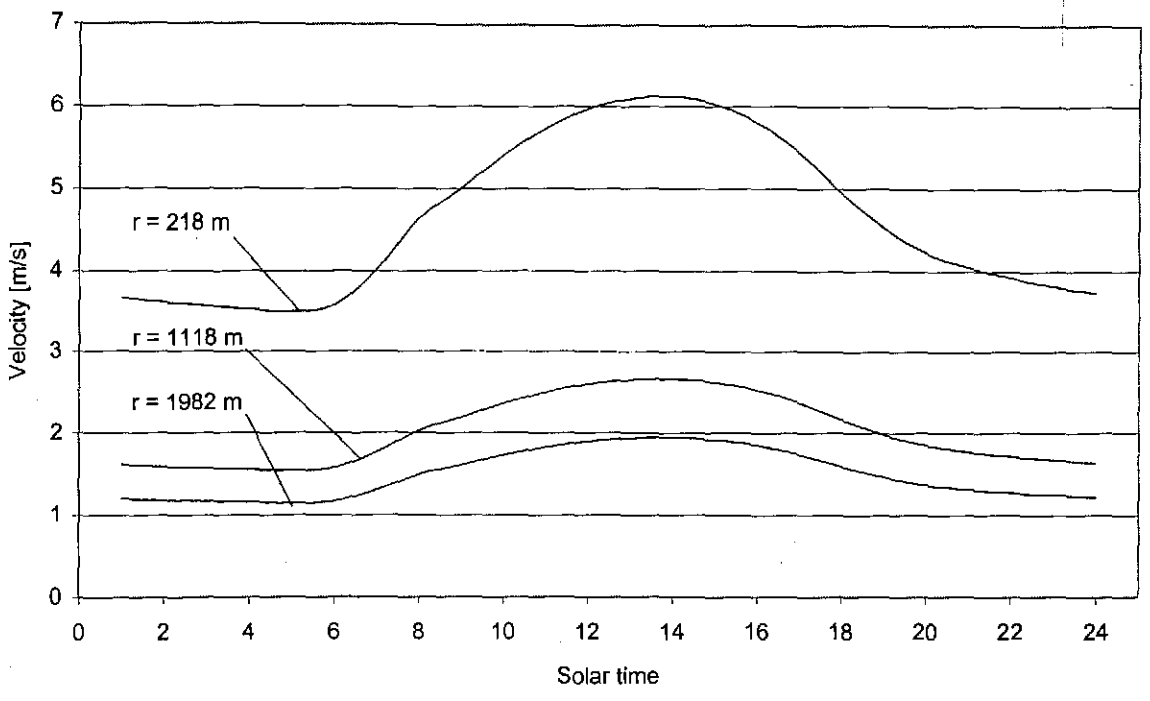

Figure 7.11: The collector air velocity at radii of 218 m, 1118 m and 1982 m on the 21 of December.

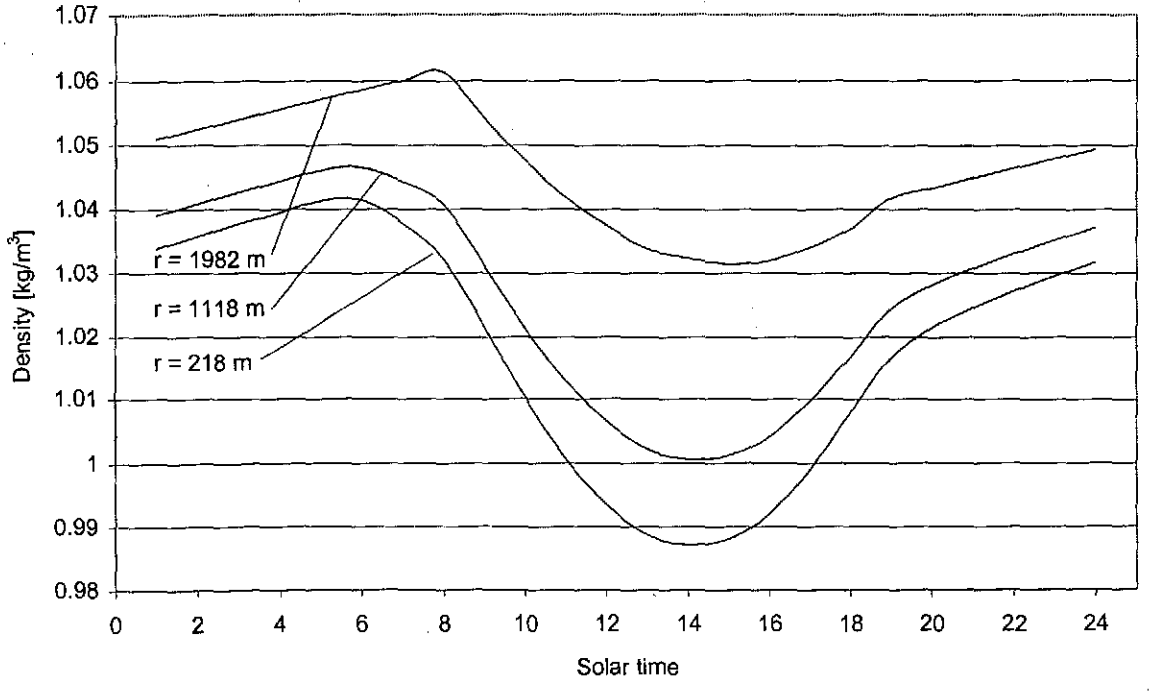

Figure 7.12: The collector density at radii of 218 m, 1118 m and 1982 m on the 21 of December.

through the collector. This is not an energy loss as the other pressure drops in the figure are, since the energy is merely transferred from enthalpy into kinetic energy. Both the collector inlet loss and the frictional losses are less then 10% of the pressure drop caused by the acceleration. Radial pressure distributions in the collector are shown in figure 7.14.

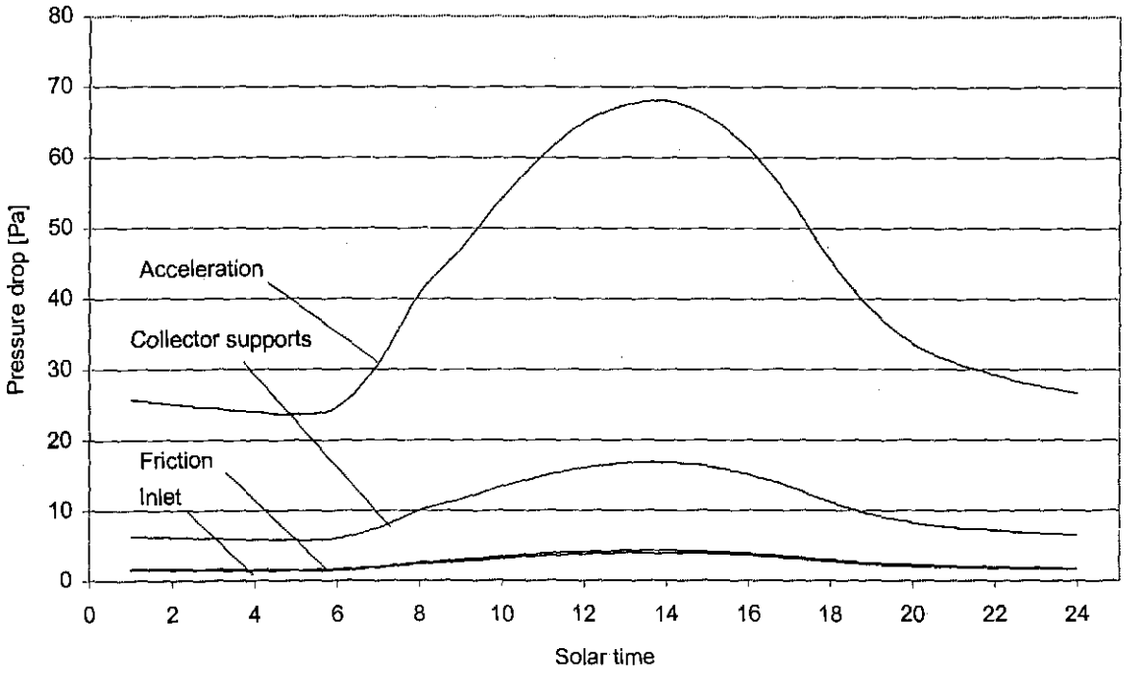

Figure 7.13: The pressure drops in the collector on the 21 of December.

7.2.4. Turbine performance

Figure 7.15 shows the variation of the turbine inlet velocity and density. Figure 7.16 shows the pressure drop over the turbine and the mass flow rate passing through the turbine. The range of the turbine pressure drop shown in the figure is from 160 Pa to 470 Pa. The mass flow rate ranges from approximately 200 000 kg/s at 5h00 (solar time) to approximately 300 000 kg/s at 14h00 (solar time). Figure 7.17 shows the turbine pressure drop as a percentage of the pressure driving potential.

7.2.5. Chimney performance

The average chimney pressure and temperature are shown in figure 7.18. These are used to determine the pressure changes in the chimney. Figure 7.19 shows the inlet and outlet chimney velocities and densities.

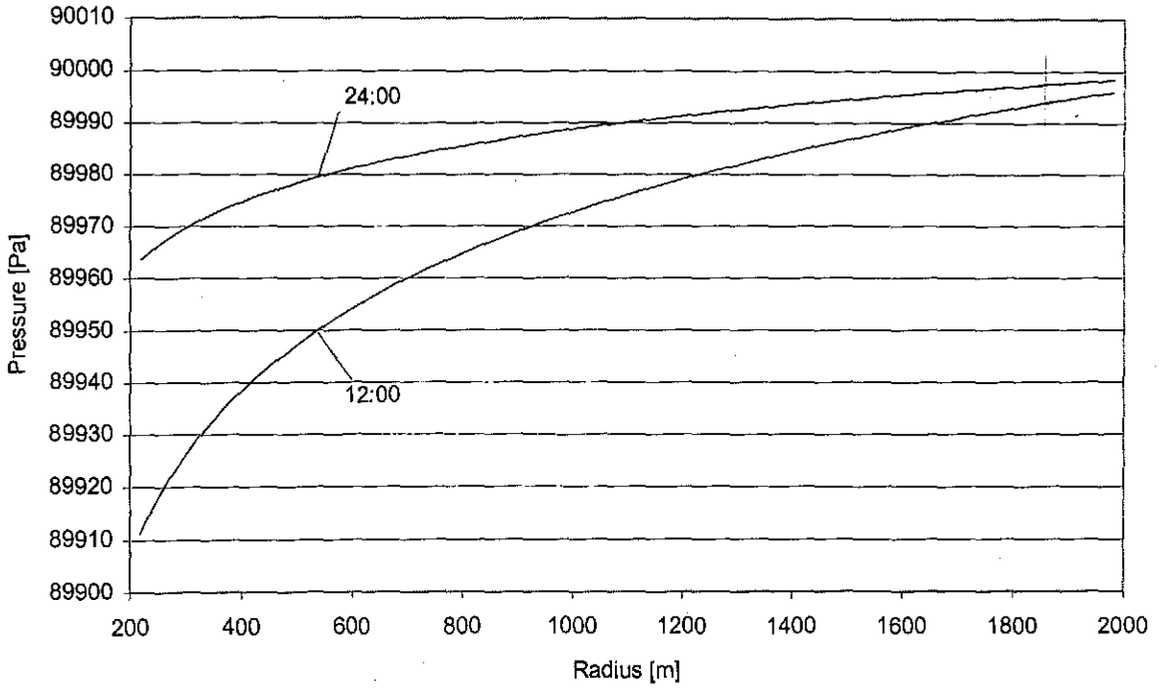

Figure 7.14: The pressure variation in the collector on the 21 of December at 12:00 and 24:00.

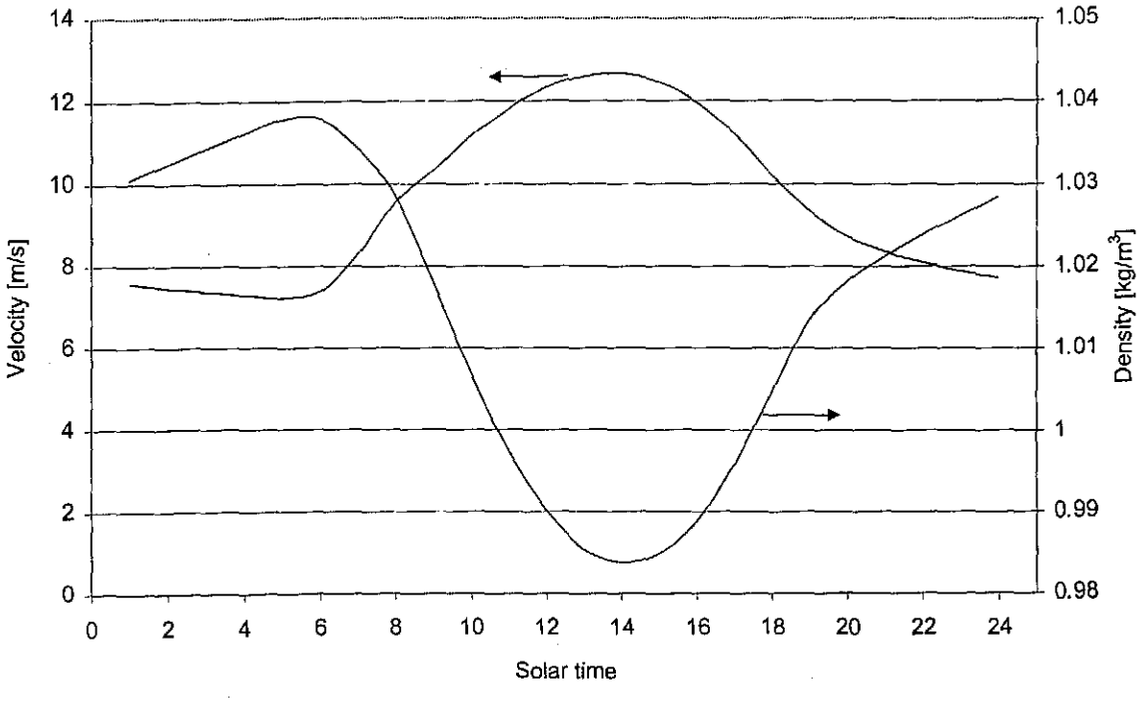

Figure 7.15: The turbine inlet velocity and density on the 21 of December.

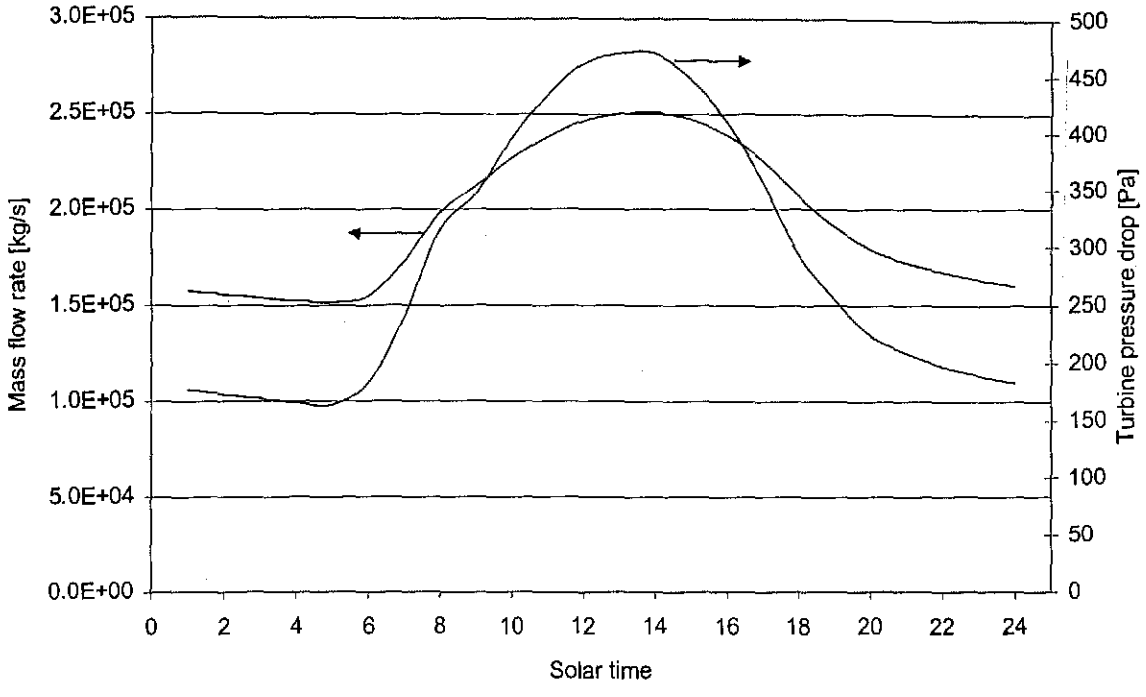

Figure 7.16: The turbine pressure drop and mass flow rate through the system on the 21 of December.

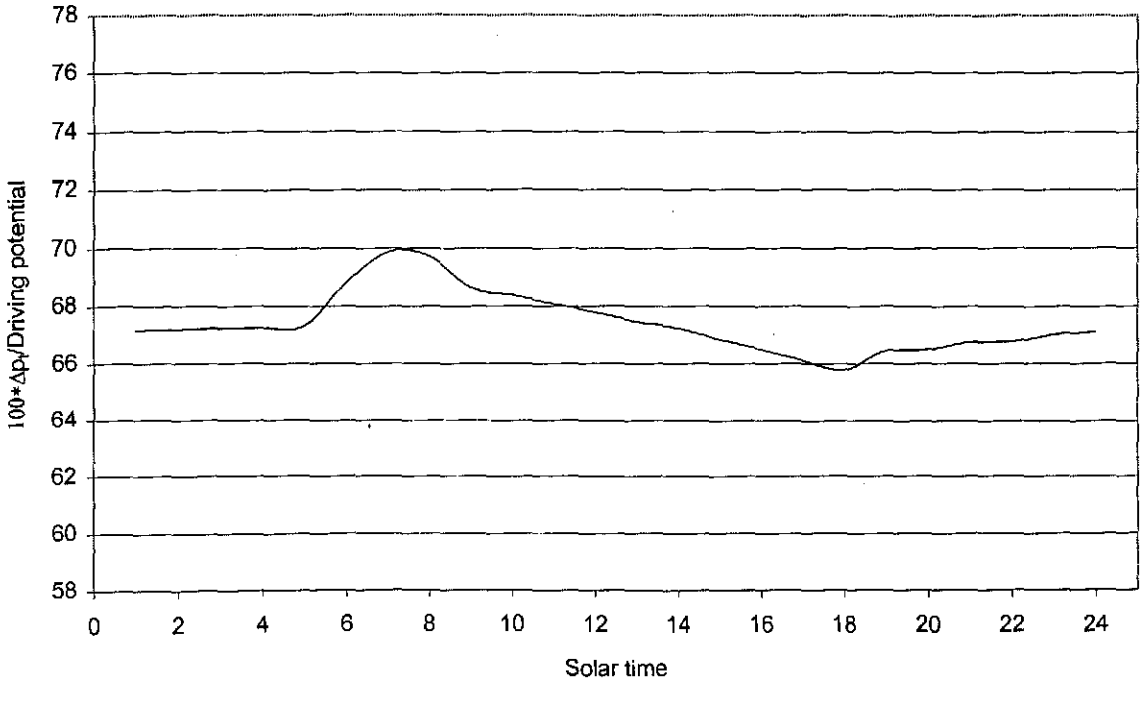

Figure 7.17: The turbine pressure drop as a percentage of the total pressure driving potential

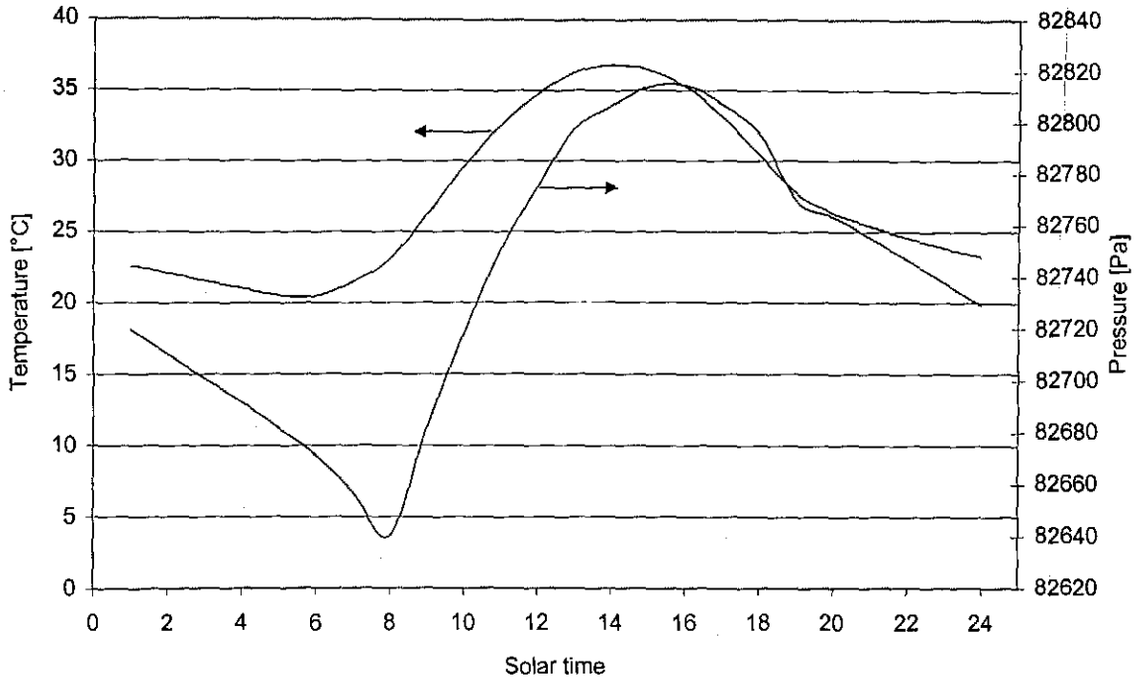

Figure 7.18: The average chimney pressure and temperature on the 21 December.

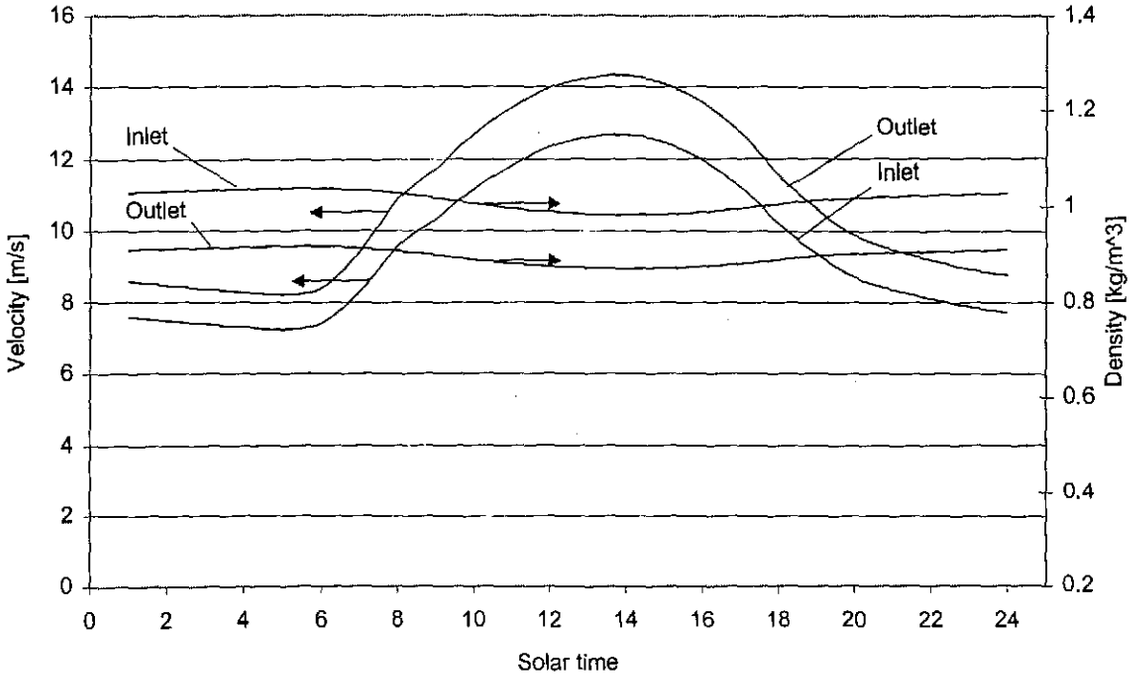

Figure 7.19: The chimney inlet and outlet velocities and densities on the 21 of December.

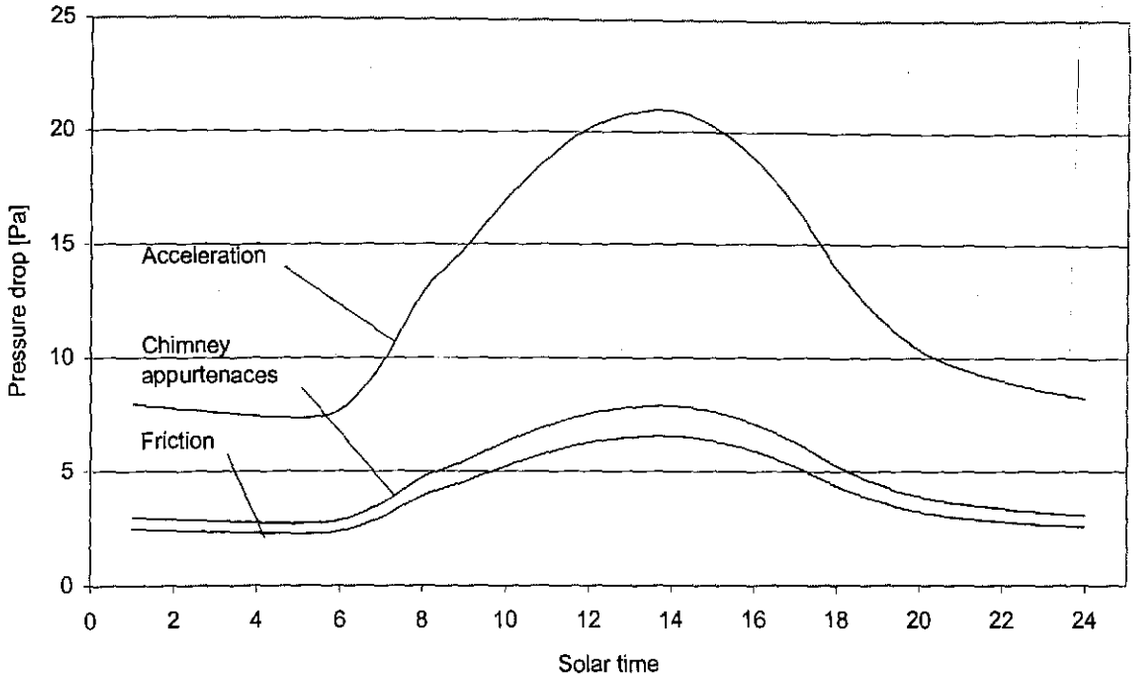

Figure 7.20: The pressure changes in the chimney on the 21 of December.

The pressure changes in the chimney are shown in figure 7.20. Once again the pressure change caused by the acceleration of the air is the greatest although it is not an energy loss, but rather transference from enthalpy to kinetic energy. Much of this kinetic energy is lost at the exit of the chimney.

A diffuser at the chimney exit would reduce this loss but the capital costs of such a diffuser would be very high. As this air exits the chimney it entrains the nearby ambient air which then moves up past the exit plane of the chimney with the chimney air. This induces a lower static pressure at the outlet of the chimney which has a positive effect on the draught of the system. The magnitudes of the dynamic pressure loss and the effective reduction in ambient pressure are shown in figure 7.21.

7.3. EFFECT OF INLET HEIGHT

By adjusting the reference plant's inlet height, it is possible to improve the overall performance of the plant as is shown in figure 7.22. It shows that by using an inlet height of approximately 4.7 m the annual power production can be increased from the reference plant's 367 GWh/annum to 406 GWh/annum.

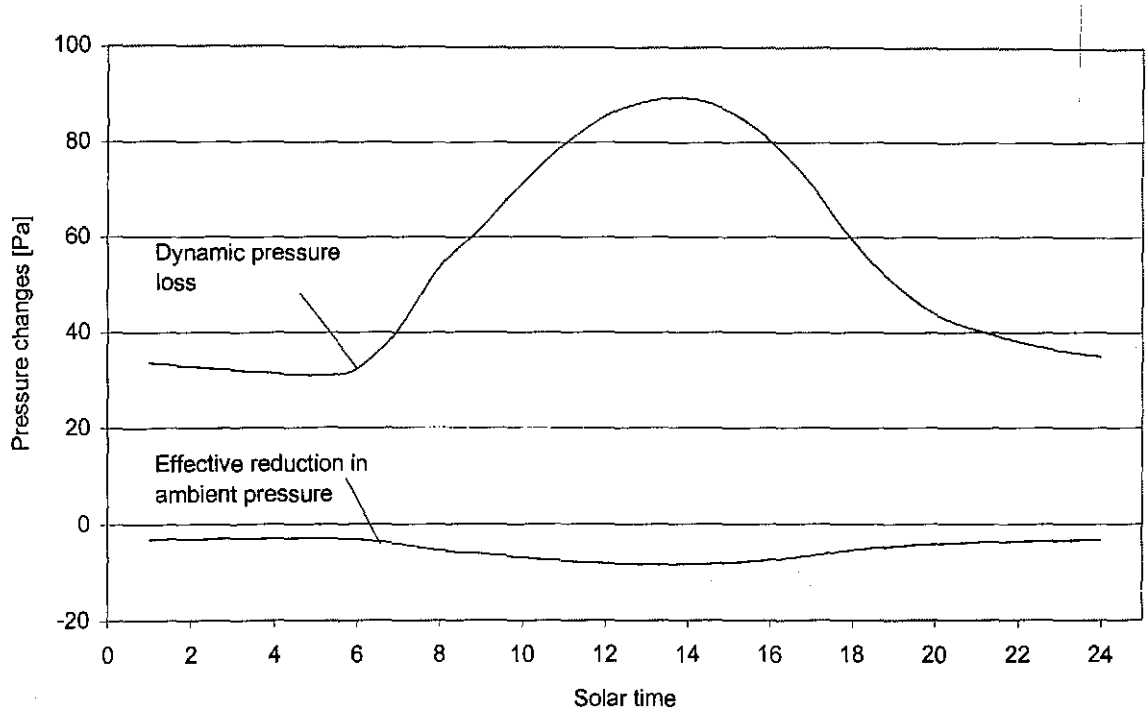

Figure 7.21: The chimney exit dynamic pressure loss and the effective reduction in ambient pressure on the 21 of December.

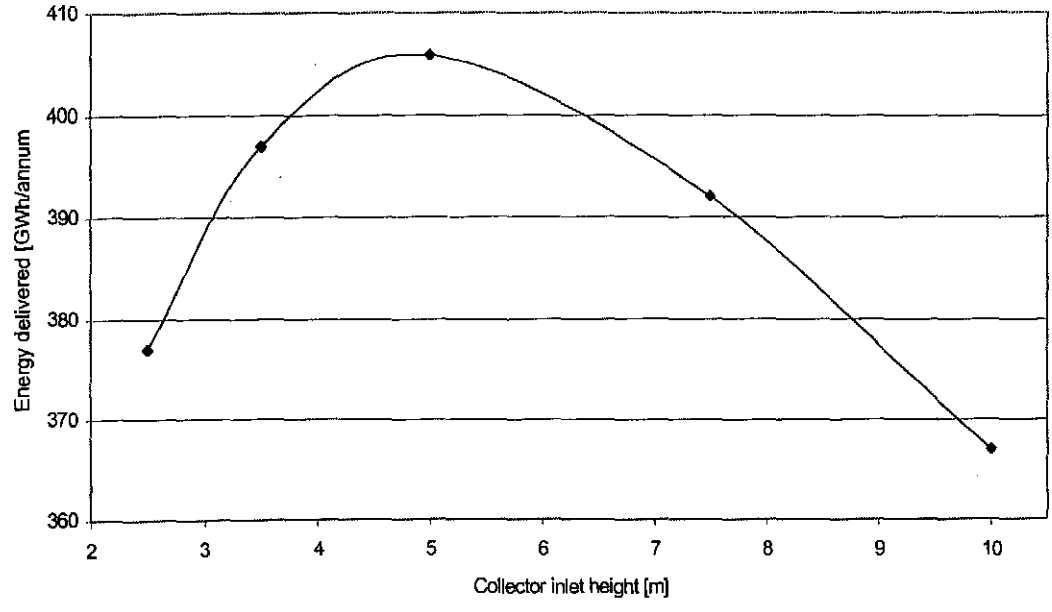

F

igure 7.22: The effect of varying the collector inlet height.

8. CONCLUSION

The solar chimney power plant is possibly one solution to help alleviate the problems associated with pollution and the sometimes limited local fossil fuel deposits in parts of world. The solar chimney power plant is capable of storing energy during the day so that power may be generated during the night as well.

In order to facilitate the study of a solar chimney power plant performance, a reference plant was defined with plant dimensions and meteorological conditions prevalent at a reference location. This also facilitates the further study of the system by other researchers who could use the reference plant for purposes of comparison.

In order to evaluate its performance the reference solar chimney power plant was modelled using a mathematical model based on energy and draught equations. These were solved numerically subject to boundary conditions, which consisted of the environmental conditions that were applicable to a period of a year at the reference location.

The power delivered varies considerably throughout each day and also during the year. On the 21 of December the plant delivers approximately 118 MW at 13h00, and only 24.5 MW at 5h00. On the 21 of June however the power delivered is only approximately 53 MW at 13h00 and 12 MW at 5h00. This difference between the winter and summer values may be attributed to the fluctuation of solar radiation during the year and also to the decrease of the plant's effectiveness during the winter months.

On the 21 of December the following applies to the reference plant: The temperature rise as the air moves through the collector is approximately 15 °C at 14h00 and 4.5 °C at 6h00. The pressure drop across the collector due to the inlet pressure loss, the collector supports, the friction on the ground and roof and the acceleration is approximately 90 Pa at 14h00 and 37 Pa at 6h00. The pressure drop through the chimney due to the appurtenances, friction and acceleration is approximately 40 P at 14h00 and 12 Pa at 6h00. The dynamic pressure loss at the chimney exit ranges between approximately 90 Pa and 31 Pa at 14h00 and 6h00 respectively. The effective reduction in ambient pressure ranges between 2.2 Pa and 6.5 Pa at 14h00 and 6h00 respectively.

The mass flow rate of air through the system is approximately 300 000 kg/s at 14h00 and 200 000 kg/s at 6h00. The velocity of the air entering the collector is approximately 2 m/s and at the collector exit it is approximately 6 m/s at 14h00 and 3.5 m/s and 1.1 m/s at 6h00. At the inlet to the turbine the air velocity at 14h00 and 6h00 is approximately 12.7 m/s and 7.5 m/s respectively. The pressure drop over the turbine ranges from approximately 470 Pa to 160 Pa at 14h00 and 6h00 respectively.

The total energy delivered by the reference plant is 367 GWh/annum but by reducing the collector inlet height to 4.7 m, this can be increased to a value of approximately 406 GWh/annum

The present study did not take the effects of humidity into account. A part of the solar chimney concept is to use the green house effect that is present in the collector for agricultural purposes if sufficient water is available. This could be done by planting crops in the outer annulus of the collector where the air velocities are not high enough to damage the crops or cause wind erosion. The moisture given off by the crops would increase the humidity of the collector air, which would subsequently become less dense. This would have a positive effect on the draught of the system. The possibility of condensation in the chimney should also be investigated.

The effects of the solar chimney system on the environment should also be analysed. The large collector surface, which is warmer than the ambient air will have a warming effect on the air just above it. This may affect the energy transferred to the ambient air via convection. The present model of the system could be modified to incorporate the heating of the ambient air. This heating effect may cause movement of the ambient air that should also be taken into account.

The turbine located at the base of the chimney should be analysed in order to optimise its performance. The present study assumed a constant efficiency for all pressure drops, and mass flow rates. This too, should be improved in order to make accurate predictions about the overall system performance.

9. REFERENCES

63SW1 Swinbank, W.C., Long-wave Radiation from Clear Skies, Quart. J.R. Meteorol. Soc., Vol. 89, 1963.

74DU1 Duffie, J.A., and Beckman, W.A., Solar Energy Thermal Processes, John Wiley and Sons, 1974.

75GN1 Gnielinski, V., Forsch. Ing. Wesen, Vol. 41, No. 1, 1975.

82AN1 Anon., Heat Transfer and Fluid Flow data Book, General Electric Co., Corporate Research Division, New York, 1982.

83HA1 Haaf, W., Freidrich, K., Mayr, G. and Schlaich, J., Solar Chimneys, Part1, Principle and Construction of the Pilot Plant in Manzanares, International Journal of Solar Energy, Vol. 2, 1983.

83HA2 Haaland, S.E., Simple Explicit Formulas for the Friction Factor in Turbulent Pipe Flow, Trans. ASME, J. Fluids Engineering, Vol. 105, No. 3. pp. 89 – 90, 1983.

84BE1 Bejan, A., Convection Heat Transfer, John Wiley and Sons, 1984.

84HA1 Haaf, W., Solar Chimneys, Part 2, Preliminary Test Results from the Manzanares Pilot Plant, International Journal of Solar Energy, Vol. 2, 1984.

87MU1 Mullet, L.B., The Solar Chimney-Overall Efficiency, Design and Performance, International Journal of Ambient Energy, Vol. 8, 1987.

88PA1 Padki, M.M. and Sherif, S.A., Fluid Dynamics of Solar Chimneys, Porceedings of the ASME Winter Annual Meeting, 1988.

89FR1 Fried, E. and Idelchik, I.E., Flow Resistance: A Design Guide for Engineers, Hemisphere Publ. Co., New York, 1989.

89PA1 Padki, M.M. and Sherif, S.A., Solar Chimneys for Medium-to-Large Scale Power Generation, Proceedings of the Manila International Symposium on the Development and Management of Energy Resources, Vol. 1, 1989.

89PA2 Padki, M.M., Sherif, S.A. and Chan, A.B., Solar chimneys for Power Generation for Rural Areas, Seminar on Energy Conservation and Generation Through Renewable Sources, 1989.

91DU1 Duffie, J.A., and Beckman, W.A., Solar Engineering of Thermal Processes, Second Edition, John Wiley & sons ,Inc, 1991.

94DU1 Du Preez, A.F., and Kröger, D.G., The Influence of a Buoyant Plume on the Performance of a Natural Cooling Tower, 9th IAHR Cooling Tower and Spraying Pond Symposium, Brussels, 1994.

94PO1 Poulikakos, D., Conduction Heat Transfer, Prentice Hall, New Jersey, 1994.

94SC1 Schlaich, J., The Solar Chimney :Electricity from the Sun, Deutsche Verlags-Anstalt, Stuttgart 1994.

96RA1 Rao, S.S., Engineering Optimisation Theory and Practice, Third Edition, John Wiley and Sons, 1996.

99BU1 Buys, J.D., Personal communication, 1999.

98KR1 Kröger D.G., Air Cooled Heat Exchangers and Cooling Towers, Begell House, New York, 1998.

99BL1 Blaine, D.C., and Kröger, D.G., Analysis of the Driving Potential of a Solar Chimney Power Plant, South African Institute of Mechanical Engineering, R & D Journal, Vol. 15, pp. 85-94, 1999.

99HA1 Harms, T.M., Personal communication, 1999.

99SA01 South African Weather Bureau, Department of Environmental Affairs, 1999.

99KR1 Kröger D.G. and Buys J.D., Radial Flow Boundary Layer Development Analysis, South African Institute of Mechanical Engineering, R & D Journal, 1999.

00GA1 Gannon, A.J. and Von Backström, W., Solar Chimney Cycle Analysis with System Losses and Solar Collector Performance, Solar 2000, 2000.

APPENDIX 1. REFERENCE PLANT SPECIFICATIONS

The following specifications apply to an arbitrary solar chimney power plant also referred to as the reference plant.

Table A1.1. Collector Dimensions

Collector inlet radius	r_i	= 2000 m
Collector outlet radius	r_o	= 200 m
Collector inlet height	H_i	= 10 m
Collector roof shape	H	= $H_i (r_i/r)^b$ m (with b = 0.5)
Radial pitch of supports	P_{sr}	= 10 m
Tangential pitch of supports	P_{st}	= 10 m
Collector support diameter	d_s	= 0.15 m
Roof thickness	t_r	= 0.005 m
Roof roughness	e_r	= 0.0 m
Drag coefficients of supports	C_{sD}	= 1
Collector inlet loss coefficient	K_i	= 1
Upper heat transfer coefficient	h_{ra}	= 5.7 W/m^{2}K

Table A1.2. Chimney Dimensions

Chimney height	H_c	= 1500 m
Chimney inside diameter	d_c	= 160 m
Drag coefficient due to appurtenances (based on chimney cross sectional area)	K_{cD}	= 0.1
Inside surface roughness	e_c	= 2×10^{-3} m

Table A1.3. Ground Properties (Granite)

Density	ρ_g	= 2640 kg/m^3
Specific Heat	c_{pg}	= 820 J/kgK
Conductivity	k_g	= 1.73 W/mK
Absorbtivity	α_g	= 0.9
Emissivity	ε_g	= 0.9
Ground roughness	e_g	= 0.05 m

Table A1.4. Roof Properties (5mm thick green of edge Glass)

Density	ρ_r	= 2700 kg/m^3
Specific Heat	c_{pr}	= 840 J/kgK
Thermal conductivity	k_r	= 0.78 W/mK
Absorbtivity	α_r	= 0
Emissivity	ε_r	= 0.87
Extinction coefficient	e_c	= 32 /m

Table A1.5. Ambient Conditions

Air pressure	p_a	= 90 000 Pa
Wind velocity	v_w	= 0 m/s
Relative humidity	θ	= 0 %
Cloud cover		= 0 %
Ambient temperature	T_a	= (as per Appendix 2)
Solar radiation	I_h, I_d	= (as per Appendix 2)
Latitude	Lat	= 27.67° South
Longitude	Long	= 23.00° East
Sky temperature	T_{sky}	= $0.0552T_a^{1.5}$

APPENDIX 2. METOROLOGICAL DATA OF REFERENCE LOCATION

A2.1. INTRODUCTION

In order to model the solar chimney power plant it is necessary to model the environment at the reference location. This location was selected near Sishen in South Africa. The co-ordinates of this location are as follows:

Latitude 27.67° South
Longitude 23.00° East

The main influence that the environment will have on the solar chimney power plant's performance will be as a result of the ambient temperature and the radiation prevalent at the location.
Other influences might include the humidity and wind conditions.

A2.2. EFFECTIVE AMBIENT TEMPERATURE

The ambient temperature is the temperature that occurs at approximately 1.5 m above ground level outside the solar chimney system. Each temperature is the average temperature that occurred in that hour, for an average day in that month. The ambient temperature data recorded by the weather station is shown in table A2.1.

A2.3. SOLAR RADIATION

The total solar radiation prevalent at a location is comprised of beam and diffuse radiation. The data used for the environment model consists of total radiation and diffuse radiation. Thus the beam radiation is calculated using equation (2.23). The distinction between beam and diffuse radiation is necessary since the properties that describe the behaviour of each type of radiation differ. The data is shown in table A2.2. The hours not indicated in the table have negligible radiation.

Table A2.1: Ground Level Ambient Temperature at Reference Location, (°C)

	1	2	3	4	5	6	7	8	9	10	11	12	13	14	15	16	17	18	19	20	21	22	23	24
Jan	25.52	25.09	24.66	24.33	23.8	23.37	22.94	22.51	24.1	25.9	27.6	29	30	30.5	30.7	30.5	30.1	29.3	28.1	27.67	27.24	26.81	26.38	25.95
Feb	24.89	24.46	24.03	23.6	23.17	22.74	22.31	21.88	22.7	24.5	26.2	27.6	28.7	29.4	29.5	29.3	28.7	27.9	27.47	27.04	26.61	26.18	25.75	25.32
Mar	22.59	22.16	21.73	21.3	20.87	20.44	20.01	19.58	20.7	22.8	24.5	25.9	26.8	27.4	27.5	27.3	26.5	25.6	25.17	24.74	24.31	23.88	23.45	23.02
Apr	18.19	17.76	17.33	16.9	16.47	16.04	15.61	15.18	16.5	18.8	20.6	22	23	23.6	23.9	23.6	23	21.2	20.77	20.34	19.91	19.48	19.05	18.62
May	15.96	15.53	15.1	14.67	14.24	13.81	13.38	12.95	12.52	14.8	16.9	18.4	19.5	20.2	20.4	20.3	19.4	18.97	18.54	18.11	17.68	17.25	16.82	16.39
Jun	13.16	12.73	12.3	11.87	11.44	11.01	10.58	10.15	9.72	11.3	13.6	15.4	16.5	17.3	17.7	17.5	16.6	16.17	15.74	15.31	14.88	14.45	14.02	13.59
Jul	14.06	13.63	13.2	12.77	12.34	11.91	11.48	11.05	10.62	11.4	13.8	15.7	17	17.9	18.3	18.2	17.5	17.07	16.64	16.21	15.78	15.35	14.92	14.49
Aug	14.79	14.36	13.93	13.5	13.07	12.64	12.21	11.78	11.35	13.7	15.9	17.7	19.1	20	20.5	20.5	19.9	17.8	17.37	16.94	16.51	16.08	15.65	15.22
Sep	19.59	19.16	18.73	18.3	17.87	17.44	17.01	16.58	16.15	18.5	20.6	22.2	23.5	24.3	24.7	24.7	24.1	22.6	22.17	21.74	21.31	20.88	20.45	20.02
Oct	22.09	21.66	21.23	20.8	20.37	19.94	19.51	19.08	19.4	21.5	23.3	24.8	25.9	26.6	26.9	26.9	26.3	25.1	24.67	24.24	23.81	23.38	22.95	22.52
Nov	22.52	22.09	21.66	21.23	20.8	20.37	19.94	20	22.2	24.1	25.7	27	27.9	28.5	28.6	28.4	27.9	27	25.1	24.67	24.24	23.81	23.38	22.95
Dec	24.92	24.49	24.06	23.63	23.2	22.77	22.34	21.91	24	25.8	27.4	28.6	29.7	30.1	30.4	30.3	29.7	28.9	27.5	27.07	26.64	26.21	25.78	25.35

Table A2.2: Total (I_h) and Diffuse (I_d) Solar Radiation on a Horizontal Surface at Reference Location, ($W.m^2$)

	6		7		8		9		10		11		12		13		14		15		16		17		18	
	I_h	I_d	I_h	I_d	I_h	I_d	I_h	I_d	I_h	I_d	I_h	I_d	I_h	I_d	I_h	I_d	I_h	I_d	I_h	I_d	I_h	I_d	I_h	I_d	I_h	I_d
Jan	138	52	357	89	572	108	762	126	909	136	1003	140	1035	135	1003	140	909	136	762	130	572	114	357	82	138	40
Feb	68	46	279	86	496	109	691	124	845	144	942	151	976	156	942	160	845	161	691	145	496	114	279	75	68	24
Mar	0	0	190	72	406	102	604	121	763	130	865	138	900	144	865	138	763	145	604	133	406	102	180	54	0	0
Apr	0	0	100	50	299	84	489	112	644	129	745	134	780	148	745	142	644	129	489	108	299	78	110	31	0	0
May	0	0	35	18	220	66	407	85	562	101	664	106	700	105	664	100	562	96	407	77	220	48	35	11	0	0
Jun	0	0	19	10	190	63	368	88	517	109	616	117	650	111	616	105	517	93	368	70	190	44	19	6	0	0
Jul	0	0	35	17	220	66	407	90	562	107	664	113	700	112	664	106	562	96	407	77	220	48	35	12	0	0
Aug	0	0	99	50	295	91	483	106	636	127	735	125	770	123	735	125	636	114	483	101	295	71	99	32	0	0
Sep	0	0	182	78	388	109	578	127	730	139	827	149	861	155	827	149	730	146	578	121	388	97	182	58	0	0
Oct	66	45	272	95	483	121	673	141	822	156	917	165	950	181	917	183	822	173	673	155	483	135	272	90	66	28
Nov	135	62	348	90	558	112	743	126	887	133	979	137	1010	131	979	137	887	142	743	134	558	117	348	87	135	45
Dec	157	58	375	83	587	103	773	108	917	119	1009	121	1040	114	1009	131	917	128	773	124	587	116	375	86	157	49

APPENDIX 3. SAMPLE OF OUTPUT FILES GENERATED BY THE 'SOLCHIM' CODE

A3.1. TIME PROPERTY DISTRIBUTION

The 'time.out' file contains a list of collector temperatures, the mass flow rate, the power output and accumulative energy generated (arranged according to ascending time). This file is appended line for line at the end of each modelled hour. A section of a sample 'time.out' file is shown in table A3.1.

A3.2. RADIAL PROPERTY DISTRIBUTION

The 'radi.out' file contains a list of collector temperatures, pressures and heat transfer coefficients (arranged according to descending radius, for each day). This file is appended once during every modelled day on the hour specified by the variable *hour_sam*. A section of a sample 'radi.out' file is shown in table A3.2.

A3.3. GROUND TEMPERATURE DISTRIBUTION

The 'ground.out' file contains a list of ground temperature distributions taken from below the chimney exit (arranged according to ascending time). This file is appended line for line at the end of each modelled hour. A section of a sample 'ground.out' file is shown in table A3.3.

Table A3.1. A sample of two sections of the 'time.out' output file.

Day1: 1
Radius: 218

			Tsky	Tr	T	Ta	Tgl	Power	Dpt	m	accumP
			[°C]	[°C]	[°C]	[°C]	[°C]	[MW]	[Pa]	[kg/s]	[GWh]
jul	21	1h00	-4.263	12.172	16.893	14.206	21.659	12.06	105.3	123349.4	187.3
jul	21	2h00	-4.867	11.691	16.434	13.776	21.188	11.91	104.6	122888	187.3
jul	21	3h00	-5.469	11.22	15.984	13.346	20.737	11.82	104.1	122634.8	187.3
jul	21	4h00	-6.072	10.755	15.541	12.916	20.304	11.78	104	122556.5	187.3
jul	21	5h00	-6.674	10.297	15.104	12.486	19.885	11.78	104.1	122624.6	187.4
jul	21	6h00	-7.275	9.844	14.672	12.056	19.477	11.81	104.3	122817	187.4
jul	21	7h00	-7.876	9.633	14.327	11.626	19.329	12.43	108.8	124087.8	187.4
jul	21	8h00	-8.477	11.169	14.655	11.196	21.028	17.97	144.4	135022.7	187.4
jul	21	9h00	-9.077	13.866	15.856	10.766	24.606	31.99	212.2	162880.3	187.4
jul	21	10h00	-7.549	17.312	18.088	11.86	28.944	42.79	252.1	181991.1	187.5
jul	21	11h00	-4.244	21.201	21.197	14.22	33.283	49.61	272.4	193212.3	187.5
jul	21	12h00	-1.6	24.223	23.917	16.1	36.721	57.71	298.4	203261.8	187.6
jul	21	13h00	0.261	25.813	25.632	17.42	38.563	61.36	308	208222	187.6
jul	21	14h00	1.532	25.924	26.289	18.32	38.535	58.27	294.5	206284.7	187.7
jul	21	15h00	2.126	24.486	25.855	18.74	36.584	49.11	260.3	197072.4	187.7
jul	21	16h00	2.013	21.621	24.421	18.66	33.025	35.96	209.5	180181.2	187.8
jul	21	17h00	1.051	18.199	22.444	17.98	29.175	24.8	164.1	159689	187.8
jul	21	18h00	-0.027	16.415	21.02	17.216	27.013	19.71	143.6	145725.9	187.8
jul	21	19h00	-0.634	15.579	20.165	16.786	25.726	16.58	128.3	137631.9	187.8
jul	21	20h00	-1.24	14.891	19.502	16.356	24.765	14.97	120.3	132819.2	187.9
jul	21	21h00	-1.845	14.28	18.914	15.926	23.986	13.92	115	129456.3	187.9
jul	21	22h00	-2.451	13.718	18.373	15.496	23.32	13.21	111.3	127127	187.9
jul	21	23h00	-3.055	13.186	17.864	15.066	22.73	12.72	108.8	125501.1	187.9
jul	21	24h00	-3.659	12.677	17.376	14.636	22.191	12.37	107	124370.9	187.9
dec	21	1h00	11.086	25.816	29.961	25.04	37.401	27.04	176.9	157524.7	351.1
dec	21	2h00	10.471	25.222	29.391	24.61	36.662	25.99	172.5	155555.1	351.2
dec	21	3h00	9.857	24.649	28.843	24.18	35.976	25.13	168.9	153915.2	351.2
dec	21	4h00	9.272	24.106	28.322	23.77	35.336	24.34	165.5	152409.8	351.2
dec	21	5h00	8.63	23.558	27.801	23.32	34.728	23.87	163.6	151451.4	351.2
dec	21	6h00	8.017	24.326	27.776	22.89	35.505	27.22	182.6	154710.3	351.3
dec	21	7h00	7.405	26.899	28.789	22.46	38.738	39.99	239.5	172702.5	351.3
dec	21	8h00	6.793	29.961	30.426	22.03	43.407	60.86	315.8	198219	351.3
dec	21	9h00	9.629	34.249	33.556	24.02	48.813	72.24	346.8	212082.3	351.4
dec	21	10h00	12.202	38.373	36.927	25.82	54.162	88.98	395.4	226611	351.5
dec	21	11h00	14.524	41.772	39.864	27.44	58.735	103.4	433.4	237922	351.6
dec	21	12h00	16.306	44.212	42.103	28.68	62.107	114.55	460.9	246098.7	351.7
dec	21	13h00	17.861	45.734	43.636	29.76	64.024	119.17	469.9	249915.5	351.8
dec	21	14h00	18.467	45.942	44.138	30.18	64.286	119.79	469.7	250889.4	351.9
dec	21	15h00	18.87	45.027	43.814	30.46	62.885	112.08	446.8	247008	352.1
dec	21	16h00	18.697	42.823	42.576	30.34	59.825	98.77	409.2	238666	352.2
dec	21	17h00	17.89	39.264	40.405	29.78	55.215	80.73	356.6	225409.4	352.2
dec	21	18h00	16.738	34.879	37.675	28.98	49.793	60.56	294	206958.1	352.3
dec	21	19h00	14.783	31.081	35.017	27.62	45.407	48.31	256.1	191154.2	352.4
dec	21	20h00	14.165	29.604	33.62	27.19	43.055	39.43	224.2	179043.7	352.4
dec	21	21h00	13.549	28.643	32.693	26.76	41.448	35.14	208.7	171968.2	352.4
dec	21	22h00	12.932	27.833	31.907	26.33	40.187	32.18	197.1	167203.6	352.5
dec	21	23h00	12.316	27.111	31.21	25.9	39.141	30.04	189	163061.6	352.5
dec	21	24h00	11.701	26.447	30.569	25.47	38.232	28.39	182.4	160058.6	352.5

Table A3.2. A sample of two sections of the 'radi.out' output file.

Day1: 1
Hour_sam: 24

radius [m]	Ta [°C]	Tr [°C]	T [°C]	Tg1 [°C]	Tg11 [°C]	P [Pa]	hg [W/mK]	hr [W/mK]
Jun 21 12h00								
1982	15.46	21.042	15.646	33.287	38.971	89997.6	8.13	3.38
1946	15.46	21.714	15.967	35.089	39.489	89997.3	6.58	2.84
1910	15.46	22.014	16.263	35.884	39.719	89996.9	6	2.63
1874	15.46	22.201	16.541	36.375	39.868	89996.5	5.66	2.51
1838	15.46	22.331	16.808	36.715	39.962	89996.1	5.44	2.43
1802	15.46	22.427	17.065	36.966	40.041	89995.7	5.29	2.37
1766	15.46	22.5	17.313	37.156	40.111	89995.3	5.17	2.33
1730	15.46	22.909	17.542	37.513	40.185	89994.9	5.51	2.2
1694	15.46	22.943	17.765	37.549	40.206	89994.5	5.55	2.22
1658	15.46	22.975	17.983	37.581	40.217	89994.1	5.59	2.23
1622	15.46	23.005	18.194	37.61	40.219	89993.6	5.64	2.25
1586	15.46	23.035	18.4	37.636	40.229	89993.2	5.68	2.27
1550	15.46	23.062	18.6	37.659	40.25	89992.7	5.73	2.29
1514	15.46	23.088	18.795	37.679	40.251	89992.2	5.78	2.31
1478	15.46	23.113	18.984	37.695	40.252	89991.7	5.83	2.32
1442	15.46	23.136	19.167	37.707	40.253	89991.2	5.88	2.34
1406	15.46	23.158	19.346	37.717	40.254	89990.7	5.93	2.36
1370	15.46	23.178	19.519	37.723	40.255	89990.2	5.99	2.39
1334	15.46	23.197	19.687	37.725	40.264	89989.6	6.04	2.41
1298	15.46	23.214	19.85	37.724	40.264	89989.1	6.1	2.43
1262	15.46	23.229	20.008	37.719	40.255	89988.5	6.17	2.45
1226	15.46	23.243	20.161	37.71	40.254	89987.9	6.23	2.48
1190	15.46	23.255	20.309	37.697	40.254	89987.3	6.3	2.5
1154	15.46	23.266	20.453	37.681	40.253	89986.6	6.37	2.53
1118	15.46	23.275	20.592	37.66	40.252	89986	6.44	2.56
1082	15.46	23.282	20.726	37.634	40.232	89985.3	6.52	2.58
1046	15.46	23.288	20.855	37.604	40.221	89984.6	6.6	2.61
1010	15.46	23.292	20.98	37.57	40.219	89983.9	6.68	2.65
974	15.46	23.293	21.1	37.531	40.197	89983.1	6.77	2.68
938	15.46	23.293	21.216	37.486	40.185	89982.3	6.86	2.71
902	15.46	23.291	21.327	37.437	40.164	89981.5	6.96	2.75
866	15.46	23.287	21.434	37.381	40.151	89980.6	7.06	2.79
830	15.46	23.281	21.537	37.32	40.128	89979.7	7.17	2.83
794	15.46	23.273	21.635	37.252	40.107	89978.8	7.28	2.87
758	15.46	23.262	21.729	37.177	40.083	89977.8	7.41	2.92
722	15.46	23.249	21.819	37.096	40.05	89976.7	7.54	2.97
686	15.46	23.233	21.904	37.006	40.017	89975.6	7.68	3.02
650	15.46	23.214	21.985	36.907	39.982	89974.4	7.83	3.08
614	15.46	23.193	22.062	36.8	39.947	89973.2	8	3.14
578	15.46	23.168	22.135	36.682	39.903	89971.8	8.17	3.21
542	15.46	23.14	22.203	36.553	39.857	89970.4	8.37	3.28
506	15.46	23.108	22.267	36.412	39.802	89968.8	8.58	3.36
470	15.46	23.072	22.327	36.256	39.746	89967.1	8.81	3.45
434	15.46	23.031	22.383	36.085	39.688	89965.2	9.08	3.54
398	15.46	22.986	22.435	35.895	39.61	89963.1	9.37	3.65
362	15.46	22.934	22.482	35.683	39.521	89960.8	9.7	3.77
326	15.46	22.876	22.525	35.446	39.431	89958.2	10.08	3.92
290	15.46	22.81	22.563	35.179	39.31	89955.1	10.53	4.08
254	15.46	22.735	22.597	34.873	39.176	89951.5	11.06	4.28
218	15.46	22.649	22.627	34.519	38.999	89947.2	11.7	4.52

Dec 21 12h00

1982	28.68	40.926	29.009	59.182	38.799	89996.1	10.27	4.14
1946	28.68	42.366	29.591	62.528	39.386	89995.5	8.31	3.48
1910	28.68	43.012	30.133	64.003	39.648	89994.9	7.58	3.22
1874	28.68	43.412	30.647	64.912	39.816	89994.2	7.16	3.07
1838	28.68	43.692	31.141	65.542	39.924	89993.6	6.88	2.98
1802	28.68	43.897	31.617	66.004	40.013	89992.9	6.69	2.91
1766	28.68	44.053	32.077	66.354	40.091	89992.2	6.54	2.86
1730	28.68	44.934	32.505	67.142	40.181	89991.6	6.97	2.7
1694	28.68	45.003	32.921	67.22	40.203	89990.8	7.03	2.72
1658	28.68	45.069	33.326	67.292	40.216	89990.1	7.08	2.74
1622	28.68	45.132	33.721	67.358	40.22	89989.4	7.14	2.76
1586	28.68	45.192	34.106	67.418	40.231	89988.6	7.2	2.79
1550	28.68	45.249	34.48	67.472	40.252	89987.8	7.26	2.81
1514	28.68	45.302	34.844	67.519	40.254	89987	7.32	2.83
1478	28.68	45.353	35.198	67.561	40.256	89986.2	7.38	2.86
1442	28.68	45.4	35.543	67.596	40.258	89985.4	7.45	2.88
1406	28.68	45.444	35.877	67.625	40.26	89984.5	7.52	2.91
1370	28.68	45.485	36.202	67.647	40.261	89983.6	7.59	2.93
1334	28.68	45.523	36.518	67.662	40.27	89982.7	7.66	2.96
1298	28.68	45.557	36.824	67.671	40.27	89981.7	7.74	2.99
1262	28.68	45.588	37.122	67.673	40.262	89980.8	7.81	3.02
1226	28.68	45.616	37.41	67.668	40.26	89979.8	7.9	3.05
1190	28.68	45.64	37.689	67.655	40.26	89978.7	7.98	3.08
1154	28.68	45.66	37.96	67.635	40.258	89977.7	8.07	3.11
1118	28.68	45.677	38.221	67.607	40.255	89976.6	8.16	3.15
1082	28.68	45.691	38.475	67.571	40.235	89975.4	8.26	3.18
1046	28.68	45.7	38.719	67.527	40.223	89974.2	8.36	3.22
1010	28.68	45.706	38.955	67.474	40.22	89973	8.47	3.26
974	28.68	45.707	39.183	67.412	40.197	89971.7	8.58	3.3
938	28.68	45.705	39.402	67.341	40.183	89970.4	8.7	3.34
902	28.68	45.698	39.614	67.259	40.16	89969	8.82	3.39
866	28.68	45.687	39.817	67.167	40.145	89967.5	8.95	3.44
830	28.68	45.67	40.012	67.064	40.12	89966	9.09	3.49
794	28.68	45.65	40.199	66.95	40.096	89964.4	9.24	3.54
758	28.68	45.623	40.377	66.823	40.069	89962.7	9.4	3.6
722	28.68	45.592	40.548	66.682	40.034	89961	9.56	3.66
686	28.68	45.554	40.711	66.527	39.997	89959.1	9.74	3.73
650	28.68	45.511	40.866	66.356	39.958	89957.1	9.93	3.8
614	28.68	45.461	41.013	66.169	39.918	89955	10.14	3.87
578	28.68	45.404	41.152	65.962	39.869	89952.7	10.37	3.96
542	28.68	45.339	41.283	65.735	39.819	89950.3	10.61	4.05
506	28.68	45.265	41.407	65.485	39.758	89947.6	10.88	4.14
470	28.68	45.183	41.522	65.21	39.696	89944.7	11.18	4.25
434	28.68	45.089	41.629	64.905	39.631	89941.6	11.51	4.37
398	28.68	44.985	41.729	64.567	39.546	89938.1	11.89	4.51
362	28.68	44.867	41.82	64.19	39.449	89934.1	12.31	4.66
326	28.68	44.734	41.903	63.767	39.349	89929.7	12.79	4.84
290	28.68	44.583	41.978	63.288	39.218	89924.5	13.36	5.04
254	28.68	44.411	42.045	62.741	39.072	89918.5	14.03	5.29
218	28.68	44.212	42.103	62.107	38.881	89911.1	14.85	5.58

Table A3.3. A sample of two sections of the 'ground.out' output file.

Day1: 1

Radius: 200

Depth			0	0.002	0.0063	0.0155	0.0354	0.0782	0.17	0.37	0.79	1.71	3.67	7.89	16.96	36.48
			[°C]	[°C]	[°C]	[°C]	[°C]	[°C]	[°C]	[°C]	[°C]	[°C]	[°C]	[°C]	[°C]	[°C]
Jun	21	1h00	20.621	20.707	20.891	21.276	22.058	23.528	25.741	27.018	28.791	32.668	37.38	38.15	39	39
Jun	21	2h00	20.176	20.262	20.446	20.831	21.615	23.1	25.398	26.989	28.791	32.665	37.378	38.15	39	39
Jun	21	3h00	19.748	19.835	20.018	20.404	21.192	22.693	25.067	26.948	28.791	32.661	37.376	38.15	39	39
Jun	21	4h00	19.335	19.422	19.606	19.994	20.786	22.304	24.749	26.894	28.79	32.657	37.374	38.15	39	39
Jun	21	5h00	18.935	19.022	19.207	19.596	20.394	21.93	24.441	26.83	28.789	32.653	37.372	38.15	39	39
Jun	21	6h00	18.544	18.631	18.817	19.209	20.013	21.568	24.142	26.756	28.787	32.65	37.37	38.149	39	39
Jun	21	7h00	18.294	18.376	18.55	18.92	19.692	21.227	23.853	26.674	28.784	32.646	37.368	38.149	39	39
Jun	21	8h00	19.664	19.666	19.68	19.747	20.039	21.083	23.584	26.584	28.78	32.643	37.365	38.149	39	39
Jun	21	9h00	22.875	22.776	22.577	22.218	21.724	21.626	23.415	26.49	28.776	32.639	37.363	38.149	38.999	38.999
Jun	21	10h00	27.007	26.813	26.415	25.646	24.357	22.944	23.462	26.399	28.77	32.635	37.361	38.149	38.999	38.999
Jun	21	11h00	31.209	30.953	30.422	29.366	27.469	24.862	23.796	26.323	28.764	32.632	37.359	38.149	38.999	38.999
Jun	21	12h00	34.519	34.253	33.696	32.561	30.411	27.038	24.421	26.273	28.757	32.628	37.357	38.149	38.999	38.999
Jun	21	13h00	36.257	36.031	35.55	34.548	32.546	29.028	25.266	26.26	28.75	32.624	37.355	38.149	38.999	38.999
Jun	21	14h00	36.16	36.01	35.686	34.985	33.477	30.444	26.2	26.289	28.744	32.621	37.353	38.149	38.999	38.999
Jun	21	15h00	34.222	34.173	34.06	33.779	33.029	31.027	27.068	26.357	28.737	32.617	37.351	38.149	38.999	38.999
Jun	21	16h00	30.812	30.868	30.975	31.147	31.27	30.662	27.724	26.455	28.732	32.613	37.349	38.149	38.999	38.999
Jun	21	17h00	27.289	27.407	27.65	28.117	28.879	29.528	28.063	26.569	28.728	32.61	37.347	38.149	38.999	38.999
Jun	21	18h00	25.453	25.561	25.787	26.242	27.08	28.22	28.081	26.684	28.725	32.606	37.345	38.149	38.999	38.999
Jun	21	19h00	24.33	24.429	24.638	25.065	25.881	27.156	27.883	26.786	28.723	32.602	37.343	38.149	38.999	38.999
Jun	21	20h00	23.466	23.56	23.759	24.169	24.97	26.315	27.573	26.87	28.722	32.599	37.341	38.149	38.999	38.999
Jun	21	21h00	22.756	22.847	23.04	23.439	24.231	25.617	27.212	26.932	28.722	32.595	37.339	38.149	38.999	38.999
Jun	21	22h00	22.144	22.233	22.422	22.814	23.6	25.014	26.834	26.974	28.722	32.591	37.336	38.149	38.999	38.999
Jun	21	23h00	21.596	21.684	21.87	22.259	23.041	24.475	26.456	26.996	28.723	32.588	37.334	38.149	38.999	38.999
Jun	21	24h00	21.093	21.18	21.364	21.751	22.532	23.983	26.087	26.999	28.724	32.584	37.332	38.149	38.999	38.999
Dec	21	1h00	37.401	37.55	37.867	38.531	39.876	42.379	45.892	45.962	43.705	40.703	37.108	37.401	38.881	38.881
Dec	21	2h00	36.662	36.807	37.115	37.761	39.077	41.549	45.161	45.894	43.714	40.706	37.109	37.401	38.881	38.881
Dec	21	3h00	35.976	36.117	36.418	37.051	38.342	40.788	44.475	45.799	43.721	40.709	37.111	37.401	38.881	38.881
Dec	21	4h00	35.336	35.474	35.77	36.39	37.66	40.083	43.831	45.681	43.727	40.712	37.113	37.401	38.881	38.881
Dec	21	5h00	34.728	34.864	35.155	35.766	37.02	39.425	43.225	45.542	43.732	40.715	37.115	37.401	38.881	38.881
Dec	21	6h00	35.505	35.572	35.723	36.074	36.918	38.925	42.658	45.386	43.736	40.718	37.116	37.401	38.881	38.881
Dec	21	7h00	38.738	38.679	38.569	38.403	38.334	39.113	42.197	45.217	43.737	40.721	37.118	37.401	38.881	38.881
Dec	21	8h00	43.407	43.23	42.869	42.187	41.124	40.291	41.978	45.043	43.737	40.724	37.12	37.401	38.881	38.881
Dec	21	9h00	48.813	48.525	47.931	46.769	44.763	42.302	42.107	44.878	43.735	40.727	37.122	37.401	38.881	38.881
Dec	21	10h00	54.162	53.806	53.064	51.579	48.866	44.948	42.627	44.739	43.732	40.73	37.124	37.401	38.881	38.881
Dec	21	11h00	58.735	58.351	57.546	55.908	52.799	47.86	43.518	44.642	43.728	40.732	37.125	37.401	38.881	38.881
Dec	21	12h00	62.107	61.735	60.949	59.326	56.142	50.685	44.697	44.598	43.722	40.735	37.127	37.401	38.881	38.881
Dec	21	13h00	64.024	63.697	63.001	61.541	58.576	53.121	46.045	44.614	43.717	40.738	37.129	37.401	38.881	38.881
Dec	21	14h00	64.286	64.036	63.499	62.343	59.882	54.941	47.426	44.692	43.713	40.741	37.131	37.401	38.881	38.881
Dec	21	15h00	62.885	62.733	62.399	61.648	59.912	55.953	48.702	44.825	43.709	40.744	37.132	37.401	38.881	38.881
Dec	21	16h00	59.825	59.789	59.698	59.437	58.617	56.045	49.743	45.001	43.708	40.747	37.134	37.401	38.881	38.881
Dec	21	17h00	55.215	55.303	55.474	55.753	55.981	55.138	50.439	45.206	43.708	40.749	37.136	37.401	38.881	38.881
Dec	21	18h00	49.793	49.984	50.375	51.122	52.321	53.284	50.7	45.419	43.71	40.752	37.138	37.401	38.881	38.881
Dec	21	19h00	45.407	45.632	46.103	47.041	48.73	50.922	50.506	45.619	43.714	40.755	37.139	37.401	38.881	38.881
Dec	21	20h00	43.055	43.254	43.673	44.531	46.171	48.718	49.948	45.789	43.721	40.758	37.141	37.401	38.881	38.881
Dec	21	21h00	41.448	41.63	42.014	42.807	44.359	46.96	49.189	45.916	43.728	40.761	37.143	37.402	38.881	38.881
Dec	21	22h00	40.187	40.357	40.716	41.464	42.947	45.543	48.355	46	43.737	40.763	37.145	37.402	38.881	38.881
Dec	21	23h00	39.141	39.302	39.643	40.356	41.783	44.354	47.514	46.039	43.746	40.766	37.147	37.402	38.88	38.88
Dec	21	24h00	38.232	38.387	38.715	39.401	40.784	43.323	46.698	46.039	43.755	40.769	37.148	37.402	38.88	38.88

APPENDIX 4. VALUES FROM SAMPLE 'SOLCHIM' RUN.

This section is merely a list of the values of all the variables used in this study. It should be noted that the values were taken from the first of January at 10h00 in the morning when the transient terms will be large.

Name	*Developing region*	*Developed region*	*Units*
b	0.5	0.5	-
c_p	1006.891419	1007.211369	J/kgK
$c_{p,i-1}$	1006.878219	1007.209511	J/kgK
$c_{p,old}$	1006.890273	1007.208961	J/kgK
c_{pg}	820	820	J/kgK
c_{pr}	840	840	J/kgK
d_c	160	160	m
Drive Pot.	503.80806	503.80806	Pa
dt	60 (4 for temp gradients)	60 (4 for temp gradients)	s
Fr_D	2.2710617	2.2710617	-
g	9.81	9.81	m/s^2
H	10.23289	28.060677	m
H_c	1500	1500	m
h_g	6.657858	12.295963	W/m^2K
H_i	10	10	m
H_{i-1}	10.137797	26.261287	m
h_r	2.88198	4.706022	W/m^2K
h_{ra}	5.7	5.7	W/m^2K
h_{rgr}	5.623413	5.620415	W/m^2K
h_{rs}	5.057084	5.082588	W/m^2K
I_b	638.28333	638.28333	W/m^2
I_d	126.166667	126.166667	W/m^2
k	0.026086	0.026735	W/mK
K_{co}	-0.094334	-0.094334	-
K_{cs}	0.1	0.1	-
k_g	1.73	1.73	W/mK
K_i	1	1	-
k_{i-1}	0.026055	0.026731	W/mK
k_{old}	0.026083	0.02673	W/mK

k_r	0.78	0.78	W/mK
K_{ti}	0.25	0.25	-
m	216442.204096	216442.204096	kg/s
m_{old}	211283.369578	211283.369578	kg/s
p	89996.082437	89938.521131	Pa
p_a	90000	90000	Pa
p_{aHco}	75430.778141	75430.778141	Pa
p_c	82681.88356	82681.88356	Pa
p_{cold}	82682.775735	82682.775735	Pa
p_i	89997.009616	89997.009616	Pa
p_o	89932.988978	89932.988978	Pa
Power	$7.201239*10^7$	$7.370524*10^7$	W
P_r	10	10	m
Pr	0.7	0.7	-
P_t	10	10	m
q_i	530.269208	530.269208	W/m^2
r	1910	254	m
R	287.079987	287.079987	Nm/kgK
Re_c	$93.3917*10^6$	$93.3917*10^6$	-
Re_h	$1.961665*10^6$	$14.44813*10^6$	-
r_i	2000	2000	m
r_{i-1}	1946	290	m
r_o	200	200	m
T	298.281361	306.709481	K
T_a	297.233327	297.233327	K
T_c	299.43546	299.43546	K
T_{cold}	299.376342	299.376342	K
T_g	323.468219	322.422016	K
$T_{g,j=2}$	323.171357	322.13334	K
T_{gold}	323.461629	322.41558	K
T_{i-1}	297.891695	306.665054	K
T_{i-2}	297.471725	306.614755	K
T_o	306.74796	306.74796	K
T_{old}	298.279541	306.705549	K
T_r	306.540335	307.507588	K
$T_{r,i-1}$	306.088408	307.62252	K

T_{rold}	306.536791	307.503808	K
T_{sky}	282.868982	282.868982	K
v	1.676819	4.730609	m/s
v_c	11.192004	11.192004	m/s
v_{co}	11.96829	11.96829	m/s
v_{cold}	10.922972	10.922972	m/s
v_i	1.641611	1.641611	m/s
v_{i-1}	1.659066	4.426405	m/s
v_{old}	1.636669	4.616991	m/s
v_{ti}	10.538497	10.538497	m/s
z_1	0	0	m
z_2	0.002	0.002	m
Δp_{acc}	0.031716	0.031716	Pa
Δp_{cacc}	15.391654	15.391654	Pa
Δp_{cf}	4.716167	4.716167	Pa
Δp_{chim}	25.780142	25.780142	Pa
Δp_{co}	-6.076932	-6.076932	Pa
Δp_{coll}	64.020637	64.020637	Pa
Δp_{cs}	5.672321	5.672321	Pa
Δp_f	0.044118	0.044118	Pa
Δp_i	2.840309	2.840309	Pa
Δp_s	0.397938	3.027018	Pa
Δp_t	338.644068	338.644068	Pa
Δp_{ti}	14.180802	14.180802	Pa
Δr	36	36	m
Δz_1	0.002	0.002	m
Δz_2	0.0043	0.0043	m
μ	$1.838797*10^{-5}$	$1.877356*10^{-5}$	kg/ms
μ_c	$1.844267*10^{-5}$	$1.844267*10^{-5}$	kg/ms
μ_{cold}	$1.843995*10^{-5}$	$1.843995*10^{-5}$	kg/ms
μ_{old}	$1.838642*10^{-5}$	$1.877094*10^{-5}$	kg/ms
π	3.141593	3.141593	-
ρ	1.0511	1.021676	kg/m^3
ρ_a	1.054726	1.054726	kg/m^3
ρ_b	0.04426	0.04426	-

ρ_c	0.961843	0.961843	kg/m^3
ρ_{co}	0.899456	0.899456	kg/m^3
ρ_{cold}	0.962043	0.962043	kg/m^3
ρ_d	0.093463	0.093463	-
ρ_g	2640	2640	kg/m^3
ρ_i	1.053962	1.053962	kg/m^3
ρ_{i-1}	1.052476	1.052476	kg/m^3
ρ_{old}	1.051219	1.051219	kg/m^3
ρ_o	1.0214884	1.0214884	kg/m^3
ρ_r	2700	2700	kg/m^3
σ	$5.67*10^{-8}$	$5.67*10^{-8}$	W/m^2K^4
$\tau_{b\alpha}$	0.845492	0.845492	-
$\tau_{d\alpha}$	0.823391	0.823391	-

A5.1. THE AIR ENERGY EQUATION

An order of magnitude analysis follows concerning the kinetic energy, radial conduction and specific heat gradient terms in the air energy equation (equation 2.1). This analysis is done using values from the code (after it had stabilised) at a model time on the first if January of 10h00 because transient terms will be greatest at approximately this time. These values can be found in Appendix 4. This equation can be simplified to read

$$q_r \Delta\theta r \Delta r + q_g \Delta\theta r \Delta r = \frac{\partial}{\partial r}\left(m_{\Delta\theta} c_p T + \frac{1}{2} m_{\Delta\theta} v^2 - kHr\Delta\theta \frac{\partial T}{\partial r} \right)\Delta r + \frac{\partial}{\partial t}\left(\rho c_p \Delta\theta r \Delta r H T + \frac{1}{2} \rho \Delta\theta r \Delta r H v^2 \right) \quad \text{(A5.1)}$$

Beginning with the first term on the right hand side, and applying the differential operator

$$\frac{\partial}{\partial r}\left(m_{\Delta\theta} c_p T + \frac{1}{2} m_{\Delta\theta} v^2 - kHr\Delta\theta \frac{\partial T}{\partial r} \right) = c_p T \frac{\partial m_{\Delta\theta}}{\partial r} + m_{\Delta\theta} c_p \frac{\partial T}{\partial r} + m_{\Delta\theta} T \frac{\partial c_p}{\partial r} + m_{\Delta\theta} v \frac{\partial v}{\partial r} + \frac{1}{2} v^2 \frac{\partial m_{\Delta\theta}}{\partial r} - kHr\Delta\theta \frac{\partial^2 T}{\partial r^2} - Hr\Delta\theta \frac{\partial T}{\partial r}\frac{\partial k}{\partial r} - kr\Delta\theta \frac{\partial T}{\partial r}\frac{\partial H}{\partial r} \quad \text{(A5.2)}$$

Applying the equation to the entire annulus (i.e. $\Delta\theta = 2\pi$), and substituting the values into each term in turn, and making use of equation (2.5) yields

$$c_p T \frac{\partial m_{\Delta\theta}}{\partial r} = -c_p T \Delta\theta r H \frac{p}{RT^2}\frac{\partial T}{\partial t}$$

$$= -1007.211369 \cdot 306.709481 \cdot 2\pi \cdot 254 \cdot 28.060677 \frac{89938.521131}{287.079987 \cdot 306.709481^2} \times \frac{306.709481 - 306.705549}{4} = -45.2899 \cdot 10^3 \text{ W/m}$$

$$m_{\Delta\theta} c_p \frac{\partial T}{\partial r} = -216442.204096 \cdot 1007.211369 \frac{306.709481 - 306.665054}{254 - 290} = 269.0339 \cdot 10^3 \text{ W/m}$$

$$m_{\Delta\theta} T \frac{\partial c_p}{\partial r} = -216442.204096 \cdot 306.709481 \frac{1007.211369 - 1007.209511}{254 - 290} = 3.4262 \cdot 10^3 \text{ W/m}$$

$$m_{\Delta\theta} v \frac{\partial v}{\partial r} = -216442.204096 \cdot 4.730609 \frac{4.730609 - 4.426405}{254 - 290} = 8.6521 \cdot 10^3 \text{ W/m}$$

$$\frac{1}{2} v^2 \frac{\partial m_{\Delta\theta}}{\partial r} = \frac{1}{2} v^2 \Delta\theta r H \frac{p}{RT^2} \frac{\partial T}{\partial t}$$

$$= 0.5 \cdot 4.730609^2 \cdot 2\pi \cdot 254 \cdot 28.060677 \frac{89938.521131}{287.079987 \cdot 306.709481^2} \frac{306.709481 - 306.705549}{4}$$

$$= 1.6404 \text{ W/m}$$

$$kHr\Delta\theta \frac{\partial^2 T}{\partial r^2} = 0.026735 \cdot 28.060677 \cdot 254 \cdot 2\pi$$

$$\times \frac{\left(\frac{306.709481 - 306.665054}{254 - 290} - \frac{306.665054 - 306.614755}{290 - 326} \right)}{254 - 290} = -5.4247 \cdot 10^{-3} \text{ W/m}$$

$$Hr\Delta\theta \frac{\partial T}{\partial r} \frac{\partial k}{\partial r} = 28.060677 \cdot 254 \cdot 2\pi \frac{306.709481 - 306.665054}{254 - 290} \frac{0.026735 - 0.026731}{254 - 290}$$

$$= 6.1406 \cdot 10^{-6} \text{ W/m}$$

$$kr\Delta\theta \frac{\partial T}{\partial r} \frac{\partial H}{\partial r} = 0.026735 \cdot 254 \cdot 2\pi \frac{306.709481 - 306.665054}{254 - 290} \frac{28.060677 - 26.261287}{254 - 290}$$

$$= 2.6318^{-3} \text{ W/m}$$

It can be seen that the radial gradients of the conduction term, the kinetic energy term and the specific heat term are negligible (an order of magnitude smaller) when compared to the enthalpy (temperature gradient) term.

Now the last term in the second set of parenthesis in equation (A5.1) should be analysed. Applying the differential operator to the terms in brackets yields:

$$\frac{\partial}{\partial t}\left(\frac{1}{2}\rho\Delta\theta r\Delta rHv^2\right) = \Delta\theta r\Delta rH\frac{\partial}{\partial t}\left(\frac{1}{2}\rho v^2\right) \propto \Delta\theta rH\frac{\partial}{\partial t}\left(\frac{1}{2}\rho v^2\right) = \Delta\theta rH\frac{1}{2}v^2\frac{\partial\rho}{\partial t} + \Delta\theta rH\rho v\frac{\partial v}{\partial t} \qquad \text{(A5.3)}$$

Substituting the values from Appendix 4 into each term in turn yields

$$\Delta\theta rH\frac{1}{2}v^2\frac{\partial\rho}{\partial t} = 2\pi \cdot 254 \cdot 28.060677 \cdot 0.5 \cdot 4.730609^2 \frac{1.021676 - 1.021873}{60} = -1.6452 \text{ W/m}$$

$$\Delta\theta rH\rho v\frac{\partial v}{\partial t} = 2\pi \cdot 254 \cdot 28.060677 \cdot 1.021676 \cdot 4.730609\frac{4.730609 - 4.426405}{60} = 1.0974 \cdot 10^3 \text{ W/m}$$

Thus it is clear that the changes in kinetic energy with respect to time are negligible when compared to the enthalpy (temperature gradient) term analysed above.

A5.2. ROOF EQUATION

In order to establish whether or not the roof can be modelled by ignoring the temperature difference across it i.e. assuming an infinite value for its thermal conductivity (k_r), it is necessary to compare the roof's internal resistance to conduction heat transfer with its external resistance to convection heat transfer. This is done using an analytical solution to the problem. The vertical temperature distribution (along z) within the roof (as shown in figure 2.3) with different heat transfer coefficients (h_a and h_r) between the ambient air and the roof and the collector air and the roof respectively is given by [94PO1]

$$T(z) = \frac{-(T_a - T)}{(h_{ra}/h_r) + (h_{ra}/k_r)t_r + 1}\left(1 + \frac{h_{ra}}{k_r}z\right) + T_a \qquad \text{(A5.4)}$$

Using the values given in Appendix 4 from near the collector outlet, equation (A5.4) can be applied to the glass in the collector. The results are shown in figure A5.1.

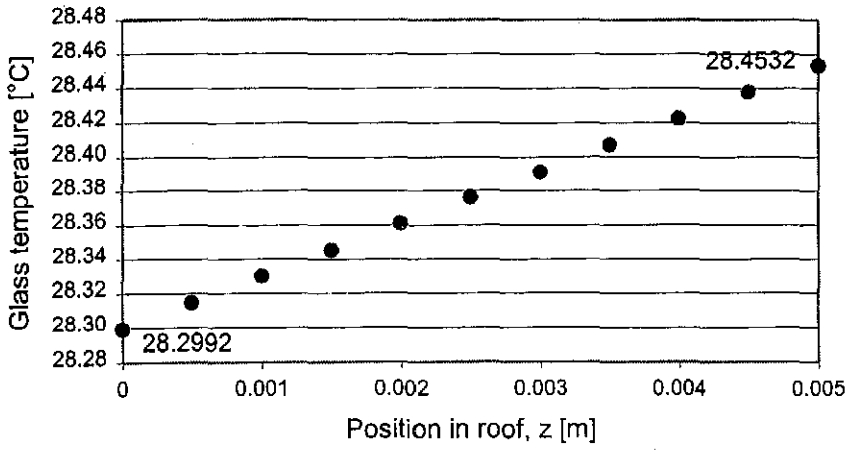

Figure A5 1. Vertical temperature distribution within the glass as predicted by equation (A5.4)

The deviation caused by assuming that the temperatures of the surfaces are equal to the average temperature can be approximated as follows:

$$\text{deviation} = 0.5(28.4532 + 28.2992) - 28.2992 = 0.077 \text{ K}$$

The difference is negligible and the assumption of a uniform temperature is thus justified.

In order to determine whether or not the term for radial conduction within the roof is negligible its magnitude may be compared to one of the other terms in the energy equation for the roof, namely the term for axial convective heat transfer. Using values at the collector outlet (found in Appendix 4), and considering an annular ($\Delta\theta=2\pi$) control volume of the roof, the radial heat transferred between the 137.6 m and 176.0 m radii via conduction is given by

$$k_r r 2\pi t_r \frac{\partial T_r}{\partial r} = 0.78 \cdot 254 \cdot 2\pi \cdot 0.005 \frac{307.507588 - 307.62252}{254 - 290} = 0.01987 \text{ W}$$

The heat transferred to the air by the roof between the 254 m and 290 m radii is given as

$$\begin{aligned} h_r r 2\pi \Delta r (T_r - T) &= 4.706022 \cdot 254 \cdot 2\pi \cdot (290 - 254) \cdot (307.507588 - 306.709481) \\ &= 215.7899 \cdot 10^3 \text{ W} \end{aligned}$$

Thus the radial heat flux in the roof is negligible.

A5.3. THE MOMENTUM EQUATIONS

An order of magnitude analysis is performed on the terms in equation (3.22) to establish that the transient term is negligible. This equation is can be simplified to read

$$\Delta M = \frac{\partial}{\partial r}(\rho v^2 H r \Delta\theta)\Delta r + \frac{\partial}{\partial t}(\rho H v r \Delta\theta)\Delta r \qquad \text{(A5.5)}$$

Applying the derivatives yields

$$\frac{\Delta M}{\Delta r \Delta \theta r} = v^2 H \frac{\partial \rho}{\partial r} + \rho v^2 \frac{\partial H}{\partial r} + 2\rho v H \frac{\partial v}{\partial r} + H v \frac{\partial \rho}{\partial t} + \rho v \frac{\partial H}{\partial t} + \rho H \frac{\partial v}{\partial t} \qquad \text{(A5.6)}$$

Substituting values from Appendix (using properties from near to the collector outlet since these yield the highest radial momentum changes) to compare the order of the magnitudes of each of these terms

$$v^2 H \frac{\partial \rho}{\partial r} = 4.730609^2 \cdot 28.060677 \frac{1.021676 - 1.021873}{254 - 290} = 0.003436\ \mathrm{N/m^2}$$

$$\rho v^2 \frac{\partial H}{\partial r} = 1.021676 \cdot 4.730609^2 \frac{28.060677 - 26.261287}{254 - 290} = -1.1428\ \mathrm{N/m^2}$$

$$2\rho v H \frac{\partial v}{\partial r} = 2 \cdot 1.021676 \cdot 4.730609 \cdot 28.060677 \frac{4.730609 - 4.426405}{254 - 290} = -2.2920\ \mathrm{N/m^2}$$

$$H v \frac{\partial \rho}{\partial t} = 28.060677 \cdot 4.730609 \frac{1.021676 - 1.021867}{60} = -422.5687 \cdot 10^{-6}\ \mathrm{N/m^2}$$

$$\rho H \frac{\partial v}{\partial t} = 1.021676 \cdot 28.060677 \frac{4.730609 - 4.616991}{60} = 54.2884 \cdot 10^{-3}\ \mathrm{N/m^2}$$

It is thus clear that the last two of these terms i.e. the transient terms are negligible.

A similar analysis is performed on the terms in equation (3.50) repeated here for clarity.

$$\Delta p_{cacc} = \frac{1}{A_c}\left[m(v_{co} - v_{ci}) + \frac{\partial}{\partial t}(\rho_c A_c H_c v_c) \right]$$

This can be written as

$$\Delta p_{cacc} = \left(\frac{m}{A_c}\right)^2 \left(\frac{1}{\rho_{co}} - \frac{1}{\rho_{ci}}\right) + \frac{H_c}{A_c}\frac{\partial m}{\partial t} \approx \left(\frac{m}{A_c}\right)^2 \left(\frac{1}{\rho_{co}} - \frac{1}{\rho_{ci}}\right) + \frac{H_c}{A_c}\frac{m - m_{old}}{\Delta t}$$

Substituting the values from Appendix 4 into this equation yields

$$\left(\frac{m}{A_c}\right)^2\left(\frac{1}{\rho_{co}}-\frac{1}{\rho_{ci}}\right)=\left(\frac{4\cdot 216442.204096}{\pi\cdot 160^2}\right)^2\left(\frac{1}{0.899456}-\frac{1}{1.0214884}\right)=15.3917\ \text{Pa}$$

$$\frac{H_c}{A_c}\frac{m-m_{old}}{\Delta t}=\frac{4\cdot 1500}{\pi\cdot 160^2}\frac{216442.204096-211283.369579}{20\cdot 60}=0.3207\ \text{Pa}$$

Since the mass flow rate is only updated every 20 minutes (a period of time specified by the mhold parameter), the time step applicable to the transient mass flow rate term is also 20 minutes. The value of the parameter mhold was set as 20 minutes to reduce the time required for the code to reach a solution since the calculation of every new mass flow rate requires the simulation of three minutes of model time. The difference in the calculated plant performance was negligible when compared to the calculated performance using a value of unity for the parameter mhold and so it was considered an acceptable approximation.

APPENDIX 6. CALCULATION OF THE SOLAR RADIATIVE PROPERTIES

A6.1 SURFACE SOLAR RADIATIVE PROPERTIES

The angle between a beam from the sun and the vertical is called the zenith angle denoted as θ. This can be found using the relation for a surface parallel to the horizon [91DU1]

$$\theta = \arccos(\sin(\phi_d)\sin(\phi_{lat}) + \cos(\phi_d)\cos(\phi_{lat})\cos(\omega)) \tag{A6.1}$$

where ϕ_{lat} is the latitude of the location where the radiation is measured. ω is the hour angle, solar noon being zero and each hour equalling 15° of longitude, mornings being positive and afternoons being negative. ϕ_d is the declination i.e. the angular position of the sun at solar noon with respect to the plane of the equator (South negative) in degrees as given by

$$\phi_d = 23.45\sin[360(284 + \text{day})/365] \tag{A6.2}$$

The beam reflectance of the roof is given by

$$\rho_b = \frac{1}{2}\left[\frac{\sin^2\{\arcsin(\sin\theta/1.526) - \theta\}}{\sin^2\{\arcsin(\sin\theta/1.526) + \theta\}} + \frac{\tan^2\{\arcsin(\sin\theta/1.526) - \theta\}}{\tan^2\{\arcsin(\sin\theta/1.526) + \theta\}}\right] \tag{A6.3}$$

and the beam transmittance due only to reflectance is given by

$$\tau_{br} = \frac{1}{2}\left[\frac{1 - \sin^2\{\arcsin(\sin\theta/1.526) - \theta\}/\left[\sin^2\{\arcsin(\sin\theta/1.526) + \theta\}\right]}{1 + \sin^2\{\arcsin(\sin\theta/1.526) - \theta\}/\left[\sin^2\{\arcsin(\sin\theta/1.526) + \theta\}\right]} + \frac{1 - \tan^2\{\arcsin(\sin\theta/1.526) - \theta\}/\left[\tan^2\{\arcsin(\sin\theta/1.526) + \theta\}\right]}{1 + \tan^2\{\arcsin(\sin\theta/1.526) - \theta\}/\left[\tan^2\{\arcsin(\sin\theta/1.526) + \theta\}\right]}\right] \tag{A6.4}$$

The diffuse reflectance and transmittance due only to reflectance can be approximated by setting a value of θ = 60° into equations (A6.3) and (A6.4) as follows

$$\rho_d = \frac{1}{2}\left[\frac{\sin^2\{\arcsin(\sin 60°/1.526) - 60°\}}{\sin^2\{\arcsin(\sin 60°/1.526) + 60°\}} + \frac{\tan^2\{\arcsin(\sin 60°/1.526) - 60°\}}{\tan^2\{\arcsin(\sin 60°/1.526) + 60°\}}\right] \quad \text{(A6.5)}$$
$$= 0.09434$$

$$\tau_{dr} = \frac{1}{2}\left[\frac{1 - \sin^2\{\arcsin(\sin 60°/1.526) - 60°\}/\left[\sin^2\{\arcsin(\sin 60°/1.526) + 60°\}\right]}{1 + \sin^2\{\arcsin(\sin 60°/1.526) - 60°\}/\left[\sin^2\{\arcsin(\sin 60°/1.526) + 60°\}\right]}\right.$$
$$\left. + \frac{1 - \tan^2\{\arcsin(\sin 60°/1.526) - 60°\}/\left[\tan^2\{\arcsin(\sin 60°/1.526) + 60°\}\right]}{1 + \tan^2\{\arcsin(\sin 60°/1.526) - 60°\}/\left[\tan^2\{\arcsin(\sin 60°/1.526) + 60°\}\right]}\right] \quad \text{(A6.6)}$$
$$= 0.842$$

For 5mm (t_r) glass having a "greenish cast of edge" (hence an extinction coefficient of 32) the beam transmittance considering only absorption is given by

$$\tau_{b\alpha} = e^{-32t_r/[\cos\{\arcsin(\sin\theta/1.526)\}]} \quad \text{(A6.7)}$$

Once again to find the diffuse beam transmittance considering only absorption, equation (A6.7) can be used with $\theta = 60°$ as follows

$$\tau_{b\alpha} = e^{-32\cdot 0.005/[\cos\{\arcsin(\sin 60°/1.526)\}]} \quad \text{(A6.8)}$$
$$= 0.823$$

The fraction of the solar beam radiation absorbed by the ground is given by

$$(\tau_b\alpha)_g = \tau_{br}\tau_{b\alpha}\alpha_g/\left[1-(1-\tau_{br})(1-\alpha_g)\right] = \tau_{br}\tau_{b\alpha}\alpha_g/\left[1-0.158(1-\alpha_g)\right] \quad \text{(A6.9)}$$

and for the diffuse radiation

$$(\tau_d\alpha)_g = \tau_{dr}\tau_{d\alpha}\alpha_g/\left[1-(1-\tau_{dr})(1-\alpha_g)\right] = 0.842\tau_{d\alpha}\alpha_g/\left[1-0.158(1-\alpha_g)\right] \quad \text{(A6.10)}$$

A6.2 RELATIONSHIP BETWEEN SOLAR TIME AND LOCAL TIME

The local time at any location is the commonly used time of day at that location. Solar time on the other hand is the time based only on the sun's position, and it thus has its noon at the time when the sun is at its highest position in the sky. The data found in Appendix 2 is recorded relative to solar time. The model uses this information in this form and creates output information also in solar time. It was thus

not necessary to convert any of the input or out put data from one time scale to the other. For completeness sake the equations used to do this were it necessary are listed [99SA01].

The year adjustment takes into account that in a leap cycle (four consecutive years) the radiation varies. To find this variation the year adjustment is calculated as follows

$$\text{yadj} = 0.25(2.5 - (\text{y} - 4 \cdot \text{INT}((\text{y} - 1)/4))) \tag{A6.11}$$

where INT is the true integer function and y is the year eg. 1999 or 2001 etc. Yadj cycles through 0.375, 0.125, -0.125 and –0.375 for the four years ending on a leap year.

The annual phase angle is given in radians by

$$\text{PA} = 0.0172028(\text{day} + \text{yadj}) \tag{A6.12}$$

The equation of time in minutes is given by

$$\begin{aligned}\text{EOTD} = 1440(&0.005114\sin(\text{PA} + 3.0593) + 0.006892\sin(2\text{PA} + 3.4646) \\ &+ 0.000220\sin(3\text{PA} + 3.3858) + 0.000153\sin(4\text{PA} + 3.7766))\end{aligned} \tag{A6.13}$$

The local time at which the sun is at its highest in the sky (noon in solar time or just solar noon) is given in hours and minutes (eg. 12.45 means 12 hours and 0.45 * 60 = 27 minutes, hence 12.45 means 12:27) by

$$\text{SN} = 12 + \frac{4(\text{Lst} - \text{Longitude}) + \text{EOTD}}{60} \tag{A6.14}$$

where Lst is the standard meridian for the local time zone namely 30° for locations in South Africa.

APPENDIX 7. COMPARISON BETWEEN THE CENTRAL DIFFERENCE SCHEME AND THE UPWIND SCHEME APPROXIMATIONS OF THE TEMPERATURE GRADIENTS

The central difference scheme approximates the air temperature gradient in equation (4.1) as follows

$$\frac{\partial T}{\partial r} \approx \frac{1}{2}\left(\frac{T_{i+1} - T_i}{r_{i+1} - r_i} + \frac{T_i - T_{i-1}}{r_i - r_{i-1}}\right) \qquad \text{(A7.1)}$$

while the upwind scheme makes use of the following approximation

$$\frac{\partial T}{\partial r} \approx \frac{T_{i-1} - T_i}{r_{i-1} - r_i} \qquad \text{(A7.2)}$$

Equations (A7.1) and (A7.2) have applied to three sets of neighbouring points at different radii in the collector using data generated by the upwind scheme in table (A7.1)

Table A.7. Comparison of gradient approximations

Radius [m]	Temp [°C]	Central [°C/m]	Upwind [°C/m]	Difference [°C/m]	Effective difference [°C]
1829	33.0951				
1811	33.3385	0.013400	0.013522	0.000122	0.0122
1793	33.5775				
1018	39.8638				
1000	39.9998	0.007492	0.007556	0.000064	0.0064
982	40.1335				
353	43.908				
335	43.9551	0.002561	0.002617	0.000056	0.0056
317	44.0002				

The difference between the gradients calculated by each approximation is multiplied by the number of control volumes and this is the effective difference or error. Assuming a 15K increase in the air temperature as it moves through the collector, the error would be at least three orders of magnitude smaller than the total increase. For this reason and considering the great simplification brought about in solving the equation, the upwind scheme is used for the gradient approximation.

APPENDIX 8. PROPERTIES OF AIR

The thermophysical properties of dry air from –53°C to 107°C at standard atmospheric pressure (101325 Pa).

Density: (with temperature given in degrees Kelvin)

$$\rho = p/(287.08T),\ kg/m^3 \qquad (A8.1)$$

Specific heat [82AN1]:

$$c_p = 1.045356\cdot10^{3} - 3.161783\cdot10^{-1}T + 7.083814\cdot10^{-4}T^{2} - 2.705209\cdot10^{-7}T^{3},\ J/kgK \qquad (A8.2)$$

Viscosity [82AN1]:

$$\mu = 2.287973\cdot10^{-6} + 6.259793\cdot10^{-8}T - 3.131956\cdot10^{-11}T^{2} + 8.15038\cdot10^{-15}T^{3},\ kg/ms \qquad (A8.3)$$

Thermal conductivity:

$$k = -4.937787\cdot10^{-4} + 1.018087\cdot10^{-4}T - 4.627937\cdot10^{-8}T^{2} + 1.250603\cdot10^{-11}T^{3},\ W/mK \qquad (A8.4)$$

APPENDIX 9. GROUND TEMPERATURE DISTRIBUTIONS

A9.1. INTRODUCTION

The rotation of the earth about its own axis causes a cyclic heating (daytime) and cooling (night-time) of the ground. The period of this variation is 24 hours. The annual variation of the earth's position relative to the sun (orbiting), on the other hand, causes a second cyclic effect namely the seasonal heating (summer) and cooling (winter) of the ground near to the earth's surface. The variation of the ground temperature due to this effect is important to a depth an order of magnitude higher than is the case with the daily variation. The capacitance of the ground causes it to store the heat energy in the hotter periods and release it in the cooler periods. Thus there are storage effects present between day and night, as well as between the summer and winter months.

A9.2. REFERENCE PLANT

In order to solve equation (2.19) the boundary condition equation (2.21) is required. This boundary condition states that at a depth of infinity the vertical heat flux is zero i.e. the temperature gradient is equal to zero. This is a valid assumption assuming that there are no geothermal effects present. An approximation to this condition can be made by applying the zero gradient condition at a finite depth below the surface where the temperature gradients are small. The temperature variation in the ground at a depth of 0.66 m is less than 1 percent of the temperature variation present at the surface, in both winter and summer and this is assumed to be small enough to satisfy the criteria just mentioned. (The data used to determine this depth was generated by modelling the reference plant with a deep ground domain i.e. the control volume just above the deepest one in the ground occurred at a depth of 16.69 m, with a multiplier in equation (5.6) of 2.15. The reason that the depth of this control volume is quoted and not the deepest one is because this is the depth from which the zero gradient condition is applied.)

The reference plant was thus modelled applying the zero gradient at a depth of 0.66 m and the temperature distributions are shown in figure A9.1. Although the zero gradients at a depth of approximately 0.7 m are evident, it is also apparent that the temperatures at this depth differ at different times of the year. In summer the

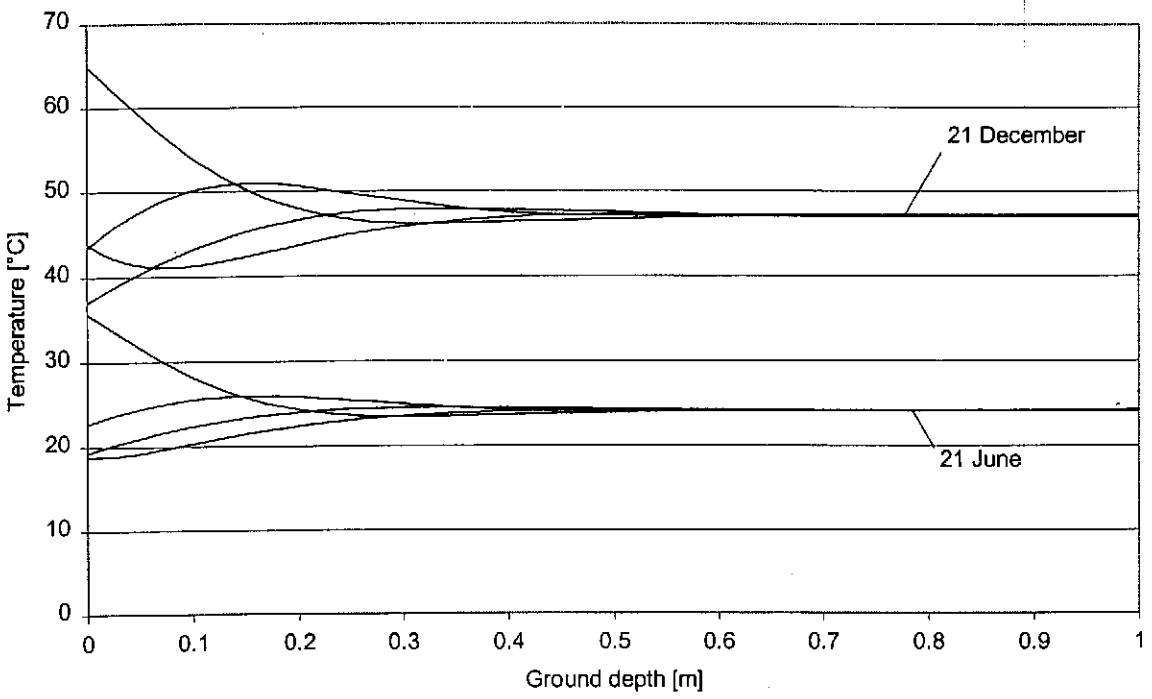

Figure A9.1: The ground temperature distributions on the 21 of June and 21 of December with the zero gradient at 0.66 m.

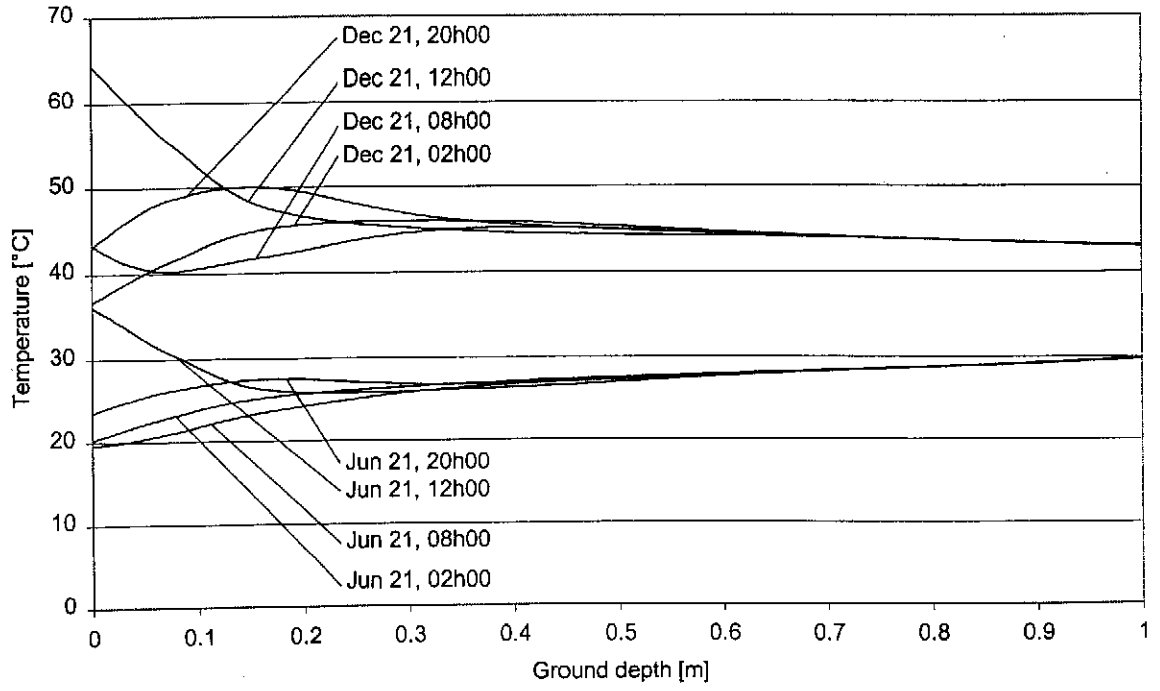

Figure A9.2: The ground temperature distributions on the 21 of June and 21 of December with the zero gradient at 16.96 m showing the daily occilations.

temperature is approximately 47°C while in winter it is 24°C. This is due to the annual variation of the average daily temperature present at the ground surface. Since there can be no discontinuities in the temperature distribution in the ground this temperature difference implies that during the year energy is transferred into and out of the ground below a depth of 0.66 m. For this reason the simulation was repeated using a depth of 16.96 m (a multiplier value of 2.15) for the zero gradient condition. The temperature distributions of this approach are shown in figures A9.2 and A9.3 (both with the same data but plotted on different axis). It is clear in figure A9.3 that there is a depth namely approximately 16 m at which no temperature variation is evident. Applying the zero gradient condition at a depth of 16.96 m is thus more suitable.

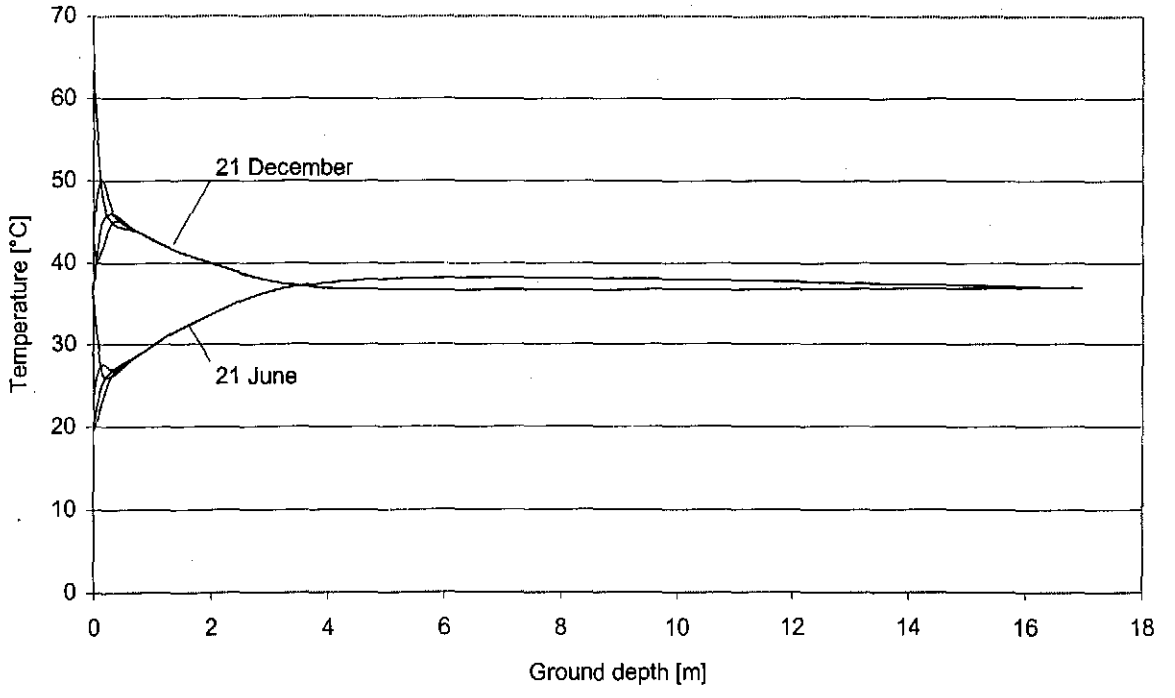

Figure A9.3: The ground temperature distributions on the 21 of June and 21 of December with the zero gradient at 16.96 m showing the daily and annual occilations.

The total energy delivered from the plant in a year as calculated applying the zero gradient at 0.66 m and 16.96 m is are equal. This is expected since after the condition of sustained response is reached the net energy entering or leaving the ground is zero. The instantaneous power delivered however differs as shown in figure A9.4. Notice the higher power output in winter and lower in summer with the zero condition applied at a depth of 16.96 m. This is due to the energy stored in the

ground (below 0.66 m) during the summer months. It is clear that by applying the model to a ground depth of 16.96 m the effects of annual storage are accounted for.

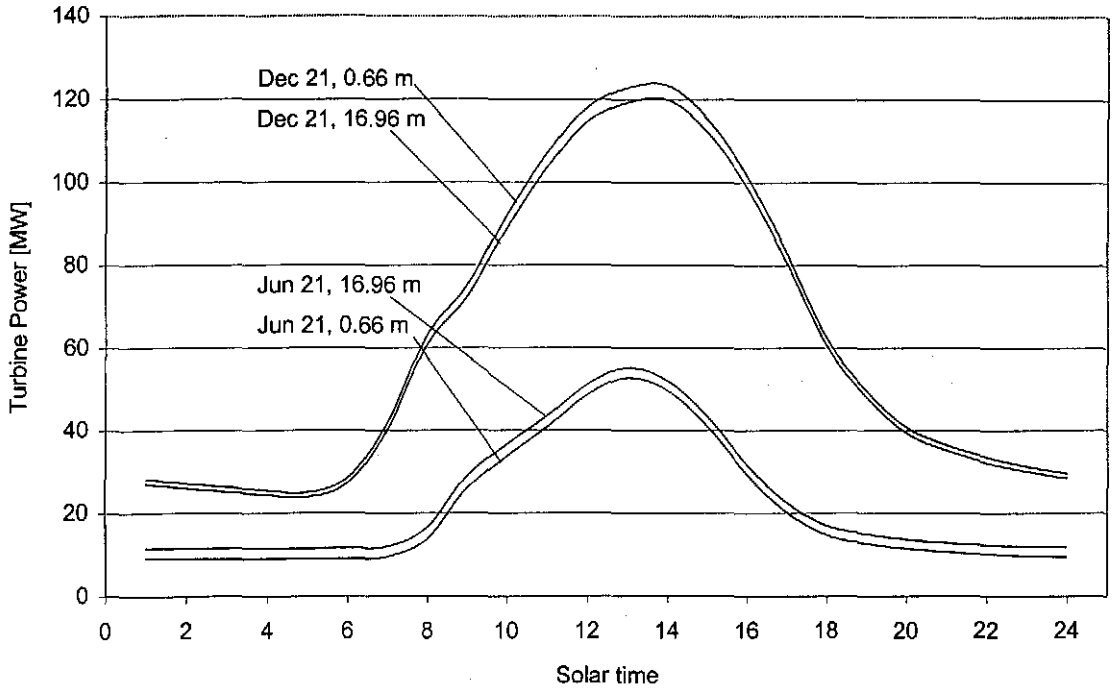

Figure A9.4: The power delivered by the refernce plant with the zero condition at 0.66 m and 16.96 m.

A9.3. EFFECTS OF GROUND PROPERTIES

In order to test the effects of the thermo-physical properties of the ground on the plant performance, a solar chimney power plant was modelled using dry sand having properties as given in table A9.1.

Table A9.1: The thermo-physical properties of dry sand

k_g	0.3 W/mK
ρ_g	1600 kg/m^3
c_{pg}	800 J/kgK

The results of this test are shown in figures A9.5 and A9.6. The temperature variations in the ground become negligible at shallower depths with sand compared to the case with granite as the ground material. In fact at a depth of 7 m the annual temperature variation is negligible.

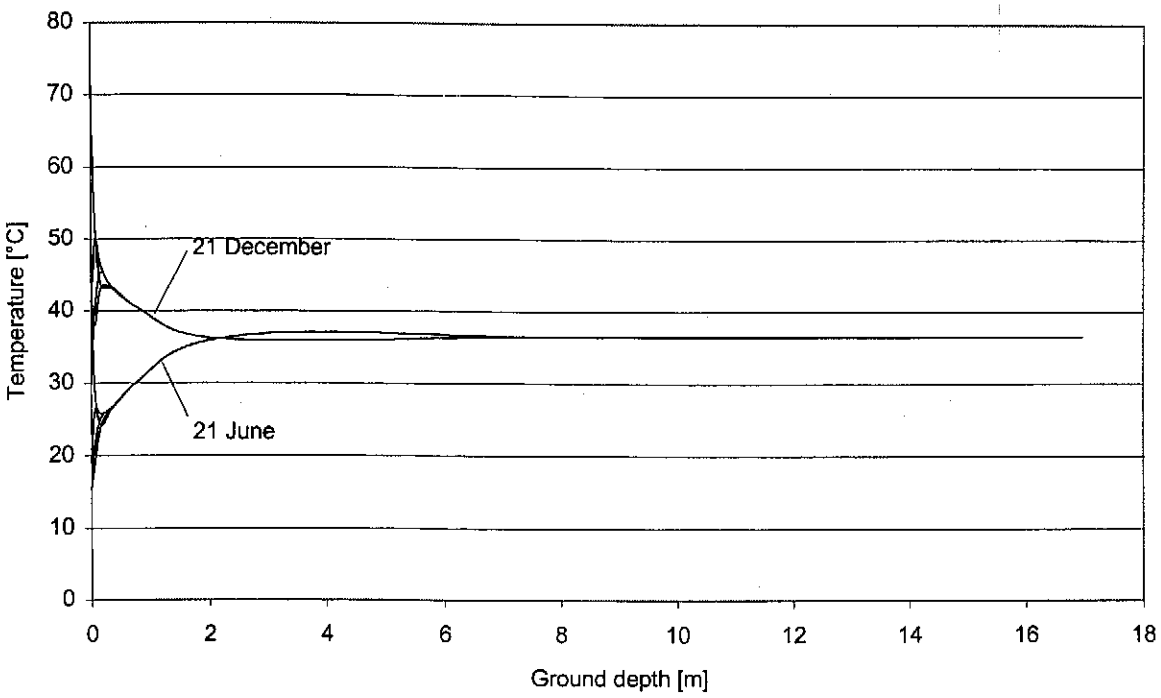

Figure A9.5: The temperature distributions in the ground (modelled as dry sand) on the 21 June and 21 December showing the annual oscillations.

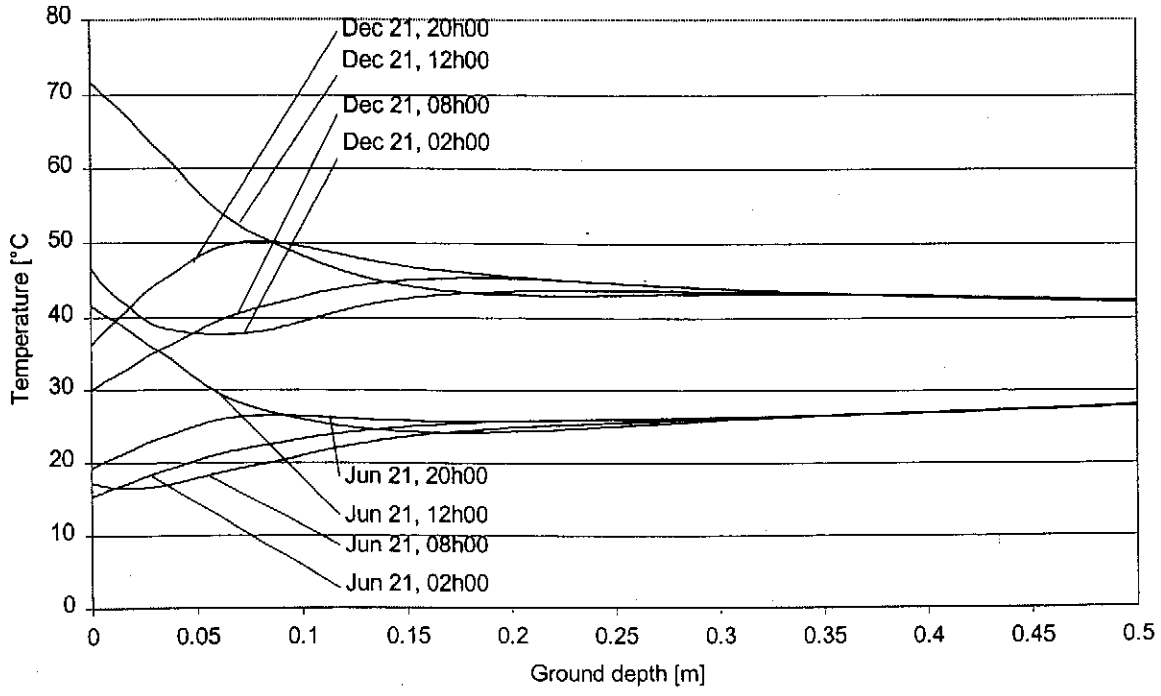

Figure A9.6: The temperature distributions in the ground (modelled as dry sand) on the 21 June and 21 December showing the daily oscillations.

The surface temperatures show greater extremes with dry sand (the surface temperature ranges between 73.0°C and 15.6°C) than with granite (the surface temperature ranges between 64.2°C and 19.6°C). The total energy generated is 380GWh/annum which is somewhat greater than the 367 generated by the reference plant.